UNIVERSITÀ
DEGLI STUDI
DI PADOVA

Sede Amministrativa: Università degli Studi di Padova
Dipartimento di Tecnica e Gestione dei Sistemi Industriali

SCUOLA DI DOTTORATO DI RICERCA
IN INGEGNERIA INDUSTRIALE

INDIRIZZO: INGEGNERIA METALLURGICA
XXII CICLO

DEVELOPMENT OF INNOVATIVE APPLICATIONS IN NON-FERROUS METALS

SVILUPPO DI APPLICAZIONI INNOVATIVE NELL'AMBITO DEI METALLI NON FERROSI

Direttore della Scuola: Ch.mo Prof. Paolo F. Bariani

Coordinatore d'indirizzo: Ch.mo Prof. Emilio Ramous

Supervisore: Ch.mo Prof. Alberto Tiziani

Dottorando: Fabio Grosselle

31 GENNAIO 2010

To my Mum with love

"La goccia d'acqua scava la pietra, non con la forza,
ma con il suo continuo cadere"

PREFACE

This doctoral thesis is the result of three years full-time studies, including courses and research at the University of Padova from January 2007 to December 2009. The experimental work was carried out at the Department of Management and Engineering (DTG), Vicenza (Italy) within Six Frame European NADIA Project - New Automotive components Designed for and manufactured by Intelligent processing of light Alloys.

Professor Alberto Tiziani and Professor Franco Bonollo were the principal supervisors.

The results were reported and published throughout the three years period and the articles included in the thesis are presented in the form they were submitted for publication or printed. The thesis consists of two parts:

PART 1 is intended to give the reader sufficient background on the influence of composition, process and defects on the performance of aluminium alloy castings, physical fundamentals and literature review as well as industrial challenges, motivation and goals.

PART 2 is a collection of five articles dealing with different aspects of aluminium foundry. The manuscripts included in this section are:

A1. Article 1
Correlation between microstructure and mechanical properties of Al-Si diecast engine blocks
F. Grosselle, G. Timelli, F. Bonollo, R.Molina, Published in Metallurgical Science and Technology, 2009.

A2. Article 2
DOE applied to microstructural and mechanical properties of Al-Si-Cu-Mg casting alloys for automotive application
F. Grosselle, G. Timelli, F. Bonollo, Accepted for publication in Materials Science & Engineering A, 2009.

A3. Article 3
Correlation between microstructure and mechanical properties of Al-Si cast alloys
F. Grosselle, G. Timelli, F. Bonollo, A. Tiziani, E. Della Corte, Metallurgia Italiana 6 (2009) 25-32.

A4. Article 4
Final correlation & models about the effect of microstructure of heat treated Al alloys on mechanical behaviour
Deliverable of NADIA project.

A5. Article 5

Validation of numerical simulation code in the development of an automotive component

F. Grosselle, G. Timelli, F. Bonollo, N. Gramegna, To be submitted for publication in Journal of Materials Processing Technology, 2009

In addition to the articles included in the thesis, parts were presented in the following publications:

P1. **Influence of solutioning heat treatment on microstructural features of an hypereutectic aluminium alloy**
F. Grosselle, G. Timelli, F. Bonollo, To be submitted for publication in Metallurgical and Materials Transactions A.

P2. **Sviluppo di un componente PCBP**
F. Grosselle, G. Zoccoletti, Die Casting & Foundry Techniques, June 2008, 77-83

P3. **Innovative and Integrated Technologies for the Development of Aeronautic Components**
N. Gramegna, F. Bonollo, E. Della Corte, F. Grosselle, M. Cocco, 2010 TMS Annual Meeting, Seattle 14-18 Febbraio 2010.

P4. **Microstructure vs properties correlation in Al-Si cast alloys**
F. Grosselle, G. Timelli, F. Bonollo, A. Tiziani, E. Della Corte, , HTDC 2008, 9-10 Aprile 2008, Montichiari (BS)

P5. **A new reference die for mechanical properties evaluation in diecasting. Part 1 - Design and process optimisation**
G. Timelli, F. Grosselle, F. Voltazza, E. Della Corte, HTDC 2008, 9-10 Aprile 2008, Montichiari (BS)

P6. **A new reference die for mechanical properties evaluation in diecasting Part 2 - Microstructural investigations and tensile testing**
G. Timelli, F. Grosselle, F. Bonollo, F. Voltazza, L. Capra, HTDC 2008, 9-10 Aprile 2008, Montichiari (BS)

P7. **Innovazione nelle tecnologie di progettazione integrando la simulazione dei processi di fabbricazione nello sviluppo del design di componenti aeronautici**
N. Gramegna, E. Della Corte, M. Cocco, D. Spaccasassi, F. Bonollo, F. Grosselle, 32° convegno AIM, Ferrara, 2008

P8. **Influenza della modifica allo stronzio e della condizione di solidificazione sulla microstruttura in leghe Al-Si da fonderia**
A. Manente, G. Timelli, F. Bonollo, F. Grosselle, 32° convegno AIM, Ferrara, 2008

Following works were presented in form of oral presentation or poster in different conferences:

P9. **Integrated approach to a component design for automotive applications**
F. Grosselle, F.Bonollo G. Timelli,S. Di Rosa, N. Gramegna, EUROMAT 2009, Glasgow (UK), 7-10 Settembre 2009.

P10. **Realizzazione di un mono-cilindro in lega di alluminio mediante approccio CAE ("Computer Aided Engineering")**
F. Bonollo, F. Grosselle, G. Timelli, R. Molina, G. Cupitò, S. Di Rosa, E. Della Corte, N. Gramegna, Enginsoft International conference 2009, Bergamo 1-2 October 2009,

P11. **Produzione di componenti automotive mediante colata in bassa pressione**
G.Timelli, F. Grosselle, F. Bonollo, B. Bonatto, R. Molina, Alumotive 2009, 2-4 Aprile 2009

P12. **Studio numerico e sperimentale del comportamento di leghe presso colate**
F. Bonollo, G. Timelli, F. Grosselle F. Voltazza, M. Paolini, S. Barison, G.Capra, L.Capra, N.Gramegna, Enginsoft CAE Users' Meeting 2008, Mestre (VE)

Finally, the following M.S. thesis have been supervised:

1. A. Tonolli, **Caratterizzazione micro strutturale di getti in lega di alluminio**, supervisors: F. Bonollo, F. Grosselle, A.A. 2006-2007.

2. N. Segato, **Processo di trafilatura nelle leghe di rame e relativa difettologia**, supervisors: F. Bonollo, F. Grosselle, A.A. 2006-2007.

3. M. Bantourakis, **Rassegna delle caratteristiche e degli impieghi di leghe Al-Si ipereutettiche**, supervisors: F. Bonollo, F. Grosselle, A.A. 2006-2007.

4. G. Valente, **Caratterizzazione microstrutturale e meccanica di getti in alluminio (EN-AC 46000 e EN-AC 46100)**, supervisors: F. Bonollo, F. Grosselle, A.A. 2007-2008.

5. E. Dal Gal, **Analisi microstrutturale e meccanica di leghe Al-Si-Cu per impieghi automobilistici**, supervisors: F. Bonollo, F. Grosselle, A.A. 2007-2008.

6. F. Miglioranza, **Analisi meccanica e microstrutturale di getti in lega di alluminio colati in bassa pressione per impieghi automobilistici**, supervisors: F. Bonollo, F. Grosselle, A.A. 2007-2008.

7. N. Pornaro, **Analisi microstrutturale e meccanica di un monocilindro in lega AlSi7Cu2 colato in bassa pressione**, supervisors: F. Bonollo, F. Grosselle, A.A. 2008-2009.

8. G. Carli, **Caratterizzazione di un componente del sistema sterzo pressocolato in lega di alluminio sottoposto a diversi trattamenti termici**, supervisors: F. Bonollo, F. Grosselle, A.A. 2008-2009.

9. A. Rancan, **Studio delle proprietà microstruttuali e di resistenza ad usura di una lega Al-Si ipereutettica per applicazioni automobilistiche,** supervisors: F. Bonollo, F. Grosselle, A.A. 2008-2009.

10. M.Scarpa, **Rassegna delle tecnologie di squeeze casting**, supervisors: F. Bonollo, F. Grosselle, A.A. 2008-2009.

11. P.Zulian, **Modellazione delle curve di invecchiamento per la lega di alluminio A319 da fonderia**, supervisors: F. Bonollo, F. Grosselle, A.A. 2009-2010.

12. P. Zanchetta, **Caratterizzazione di moduli radiatore pressocolati in lega di alluminio**, supervisors: F. Bonollo, F. Grosselle, A.A. 2009-2010.

CONTENTS

SUMMARY

Microstructural and mechanical properties of Aluminum casting are the results of the complex interactions between alloy composition, process and defects. Therefore, an exhaustive knowledge of such a interaction allows to develop component with high quality and satisfying design requirements. In addition, it allows to reduce the reject rates, to improve the process yield and the production rate leading to a lower final product cost.

It is possible to reduce both the final cost and time to market by adopting the "simultaneous engineering" approach in the product design. By means of this approach, all the aspects involved in life cycle of the component are taken into account since the first stage of development; with this aim, numerical simulation plays a key role because it allows to analyze the interaction process-component in virtual environment reducing prototyping costs and time.

The study was aimed at the analysis of the interactions between alloy, process, microstructure and mechanical behaviour for Aluminium-Silicon based castings. In addition, particular attention was paid to the development and implementation of models able to describe these interactions.

A literature review and a sufficient background of previously reported results on the influence of alloying elements, casting process and heat treatment on the properties of Aluminium based casting in terms of physical fundamentals as well as industrial challenges were carried out.

Special attention has been given to:

- The influence of solidification rate, alloy composition (especially, Copper and Titanium addition) and heat treatment on microstructural and mechanical features. With this aim, advanced statistical tools were applied.

- The influence of the primary Aluminium phase dimension as well as size and morphology of eutectic Silicon particles on casting mechanical properties. Several casting processes were taken into account. Gravity, low pressure and high pressure die casting are the most common processes in Aluminium foundry. The different filling conditions determine both different solidification rate and defect amount with an inevitable effect on overall properties.

- The age hardening modelling. The possibility to forecast the Yield Strength from quenching and ageing treatment is considerably relevant in process set-up stage.

- The use of "concurrent engineering" approach in the development of low pressure die cast mono-cylinder engine block. Casting process, solidification as well as microstructural and mechanical properties in as-cast temper and after heat treatment were analyzed and optimized by means of simulation code to obtain high quality casting. The reliability of such results was evaluated by comparing predicted values to experimental data.

SOMMARIO

Le proprietà meccaniche e microstrutturali di un getto in lega di Alluminio sono il risultato delle complesse interazioni tra composizione della lega, processo e difetti. Una conoscenza esaustiva di tali interazioni permette, quindi, di sviluppare componenti di elevata qualità che soddisfino le richieste progettuali. Tale conoscenza permette, inoltre, di ridurre la quantità di scarti, migliorare la resa del processo e la cadenza produttiva portando quindi ad un inferiore costo finale del getto. E' possibile ridurre costo finale e *time to market* utilizzando anche, in fase di sviluppo di prodotto, un approccio "simultaneous engineering". Mediante tale approccio tutti gli aspetti del ciclo di vita del componente sono considerati fin dalla fase di progettazione; a tale scopo, la simulazione di processo riveste una notevole importanza, in quanto permette di analizzare il comportamento globale del componente in un ambiente virtuale, riducendo così costi e tempi di prototipazione.

L'obiettivo di questa tesi è stato quindi l'analisi delle interazioni tra lega, processo, microstruttura e comportamento meccanico in getti in lega Alluminio-Silicio. Inoltre, particolare attenzione è stata posta allo sviluppo e alla successiva implementazione, in un software di simulazione numerica, di modelli matematici capaci di descrivere tali interazioni.

In prima analisi, è stata condotta una recensione della letteratura sull'influenza della composizione, del processo di colata e di trattamento termico sulle proprietà di getti in lega d'alluminio, analizzandone sia le caratteristiche di tipo fisico-metallurgiche così come quelle di carattere industriale.

Successivamente, nel presente lavoro è stata posta particolare attenzione ai seguenti aspetti:

- L'influenza della velocità di solidificazione, della composizione (specialmente dell'aggiunta di Rame e di Titanio) e del processo di trattamento termico sulle caratteristiche microstrutturali e meccaniche. A tale scopo sono state utilizzate tecniche avanzate di analisi statistica.

- L'influenza delle dimensioni della fase di Alluminio pro-eutettico, della morfologia e della grandezza delle particelle di Silicio eutettico sulle caratteristiche meccaniche. A tale scopo sono stati considerati il processo di colata in gravità, bassa pressione e pressocolata, che risultano essere le tecniche fusorie più utilizzate nella fonderia di Alluminio. Le diverse modalità di riempimento dello stampo, unitamente alle diverse velocità di solidificazione e alla quantità di difetti, influenzano in diverso modo sia la microstruttura che il comportamento meccanico della lega.

- La modellazione del trattamento termico d'indurimento per precipitazione. La possibilità di prevedere il valore della tensione di snervamento, a partire da parametri di tempra e di invecchiamento, riveste una notevole importanza in fase di set-up di processo.

- L'utilizzo dell'approccio "concurrent engineering" nello sviluppo di un mono-cilindrico prodotto mediante colata in bassa pressione. Il processo di colata, il processo di solidificazione, così come le proprietà microstrutturali e meccaniche allo stato as-cast e dopo trattamento termico, sono state analizzate e ottimizzate per mezzo di un software di simulazione numerica. L'attendibilità e l'affidabilità di tali risultati sono state quindi valutate comparando questi valori con quelli ottenuti dall'indagine sperimentale.

PART 1

INTRODUCTION

INTRODUCTION

The increasing attention to environment has led, in automotive industry, to a continuous growing in the use of aluminium castings in replace of ferrous castings. A reduction in the weight of passenger car decreases fuel consumption and, thus, emissions.

Due to the excellent combination among castability, mechanical and technological properties, cast Al-Si alloys are widely used in the production of automotive components.

The final mechanical properties of such alloys depend essentially on microstructure. In general, the microstructure consists in primary α-Al or Si- phases in an eutectic mixture of Al-Si. Secondary phases and intermetallic particles can be usually observed.

The size, the morphology and the distribution of these phases are influenced by the interaction between alloy composition, casting and heat treatment processes. In addition, casting process and process parameters determine the amount of defects that can be detected in the component and, consequently, the strengthening properties.

The possibility of analyzing such complex interactions and traduce them into models and correlation play a key role in industrial field to obtain components with well-knows potential and improved quality.

The following diagram summarizes how alloy composition, process (casting and heat treatment) and defect contribute to determine the microstructure and mechanical properties of casting.

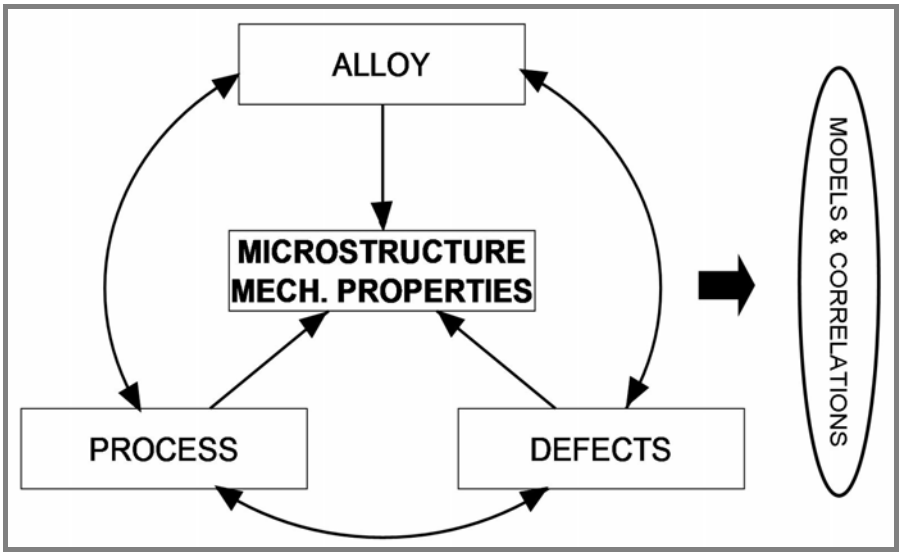

Figure 1(a). Schematic representation of the interaction between alloy/process/defect and casting microstructure and mechanical properties.

In Figure 1(b), the reference to the publication where the matter has been in detail analyzed is also reported. The nomenclature refers to that present in Preface.

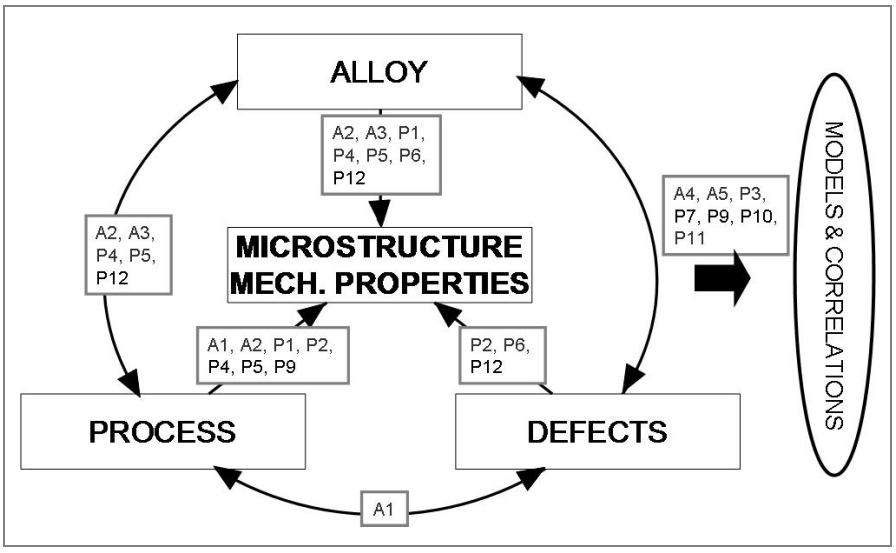

Figure 1(b). Reference to the code of publication where the interaction between alloy/process/defect and casting microstructure and mechanical properties is discussed.

The objective of this doctoral thesis is to develop new knowledge on the influence of alloy composition, processing and process parameters on the microstructural features and mechanical properties of aluminium alloy castings. Special attention has been given to:

- *Effect of α-Al and Si-eutectic particles on fracture mode;* interacting with dislocation movement, α-Al and Si-eutectic particles with their size and morphology determine the fracture mode and the final mechanical behaviour of the alloy.
- *Effect of composition on microstructure and mechanical properties;* the addition of alloying elements influences the solidification dynamics and, thus, microstructural features. In turn, mechanical properties result also affected.

- *The gravity, low-pressure and high-pressure die casting processes*; the essential feature of die casting is the use of permanent metal moulds, into which the molten alloy is either poured directly or injected under pressure, giving rise to the separate processes of gravity, low- and high-pressure die casting. Permanent moulds offer obvious advantages in terms of simplicity of production for large quantities of parts, but are subject to limitations yet to be discussed.

- *Effect of heat treatment of final mechanical properties;* due to the precipitation of secondary phase, heat treatment allows to improve the strengthening of the alloy. The possibility to predict the final Yield Stress applying a reliable model reduces the time required to setting up the process parameters.

- *Use of simulation code in design stage;* the use of simulation in design, especially within simultaneous engineering, allows to improve the overall quality of the final component reducing time and costs for its development.

The activities were mainly carried out as part of NADIA European Project - New Automotive components Designed for and manufactured by Intelligent processing of light Alloys. NADIA includes 27 Partners, and covers, into 8 WPs, the full design & production chain for automotive: materials producers & equipment

suppliers, engineering & design companies, foundries, component & car manufacturers, linked with RTD centers & Universities, focussed on materials, processing, engineering, application.
NADIA provides an integrated combination of materials, processes and the new NM^2 simultaneous engineering tools for the production of automotive demonstrators. The aim of the project is a full exploit of the potential of light multifunctional alloys for car and truck components and systems through advances in nano & micro technologies. A schematic illustration of the project structure is shown in the following Figure.

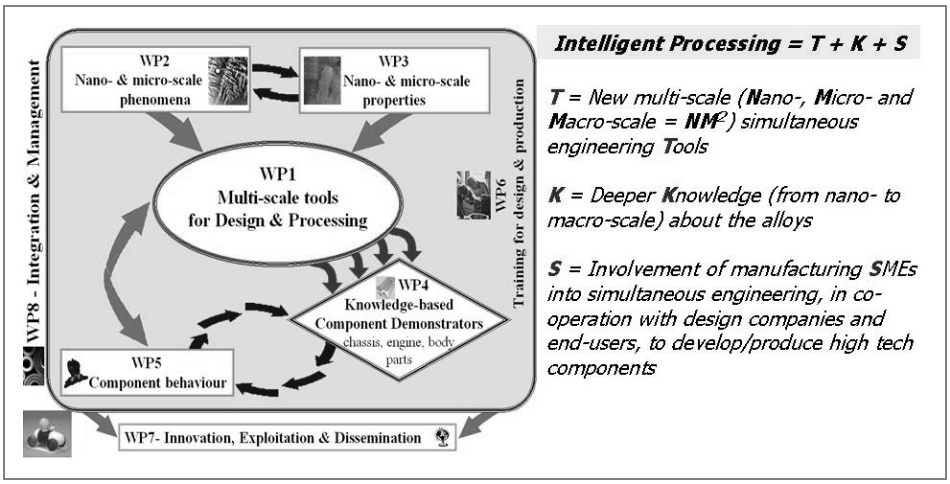

Figure 2. General NADIA structure.

1. INTRODUCTION TO Al-Si FOUNDRY ALLOYS

Aluminium casting is dominated by the automotive industry.[1,2] Roughly two thirds of all aluminium castings are automotive where the use of aluminium castings continues to grow at the expense of iron castings.[3] Although aluminium castings are significantly more expensive than ferrous castings, there is a continuing market requirement to reduce vehicle weight and to increase fuel efficiency.[1-3] In fact, the fuel consumption of a vehicle in the driving cycle and, thus the emission of CO_2 to the atmosphere, are directly related to its mass. Figure 3 (Source: Ricardo Engineering) shows the correlation between vehicle mass and the average fuel consumption for two types of engines (Gasoline and Diesel) for European passenger cars. It appears clearly that lightweight technologies, like aluminium cylinder blocks, offer a potential for fuel consumption and CO_2 emission reduction (Figure 3 (b); Source: Cahill et al, Technology Map, DG Research, EUR 19031 EN (1999)]) and how theses are the requirements which drives the replacement of ferrous parts by aluminium.

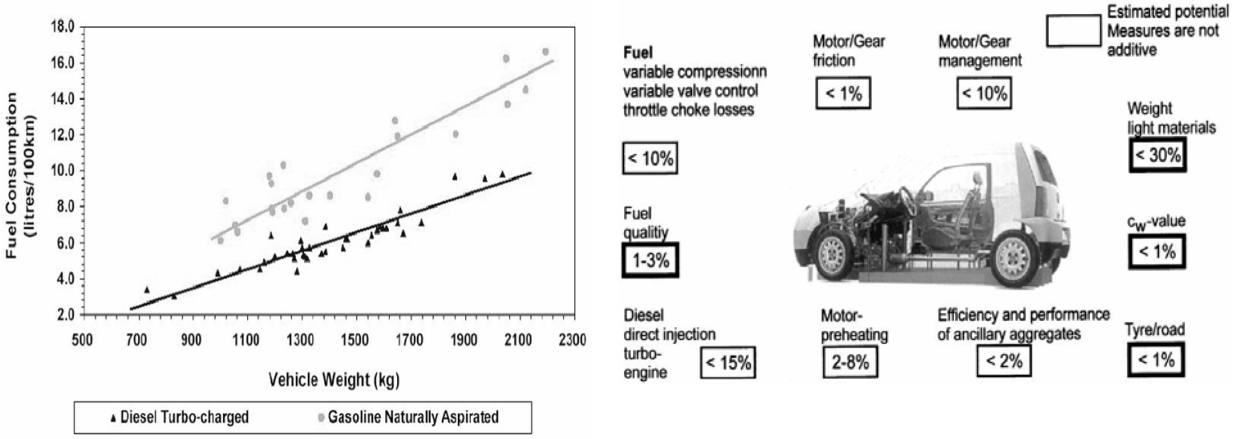

(a) (b)

Figure 3. (a) Linear relationship between fuel consumption and vehicle weight; (b) Effect of technical actions on reducing CO2 emissions

Al-Si alloy are certainly the main alloy system used for industrial production. About 90% of the total cast parts are produced with these alloys.[4]

The outstanding effect of silicon is the improvement of casting characteristics such as fluidity, hot tear resistance, and feeding reducing the volume contraction of the alloy during solidification. Silicon additions are also accompanied by a reduction in specific gravity and coefficient of thermal expansion.[4,5] Commercial alloys span the hypoeutectic and hypereutectic ranges up to about 25% Si.

In Figure 4 the phase diagram Al-Si is presented. *Hypoeutectic alloys* show Si content up to ~11%. For these alloys the solidification starts with the precipitation of primary α-Al phase. When the eutectic temperature is reached, an eutectic mixture of Al and Si form. They are mainly used in slow cooling rate processes, such us sand or gravity casting, and for applications where high strength properties are required.

The alloys with a Si content ranging from 11% to 13% are named as *eutectic alloys*. These alloys, having a short freezing range, show high fluidity[6] and a low susceptibility to shrinkage porosity[5]. Consequently, they are used for the production of casting with very thin wall thickness, especially by means of high pressure die casting process.

When Si content exceeds 13% and increases up to 25%, *hypereutectic alloys* form. In these alloys the microstructure is characterized by the precipitation of primary Si crystal and the eutectic mixture. Due to the high hardness of silicon-rich phase they are used in application where an improved wear resistance is required. On other hand, they show low ductility and are difficult to machine.

The size and the morphology of primary phases and eutectic mixture depend on the casting process and on the addition of modifier or refiner element. For example, the rapid solidification in HPDC leads to a microstructure with a fine eutectic structure, small dendritic cells and low arm spacing distance along with a reduction in grain size[4,7]. Vice-versa, in sand and permanent mould casting, the low solidification rate requires the addition of modifier elements, such us sodium or strontium, to obtain small and round eutectic Si particles. In hypereutectic alloys, phosphorus is added to control the primary silicon while in hypoeutectic alloy titanium and boron are usually added to promote α-Al nucleation and produce a fine equiaxed grain structure[5].

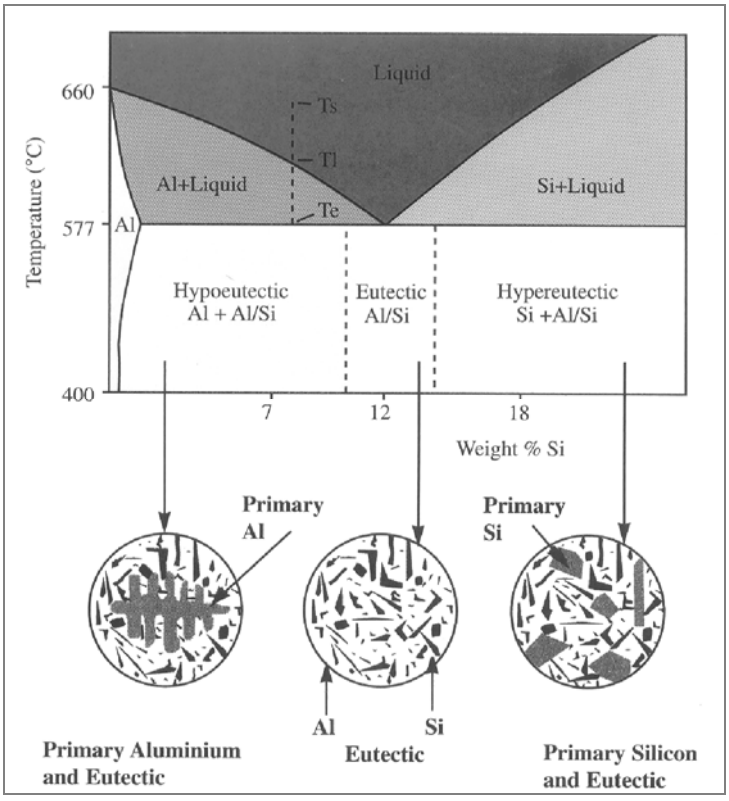

Figure 4. Al-Si equilibrium diagram

A further important classification of Al-Si alloys is between primary and secondary alloys. The *primary Al-Si alloys* are based on the electrolytically refined aluminium. Alloying elements such us silicon, magnesium or copper, are in turn separately refined and subsequently added into alloy. Since the purity of electrolytic aluminium is high, the impurity contents in these alloys lay at low level[8]. The level of impurity is much higher is *secondary alloys* as consequence of their production methods based on the remelting of scrap. The desired composition is achieved by a careful selection of scrap material as well as by molten metal treatments[8].

2. EFFECT OF ALLOYING ELEMENTS

Apart from the small amount of coexisting elements in Al-Si alloy, some elements are intentionally added into the Al-Si melt to a significant quantity so that the alloy's sensitivity to heat treatment and microstructure is changed[9]. Thus, alloying has become an effective method to improve the mechanical properties of Al-Si alloy.

In Al-Si-Mg alloys *the addition of copper* improves strength and hardness both in the as-cast and heat-treated temper, as shown in Figure 5(a).[10-13] As Samuel *et al.* reported that, during solidification, Al_2Cu can precipitate in due distinct forms in function of solidification rate. For high solidification rate, Al_2Cu phase occurs mainly in the form of fine eutectic $Al+Al_2Cu$. In turn, as the cooling rate decreases, the formation of blocky like coarse Al_2Cu precipitates prevails.[13]
Besides the $\theta(Al_2Cu)$ phases, the improvement in strengthening after heat treatment is due to the precipitation of some other precipitate phases, such us $W(AlxCu_4Mg_5Si_4)$, $S(Al_2CuMg)$ and $Q(Al_5Cu_2Mg_8Si_6)$ phases.[10,14]
As Heusler *et al.*[15] stated that, the introduction of Cu into Al–Si alloys also results in an eutectic modification; however an addition exceeding 1.2 wt.% Cu leads to regions with coarser eutectic suggesting a certain overmodification, as displayed in Figure 5(b) and described in **Article 2**.
In addition, Cu promotes the formation of shrinkage cavities and micro-porosity affecting the ductility of the alloy[16,17] as consequence of the increase in solidification interval along with a reduction of castability. Finally, resistance to general corrosion and, in specific compositions and material conditions, stress-corrosion susceptibility are also decreased.[4]

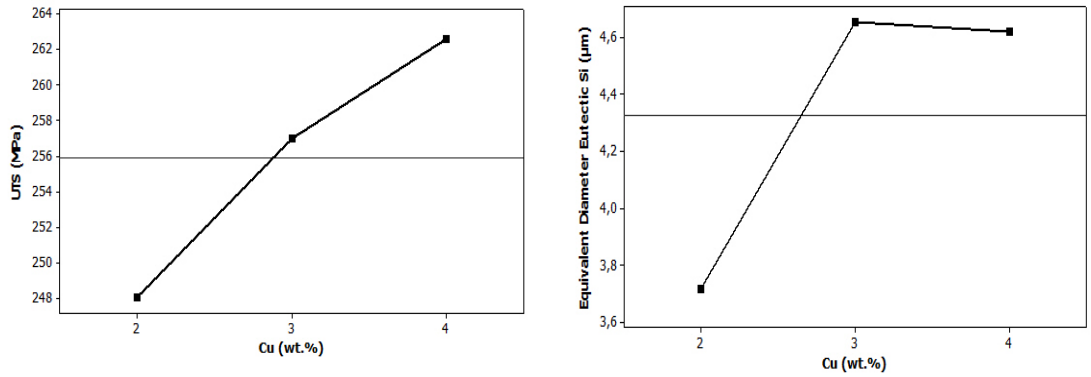

(a) (b)

Figure 5. Effect of Cu addition in (a) UTS and (b) dimension of eutectic Si particles.
[Article 2]

Generally present in Al-Si alloys in a content ranging from 0.2% to 0.4%, *magnesium* allows to improve the strengthening[18,19] of Si alloys containing copper, nickel, and other elements for the same purpose.[4] The hardening-phase β-Mg_2Si displays a useful solubility limit corresponding to approximately 0.70% Mg, beyond which either no further strengthening occurs or matrix softening takes place. However, the presence of magnesium increases the oxidation losses of liquid aluminium.

Iron is generally considered as impurity except for some high pressure die cast alloy where a content up to 1% prevents die soldering phenomena.

The effect of iron can be observed in a reduction of ductility[20,21], shock resistance and machinability. Iron-bearing phase can assume different morphology and shape in dependence of cooling rate (Figure 6) and alloy composition [22-24].

At lower iron level up to 0.8% and without addition of "neutralizer" element and for low solidification rate, the iron precipitates in form of β-Al_5FeSi needles precipitates. These needles are very hard and brittle and have relatively low bond strength to the matrix. In addition, the acicular morphology promotes the fracture mechanism increasing the tension field around particles. *Manganese* is often added in order to convert their morphology reducing the embrittlement and to alter the shape from sharp needles to a more compact type α-$Al_{15}(Fe,Mn)_3Si_2$.[4,24]

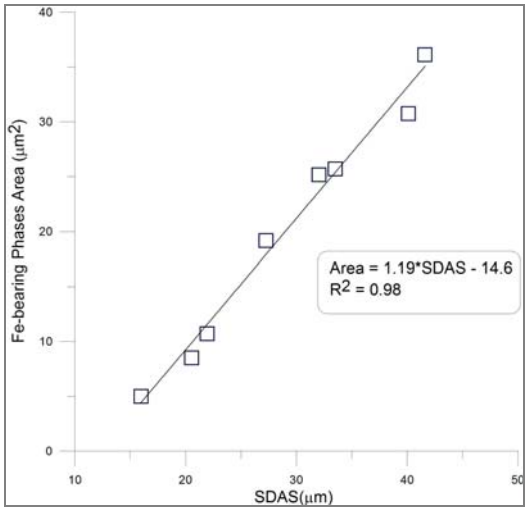

Figure 6. Effect of solidification time, in term of SDAS, on the dimension of Fe-bearing phase in A356 alloy **[Article 5]**.

Titanium and *boron* are typically added into aluminium alloy for their grain refinement action. Typically, titanium amount ranges from 0.02 to 0.15% while if the mixture Ti-B is used the content varies from 0.01-0.03% for Ti and 0.01% for B.[5]
Guzowaski[5,25] suggested that the intermetallic phase $TiAl_3$ acts as nucleant for α-Al by means peritectic reaction:

Liquid+ $TiAl_3 \rightarrow$ α-Al (solid)

When boron is present in master alloy, boride particles, TiB_2 and (Al, Ti)B_2, cover the surface of $TiAl_3$ improving the refining process. However, Mohanty and Gruzeleski[26] have recently proposed an alternative mechanism in which TiB_2 alone does not nucleate α-Al, but promotes the formation of a ternary aluminide (Al-Ti-Si) phase, acting as a nucleant for the α-phase.
Grain refinement influences positively some properties of alloys; it reduces hot tearing tendency, porosity and shrinkage distribution; at the same time, it improves distribution of intermetallic particles (especially in alloy with high content of Cu), and mechanical properties as well. However, the improvement in tensile strength and elongation is due to a better distribution of porosity or intermetallic phases rather than a reduction of grain size.[25]
In **Article 2** the influence of Ti addition on Si eutectic is also reported. By increasing Ti content, coarser Si particles were observed. However, these results seem to be in

contrast with the work of Grab *et al.*[27] where the presence TiB_2 particles reduces the size and changes the morphology of eutectic Si particles.

Strontium and *sodium*, influencing the growing kinetic of eutectic silicon, are added to modify the Al-Si eutectic structure. Modification treatment will be described in next paragraph.

The addition of *lead* at levels over 0.1% improves machinability.

Phosphorous is usually added in hypereutectic alloys. At temperature above 800°C, particles AlP can form promoting the heterogeneous nucleation of primary Si crystals.[5,28] A refined microstructure with small and homogeneously distributed Si crystal can be obtained resulting in improved wear properties. However, special attention has to be paid on the interaction between phosphorus and modifier elements. Due to their high affinity, strontium or sodium phosphate form more easily than aluminum phosphate. Consequently, modification and Si refinement result decreased. To overcome this effect, a strict control of temperature of element addition is necessary.

3. OVERVIEW OF CASTING PROCESS

Aluminium alloys are suitable to be cast by means all foundry conventional processes. These processes are high pressure die casting (HPDC), permanent mold casting (PMDC), sand casting, low pressure die casting (LPDC), plaster casting and investment casting. Other processes such as lost foam, semi-solid and squeeze casting are also developed as an evolution of existing techniques.[29]
The selection of the process is affected by several factors related to component features (dimension, weight, presence of internal cavities), to required mechanical properties and overall quality and, finally, to economic aspects (production volume and costs). A description of the more relevant processes is reported below.

Sand Casting

Sand casting consists in pouring a molten metal into a mould produced by shaping a suitable refractory. The mould cavity has to retain its shape until the complete solidification of casting and then, it can be removed. In making moulds and cores, various agents can be used for bonding the sand. The agent most often used is a mixture of clay and water. Sand bonded with oils or resins, which is very strong after baking, is used mostly for cores. Water glass (sodium silicate) hardened with CO_2 is used extensively as a bonding agent for both moulds and cores.[30].
This process allows to produce components without any limitation in component shapes and size or alloys. In addition, the cost of minimum equipment for the production of a small number of castings is low. In general, the annual production volume ranges from 1 to 100 parts/years.
The disadvantages are low dimensional accuracy and poor surface finish along with a coarse microstructure due to a low cooling rate. The use of metal internal chills is necessary in zones of casting where improved mechanical properties are required. With this aim, adequate treatments of liquid metal with the addition of modifier or refiner elements have to taken into account.
Typical component produced from this process are crankcases, gear housings, automobile transmission cases, cylinder blocks, cylinder head, truck and bus frame components, levers, brackets.

Permanent mold casting

In permanent mould casting process, the molten metal is poured into a metallic die; the filling driving force is gravity. The low velocity of liquid metal along with the absence of an external pressure doesn't permit the manufacture of components with complex geometry or thin thickness.

On the other hand, this type of process allows the production of parts with good surface finishing and good mechanical properties at quite high production rate and low equipment costs.

By controlling the metallostatic pressure, a laminar filling flow of molten metal can be observed and the soundness of casting may be assured. The good integrity of casting is achievable also by avoiding the formation of shrinkage porosity controlling the gradient of solidification and using feeders, as well. To control the solidification, special methods of cooling system are used, including water jacket or air cooled fins. The internal quality of casting is reached also by the use of filters that, placed in the gating system, prevents the inclusion of oxides or external particles decreasing the mechanical properties of casting.

To produce casting with internal cavity, cores made in metal or sand are placed into the mould prior the casting. The use of sand is possible thank to the low velocity of liquid metal and, in this case, the process is called "semi-permanent" die casting.

In order to extend the life of the permanent mould, the surfaces of the die are coated with a refractory slurry or sprayed with graphite every few casting. These coatings also allow to control the gradient of solidification, acting as thermal barrier. In addition, they make the extraction of casting at the end of solidification. These operations are served by mechanical ejectors present in various parts of the dies.

The high cooling rate achievable during solidification allows to obtained a refined microstructure, with low values of SDAS and fine eutectic Si particles.

In Figure 7, the geometry of step casting used in **Article 3** and **Article 4** and typical components obtained by permanent mould die casting are shown.

(a) (b)

Figure 7. (a) Geometry of PMDC step casting used in **Article 3** and **Article 4** and (b) typical PMDC components.

Low pressure die casting

Among the casting processes for aluminium alloys, low pressure die casting is certainly worth mentioning, thanks to its peculiarities, allowing, in several cases, an excellent compromise between quality, costs, productivity, geometrical feasibility.

In this process, the permanent die and the filling system are placed over the furnace containing the molten alloy. The filling of the cavity is obtained by forcing (by means of a pressurized gas, typically ranging from 0.3 to 1.5 bars) the molten metal to rise into a ceramic tube (which is called stalk), which connects the die to the

furnace. Once the alloy in the die cavity is solidified, the overpressure in the furnace is removed, and the residual molten metal in the tube flows again towards the furnace. The various parts of the die are then separated, and the casting is finally extracted. The peculiarity of LPDC is that the massive region of the casting has to be the last one to solidify and must be placed near to the stalk, which acts as a "virtual" feeder and allows to avoid the use of conventional feeders, improving the yield of the process, which becomes significantly high. The low injection velocity and the relatively high cycle time lead to a good control of the fluid-dynamics of the process, avoiding the defects originated by turbulence phenomena. Castings up to 70 kg weight can be produced, with tolerances of 0.3-0.6 %.
The process is particularly suitable to the production of symmetrical castings, such as automotive wheels, or castings of high quality, such as critical aerospace castings, electric motor housing, suspension brackets, etc. Some examples of low pressure die casting products are collected in Figure 8.

Figure 8. Examples of castings produced by means of the LPDC process.

High pressure die casting

Generally, this technique is used for the production of small component weighing up to about 5 kg but castings weighing as much as 20 kg, *i.e.* engine block, are also produced. The main advantage of this casting process is the high production rate, typically 40 parts/hours for a component of 5Kg. In addition, very complex geometries can be achieved with close tolerances, good surface finishes and very thin wall thickness, up to 1.0 mm.
In high pressure die casting, the molten metal is forced into the die cavity at pressure ranging from 0.7 to 700MPa.
The injection of molten metal can be subdivided in three stages. In the first phase, the piston has a low speed motion, typically 0.25m/s and lead to a preliminary filling of the die. The velocity has to be set up in order to avoid turbulence of liquid metal as well as wave phenomena. When molten metal arrives to in-gates, the first phase ends. In the second phase the filling of the cavity take place. Due to the complex geometry and very thin walls of the castings, the filling has to be as fast as possible. As consequence high velocity and high pressure are required. In Figure 9 a schematic view of typical injection-control stages during high-pressure die casting is proposed.

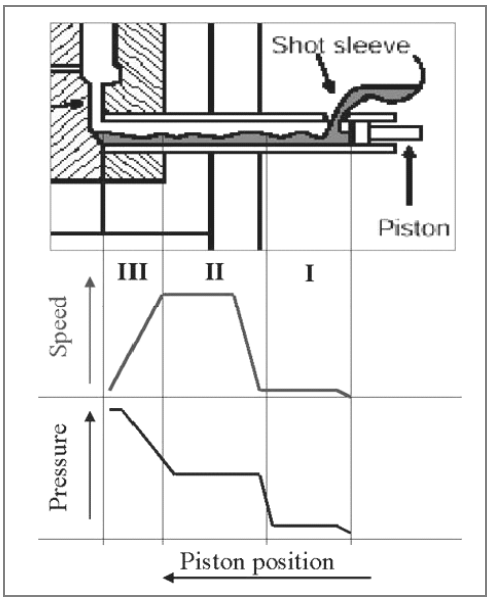

Figure 9. A schematic view of typical injection-control stages during high-pressure die casting.[29]

As consequence of high velocity of metal during filling metal cores have to be used and they are restricted to simple shapes that permit straight-line removal.
The rapid injection along with a high solidification rate due to good thermal contact between metal and water-cooled die allow to obtain a very fine microstructure. However, the turbulence due to the high filling rate inevitably causes the trapping of oxide and air promoting the formation of gas porosity and oxide inclusion. The presence of these defects decreases the mechanical properties of components, restricting the used of HPDC for application where high strength performances are not required.
The entrapped gases also make difficult the weld and heat treatment process. In the latter case, during solutioning the entrapped gases expand leading to a plastically deformation of component surface and diminishing its quality.
However, the development of several process such us vacuum die casting process, squeeze casting or semi-solid die casting has be made to overcome the problem of soundness in HPDC components.
Typical applications of HPDC aluminium alloys include gear cases, cylinder heads for air-cooled engines, cylinder blocks, cover plates, instrument cases, parts requiring corrosion resistance, escalator parts, conveyor components, aircraft and marine hardware and fittings

4. EUTECTIC NUCLEATION AND GROWTH IN UN-MODIFIED AND MODIFIED Al-Si ALLOYS.

In Al-Si alloys, the microstructure consists in a primary phase, aluminium or silicon, and a eutectic mixture of these two elements.
Eutectic phase has a primarily importance in the determination of overall properties[5] of alloy and a full comprehension of the nucleation and growing is necessary.
In un-modified alloys, the eutectic silicon crystals have plate or faceted morphology growing along definite crystallographic direction.[31]
Modification is a treatment of liquid Al-Si alloy in which a modifier element is added in order change the condition of solidification and influence the nucleation and growing mechanisms of eutectic Si.[31-36] Common elements are strontium, sodium,

calcium and antimony. These promote the precipitation of a very fine and round particles with improvements in ductility, toughness and fatigue properties.[5] In Figure 10 and Figure 11 the comparison in dimension and roundness distribution of eutectic Si between a un-modifies and modified alloy can be noted. It was established that the size distribution of eutectic Si particles follows the lognormal distribution.[37] The probability density function of the three-parameters lognormal distribution can be written as:

$$f(d) = \frac{1}{(d-\tau)\sigma\sqrt{2\pi}} \exp\left[\frac{-(\ln(d-\tau)-\mu)^2}{2\sigma^2}\right] \quad (1)$$

where d is the diameter of Si particles, τ the threshold, σ the shape and μ is the scale parameter.

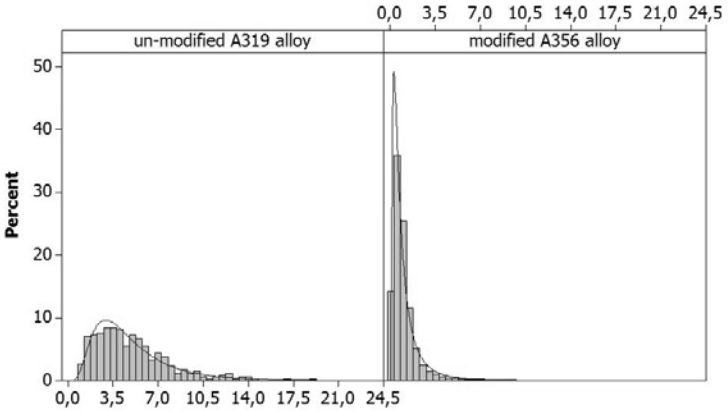

Figure 10. Comparison in Si- equivalent diameter distribution between an unmodified A319 and a modified A356 alloys **[Article 2 and Article 3]**.

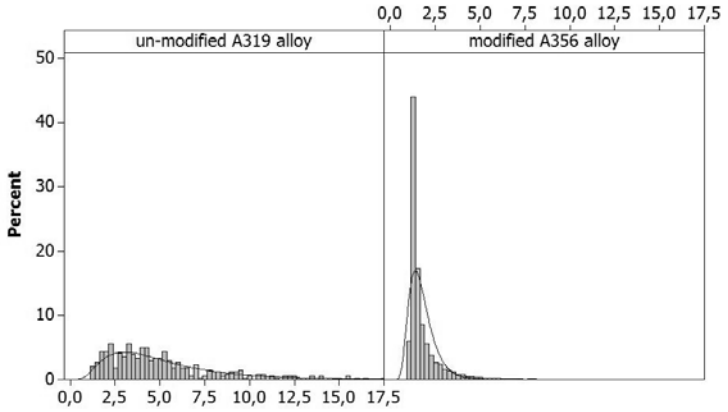

Figure 11. Comparison in Si- roundness distribution between an unmodified A319 and a modified A356 alloys **[Article 2 and Article 3]**.

Many theories were proposed to explain the mechanism of nucleation and growing both for un-modified and modified alloys.

For nucleation in un-modified alloys, Chadwick[39] and Elliot[40] suggested that due to the high disregistry between the Si particles and the Al matrix, Si nucleates in the liquid ahead of the interface Si-Al, where the Si content of the liquid is at its highest. After being nucleated, the Si particles are taken into growing Al phase after which both phases grow co-operatively.

Dahle *et al.*[41] reported that for un-modified alloys eutectic nucleates and grows from the primary α-Al particles, with the same orientation between Al eutectic phase and primary Al and a different orientation for Si. Vice-versa in modified alloy nucleation of independent eutectic grains takes place within interdendritic regions with no relation to the primary dendrites.
On other hand, Khalifa *et al.*[42] and Shankar *et al.*[43] suggested that β-iron or, in general, trace elements form impurity particles acting as nucleation site for eutectic Si.
On the same concept, Nogita *et al.*[44] proposed a model for eutectic nucleation based on the presence of AlP particles in the interface dendrite-liquid interface acting as nucleants for silicon crystals, and eutectic solidification begins from each growing crystals.
Finally, Nafisi *et al.*[45] suggested that the eutectic reaction starts with the nucleation of Al-rich spikes on the primary Al dendrites leading to localized Si enrichment within interdendritic liquid and eventual segregation of numerous small silicon particles. These particles act as nucleation sites for the eutectic Si. Based on this theory, in **Article [2]** the influence of Titanium on size of eutectic Si particles was explained.
For growing, *Twin Plane Re-entrant edge (TPRE)*[46, 47], based on the presence of re-entrant corner seems to a effective mechanism. On other hand, Hellawell *et al*[48,49] suggested *Layer Growth Mechanism* as growing mechanism of silicon. In this theory the presence of interface containing ledges promotes an easily join of liquid atoms to the solid without increasing the interfacial energy.

The most common and recent theories for modification are based on "restrict growing". Among these theories, it is worthy mentioning *Surface Energy Theory* (Thall and Chalmers, 1949[46,50]) and *Impurity Induced Twinning Theory* (Lu and Hellawell, 1987[46,49]).
In *Surface Energy Theory* the decrease in surface energy of the aluminum-silicon solid interface due to the addition of the chemical modifier suppresses growth of the silicon crystal and causes modification of the eutectic structure and under-cooling.
In *Impurity Induced Twinning Theory*, Lu and Hellawell proposed that modifier elements act as "poison" of growing mechanism of atomic silicon layers. Atoms of Sr or Na are adsorbed onto growing Si surface preventing the attachment of further silicon atoms to the crystal. Thus, the adsorbed impurity atoms induce twinning by altering the stacking sequence of atomic layers as the newly added layers seek to grow around the adsorbed impurity atom.

5. EFFECT OF SOLIDIFICATION RATE ON MICROSTRUCTURE

In general, it can be stated that a general coarsening of microstructure occurs when solidification rate decreases for the effect of an high thick of the section or a poor heat exchange between liquid metal and die as shown in Figure 12 (a) and (b) for PMDC and HPDC castings, respectively.
In detail, differences in solidification rate reflect upon dimension and distribution of α -Al phase as well as morphology and distribution of eutectic Si particles.

The amount of α-Al phase decreases as the solidification rate decreases. Changes in α-Al phase morphology can be also noted. In presence of rapid solidification, for example in HPDC, it shows mainly an equiaxed globular-geometry. The α-Al cells are little branching due to an increased undercooling governing the entire solidification process and due to the shift in the equilibrium diagram to lower temperatures.[51] Thus, the dimensions of α-Al globules increases for

lower solidification rates (typically PMDC and sand casting) and dendrite morphology can be observed. Generally, the relation between solidification time and SDAS is quantified using the following Equation 2[52]:

$$SDAS=k*t_s^{\,n} \quad (2)$$

where k and n depend on the alloy and casting process.

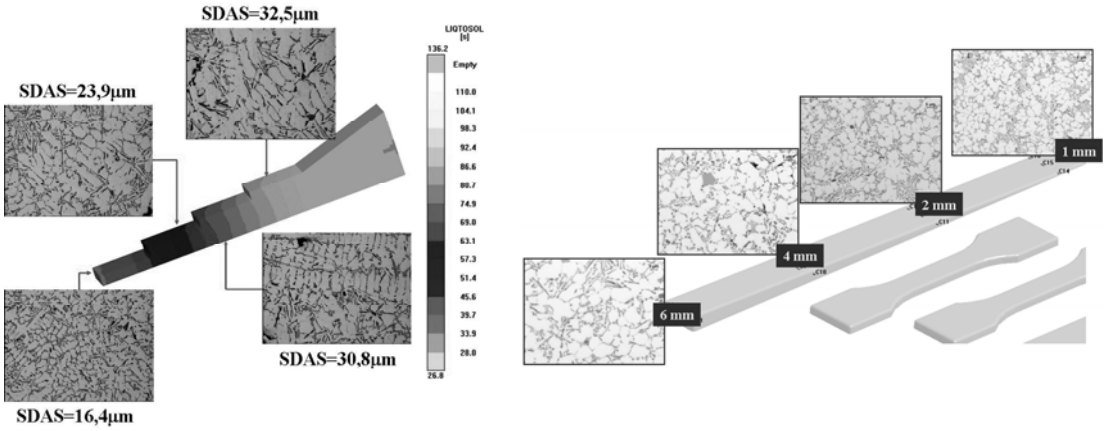

Figure 12. Microstructural comparison between PMDC **[Article [3]]** and HPDC castings **[Publications [P5]-[P6]]**.

In addition to α-Al phase feature, solidification rate also affects the size and morphology of eutectic Si particles acting as modifier. It can be established that by reducing the cooling rate, the microstructure is characterised by coarse eutectic Si particles while the formation of fine eutectic Si is predominant in case of rapid solidification. In Figure 13 it can be noted the influence of different solidification rate on the distribution of eutectic Si equivalent diameter for a HPDC and PMDC secondary EN-AC46000 alloy. For the same section thickness (~20mm), the much higher cooling rate in HPDC compared to PMDC allows to obtain a more uniform distribution of finer eutectic Si. Based on the theory of *"Surface energy"* of the aluminum-silicon solid interface, Thall and Chalmers[46,50] suggested that the rate of advance of the interface depends on a balance between the rate of heat flow from the liquid to the solid through the interface and the latent heat of fusion released during solidification. Due to the high difference in thermal conductivity and latent heat of fusion between aluminum and silicon, aluminum will solidify much faster than silicon. As the cooling rate increases, the lead of aluminum over silicon increases promoting a complete encasement of the lagging silicon crystal by the advancing aluminium.

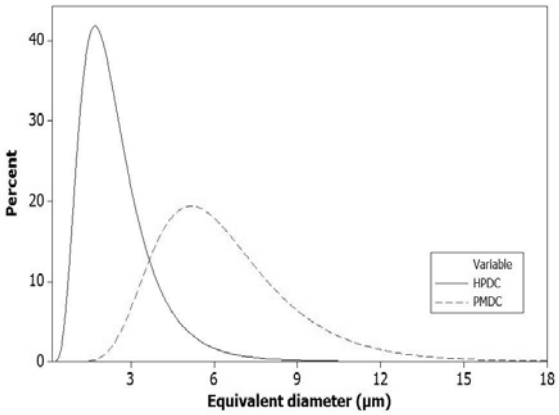

Figure 13. Influence of different solidification rate on the distribution of eutectic Si equivalent diameter for a secondary EN-AC46000 alloy.

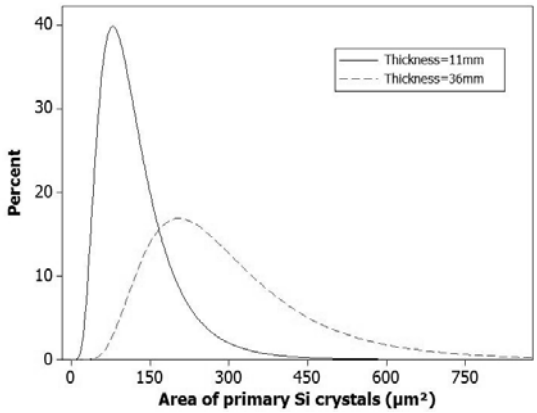

In Figure 14. Influence of solidification rate on the area distribution of primary Si crystals for a LPDC AlSi17Cu4 hypereutectic alloy.

In hypereutectic alloys, solidification rate affect also the dimension of primary Si crystals. As shown in Figure 14, by increasing the cooling rate the dimension of these particles decrease as consequence of the high undercooling, promoting the nucleation on diffusion. However, it has been demonstrated that cooling rate doesn't affect the morphology of Si crystal.

6. FRACTURE MODE AND MECHANICAL PROPERTIES

The main factors affecting the fracture mode of Al-Si foundry alloys are eutectic Si particle size and aspect ratio and the extent of particle clustering, the latter being related to the secondary dendrite arm spacing (SDAS).[53-56] In general, two general fracture modes can be observed:

- brittle fracture for as-cast temper alloy
- cellular fracture for modified or heat treated alloy

In un-modified Al-Si alloys, where the silicon forms a continuous network, the crack nucleates and propagates on the silicon cleavage planes or on other brittle intermetallic particles. [38,57] The cleavage cracks are mainly perpendicular to the macroscopic principal strain, regardless of the particle orientation. Platelet particles with their length perpendicular to the tensile direction break because of cleavage along their length. [58,59] Therefore, it is easy to hypothesize that the fracture mechanism depends on the size and shape of Si or Fe-rich brittle phases. Large and acicular particles are deleterious for mechanical properties reducing elongation to fracture and ultimate tensile strength **[Article 1-4]**. Figure 15 plots UTS and elongation to fracture as function of the product of SDAS, equivalent diameter and aspect ratio of eutectic Si particles for a PMDC and HPDC EN-AC46000 alloy. An increased value of this product reflects on a reduction of strength and ductility.

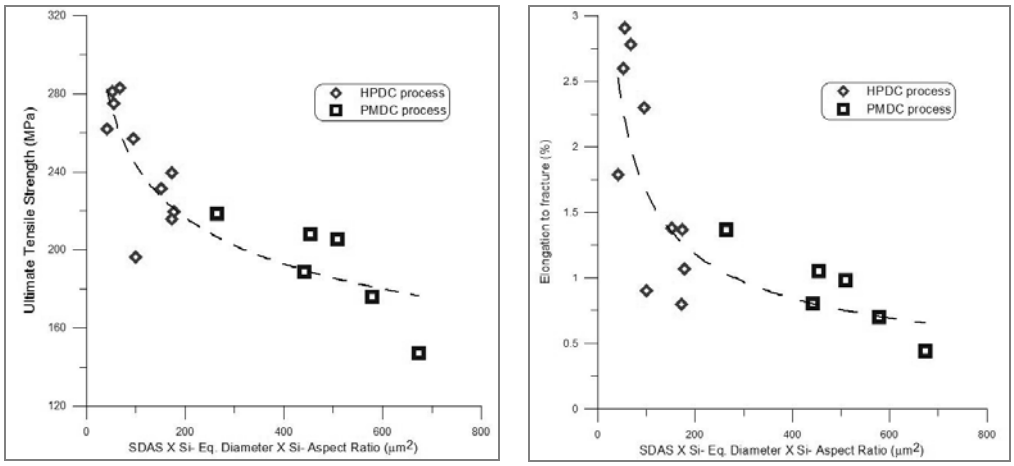

(a) (b)

Figure 15. Influence of microstructure (in terms of combined parameter SDAS x Si-Eq. Diameter x Si- Aspect ratio on (a) strength and (b) ductility of PMDC and HPDC EN-AC46000 alloy.

The microstructure also determines the mode of fracture propagation. As Caceres and Wang reported,[59] in material with large DAS, the final fracture occurs along the cell boundaries and the fracture mode is transgranular while in small DAS material, final fracture tends to concentrate along grain boundaries. The transition from transgranular to intergranular fracture mode occurs at a SDAS of about 30 μm in the un-modified alloys and 50 mm in the Sr-modified alloys and is accompanied by an increase in the ductility.

In modified Al-Si alloys the fracture presents mainly cellular morphology. The addition of modifier leads to precipitation of round or fibrous Si eutectic particles with a strong cohesion at the interface with α-Al. Thus, the brittle particles are surrounded with a relatively soft matrix and sometimes they are isolated. Consequently, under a local stress, the cells are formed around the silicon-cracked particles by plastic deformation of the matrix. [56]

Finally, in heat treated alloys, the typical ductile fracture can be observed. It occurs with the sequence of nucleation, by means growth and coalescence of voids. [56]

7. DEFECTS IN Al-Si ALLOYS

In general, cast Al-Si alloys are sensitive to the formation of defects that can strongly affect the final mechanical properties.[60-64]

Defects can form both during solidification, in form of gas or shrinkage porosity, or during filling in form of dross or oxide films. Some examples are shown in Figure 16 and 17.

In addition, hot tearing and crack can occur as consequence of differential stresses arising between regions of the castings, during solidification and subsequent cooling. The type and the amount of defect depend on the casting process. In sand and gravity casting process, the combined effect of low solidification rate and a laminar filling flow promotes shrinkage porosity rather than cold shot or oxide film. Contrarily, these latter defects are common in HPDC parts as consequence of the very high turbulence during filling.

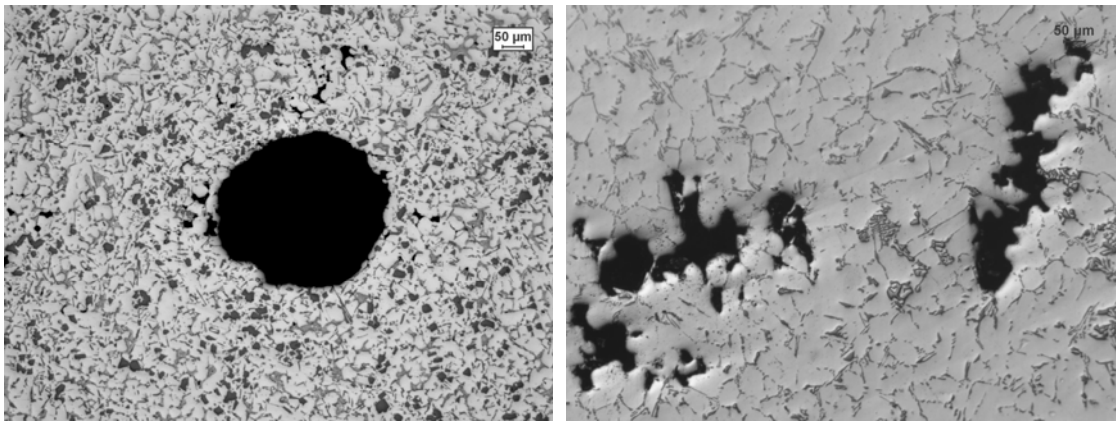

(a) (b)

Figure 16. (a) Gas and (b) shrinkage porosity in a LPDC AlSi17Cu4 and A356 alloys, respectively.

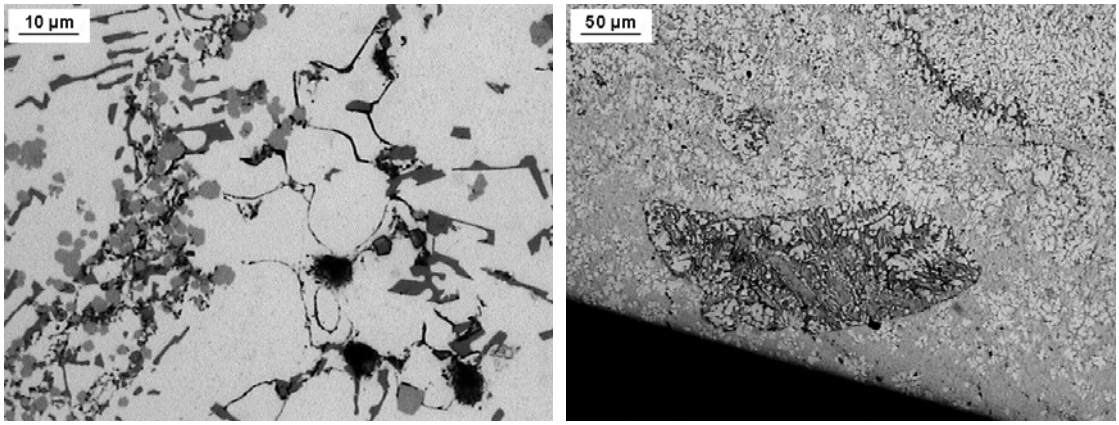

(a) (b)

Figure 17. (a) Oxide film, inclusion particles and (b) cold shot in a HPDC EN-AC 46000 alloy.

The effect of defect on mechanical properties can be noted in Figure 18. It reports the true stress-true strain curve for an AlSi7Cu2 PMDC sample with two different amounts of defects.

The presence of defects, measured to be 16% of fracture area covered, causes a strong reduction of UTS and ductility.

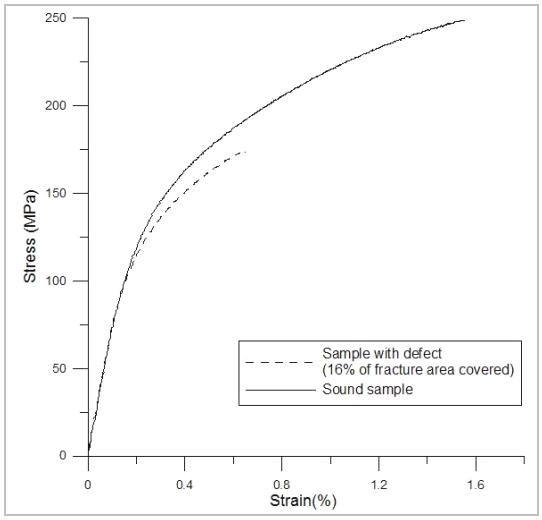

Figure 18. Effect of defects on mechanical properties of an AlSi7Cu2 PMDC sample.

Cáceres *et al.*[64] and Gokhale *et al.*[65] reported that the mechanical properties decrease monotonically with an increase in the area fraction of defects revealed on the fracture surface of gravity cast aluminium specimens. Fatigue properties are also affected by defect, reducing the initiation period of crack as well as its propagation. Thus, castings with defects have at least an order of magnitude lower fatigue life compared to defect free materials. Finally, porosity is more detrimental to fatigue life than oxide films.
In order to overcome the formation of defect attention has to be paid on gating system, as suggested by Campbell[6] and Dai *et al.*[66] , and on process parameters. Timelli *et. al.*[60] demonstrated, by means of quality mapping approach for HPDC component, how the amount and type of defects and, thus, the mechanical properties are distributed in a casting by changing the process parameters.

8. HEAT TREATMENT

8.1 Theoretical background

The use of aluminium alloy in application where high mechanical properties are required is related to the possibility to perform the heat treatment. In particular, in automotive application, such as engine bock, cylinder head or wheels, Mg and Cu are added in Al-Si alloy leading to a uniform precipitation of fine and coherent or semi-coherent Al_2Cu, Mg_2Si, Al_2CuMg and $Al_4CuMg_5Si_4$ secondary phases. Precipitates can impede the motion of dislocations increasing strength properties through a wide variety of mechanisms[67-69] among which the mainly are share and Orowan mechanisms. The improvement on mechanical properties due to heat treatment can be noted in Figure 19 where the comparison between true stress-true strain curves for an as-cast sample and T7 treated sample is provided. A detail description of the effect of heat treatment on overall microstructural and mechanical properties are reported in **Article [4]**.
The hardening process consists in three different steps: solutioning, quenching and age treatment, below described.

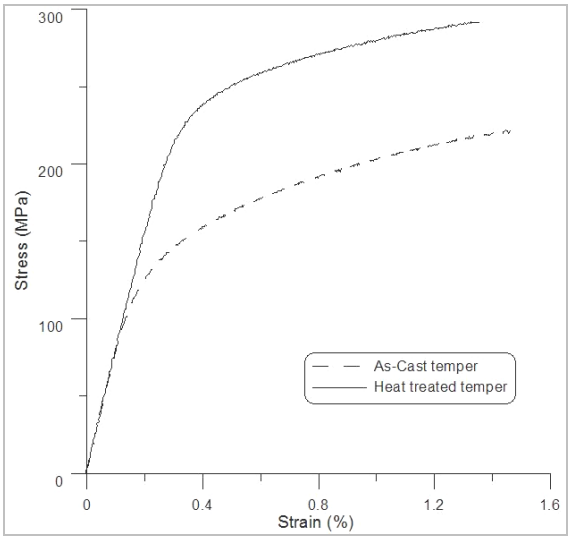

Figure 19. Comparison between as-cast and heat treated temper in terms of true stress-true strain curve for PMDC AlSi7Cu2 alloy. **[Article [2]]**

Solutioning

In Al-Si-Cu-Mg alloys, solution treatment allows to achieve a dissolution of Mg_2Si and Al_2Cu into the α-Al phase along with a microstructural homogenisation reducing segregations.

In addition, it is well known the influence of heat treatment on the morphology of eutectic Si particles, making them rounder. It has been reported that solution heat treatment changes the morphology of eutectic silicon from a polyhedral to a globular structure and that the kinetics of spheroidization and coarsening processes occur much more rapidly in a modified structure[70-71] as consequence of Rayleigh instability.[72] Silicon particles undergo necking and are broken down into fragments due to the instability of the interfaces between the two different phases and a reduction in the total interface energy, as shown in Figure 20 for a hypereutectic alloy. From the Figure can be also noted that no appreciable variation in size or roundness primary Si crystal occurs by increasing solutioning time.

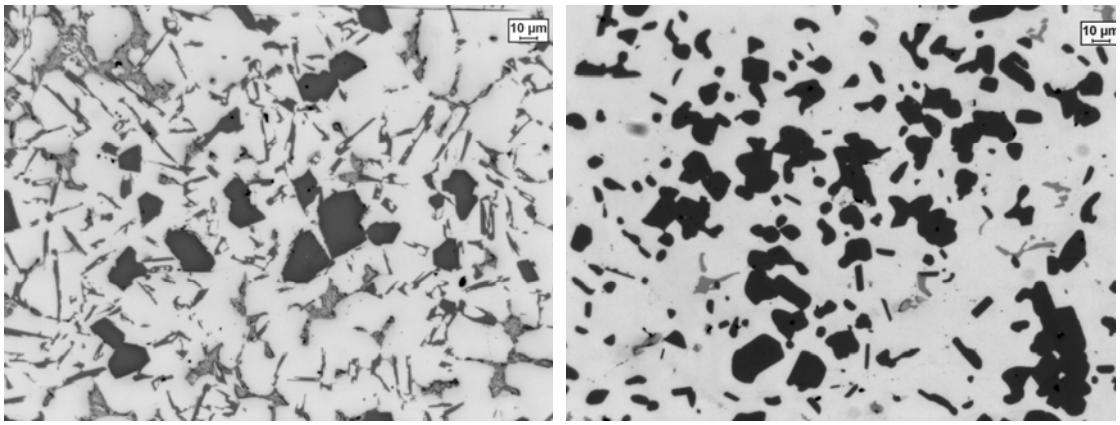

(As-Cast Microstructure) (Microstructure after 80h of solutioning)

Figure 20. Microstructure evolution in a AlSi17Cu4 hypereutectic alloy as consequence of 80h af solutioning.

Finally, modification in the morphology of Fe-rich phase (β-Fe phases undergo gradually necking and fragmentation) can be observed after long time of treatment, improving the ductility of the alloy.

However, a correct set up of time and temperature is necessary to preserve the quality of the casting. These parameters are function of alloy composition and casting process. For example, alloys containing Cu require a lower solutioning temperature (~500°C) in order to avoid the melting of low-melt phases at grain boundary. If temperature exceeds the eutectic temperature, de-cohesion between grain occur (Figure 21 with a reduction of the mechanical properties.

Another common defect due to un-correct time and/or temperature is named as "blistering". This is typical for component manufactured by means of HPDC process but it can be detected also in other casting processes. It arises in alloy containing a high content of internal as consequence of entrapped gases such as air, steam, hydrogen, or vapours formed by the decomposition of organic lubricants or binders. During treatment, the entrapped gases expand, resulting in unacceptable surface blistering and dimensional instability when the pressure inside the pores causes the skin of the component to plastically deform at elevated temperatures.

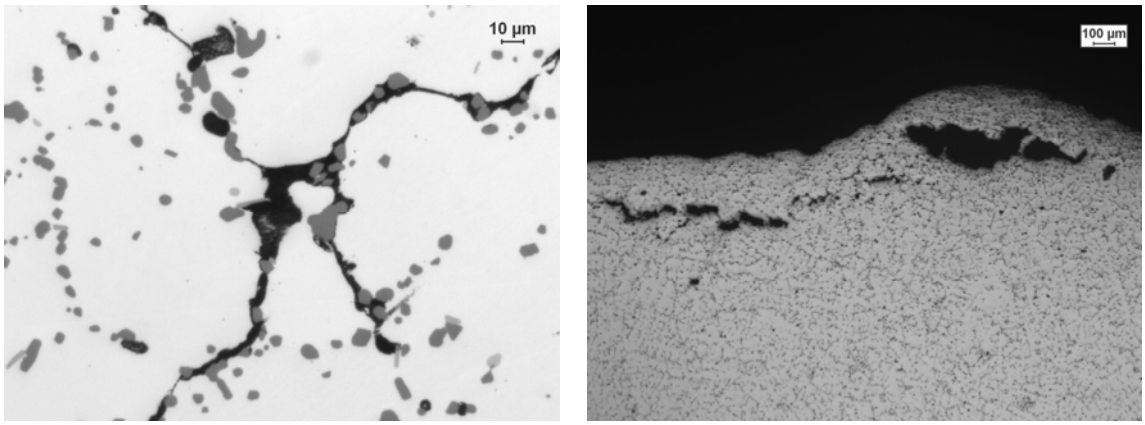

(a) (b)

Figure 21. Examples of defects due to incorrect solutioning treatment. (a) decohesion of grain and (b) blistering is sand casting.

Quenching

The amount of solute in α-Al matrix available for the precipitation during ageing depends upon quenching conditions. Quenching consists in a rapid cooling of casting (water at room temperature is the common quenching media adopted) with the aim to obtain an high degree of matrix saturation and, thus, a more efficient precipitation during ageing. In addition an increased number of vacancies occur at room temperature promoting the formation of GP-zones. However, high cooling rate lead to a high difference in local thermal gradients in sections of casting with different thickness and, thus, residual tensile stresses arise in the component. They can deform or, in the worst case, fracture the component. In general, they reduce the material mechanical performance, the stress corrosion resistance properties and promote the fatigue susceptibility as well as the onset of fractures due to wear phenomena. Polymers are often added in water at about 70°C. They delay the phase of nucleate bowling allowing better temperature uniformity in casting.

Ageing

The age-hardening mechanism is based on the formation of intermetallic compounds during decomposition of a metastable supersaturated solid solution obtained by solution treatment and quenching. A close control of time and temperature is necessary to obtain the desired properties.

For Al–Si–Cu–Mg alloys, besides the θ(Al_2Cu) and β(Mg_2Si) phases, some other precipitate phases exist such as W($Al_xCu_4Mg_5Si_4$) and S(Al_2CuMg) phases.[10] In Figure 22, experimental ageing curves for an AlSi7Cu2Mg alloy are illustrated. It can be noted that increasing ageing temperature the peak values decrease and they are reached in shorter time. In according to the results reported by Li *et al.*, above a temperature of 170°C these alloy show double aging peaks. The first peak is attained depending on the high density GP zones, while the second is acquired in terms of metastable particles. However, these results contrast those reported by Cloutier *et. al.* [14] where for the same alloy a conventional single peak was obtained.

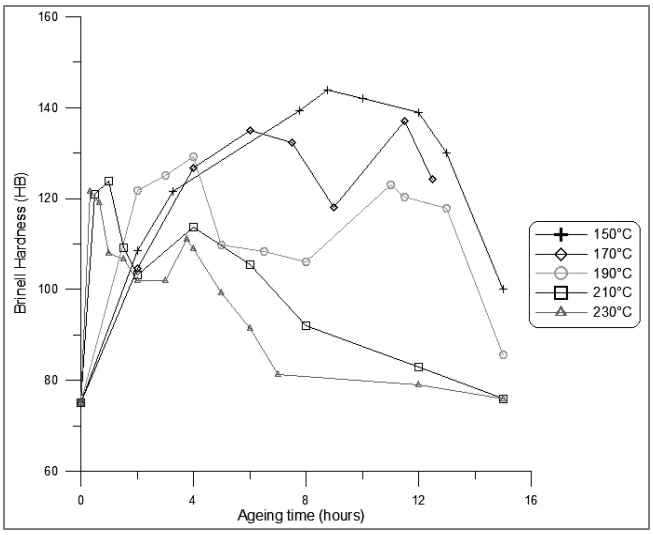

Figure 22. Ageing curves for an PMDC AlSi7Cu2(Mg) alloy.

However the increasing in tensile properties is accompanying by a reduction in ductility. The formation of β'-Mg_2Si and θ'-Al_2Cu precipitates with their needle-like shapes and brittle behaviour, increase the micro-stresses; as showed by Zhang *et al.*[73], this resulted in the reduction of α-Al matrix deformation, thus decreasing ductility. These precipitates are brittle and may fracture at very low strains during deformation, accelerating the growth of the crack.

8.2 Modelling of heat treatment

The possibility to predict the mechanical properties of casting after heat treatment is a powerful tool in an industrial process since it reflects upon a cost and time redaction in design stage.
In **Article 4**, an exhaustive description of the development and the validation of new model predicting the yield strength of a casting from quenching and ageing conditions are proposed.
The model results from the integration of Quench Factor Model (Evacho and Staley[74-76]) and the Age Hardening Model ((Rometsch and Schaffer[77-78]). It can be written as follows:

$$YS=YS_{ageing}(exp(k_1 Q^n) \quad (3)$$

where:
- YS_{ageing} depends on age hardening parameters after an ideal quenching;
- Q is quench factor considering different quench rate;
- YS is the resulting yield strength;
- k_1 is a constant which equals the natural logarithm of the fraction untransformed during quenching;
- n is Avrami's coefficient.

The final yield stress, YS_f, is calculated by re-scaling the yield strength achievable after ageing following a rapid quenching, YS_{ageing}, thorough the quench factor Q. It considers the effect of different quenching media or different section thickness on cooling rate. In Figure 23 the influence of water and air quenching on the ageing curve of PMDC A356 alloy can be observed. As the cooling rate decreases, the yield stress value also decreases.

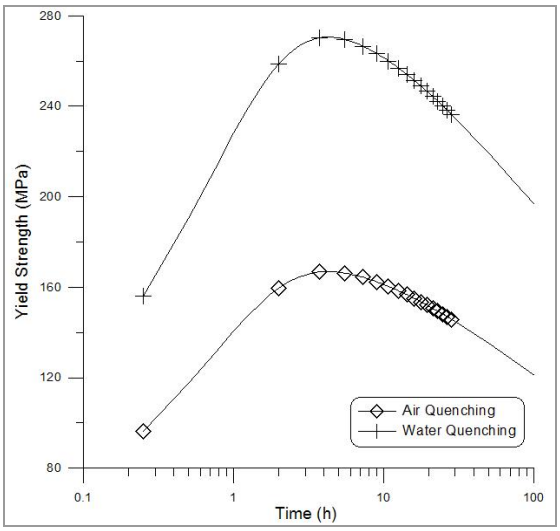

Figure 23. Modelled ageing curve for A356, PMDC alloy. The influence of quenching rate on Yield stress can be also observed **[Article 4]**.

Quench Factor

Quench Factor Analysis was initially investigated by Evacho and Staley[74] and it allows to describe the correlation between cooling rate and mechanical properties. Quench factor is typically calculated superimposing the cooling curve of quenching on the C-curve. The C-curve describes the time required, at different temperatures, for the precipitation of a constant quantity of solute; it was defined by Evancho and Staley as the reciprocal of the nucleation rate equation. The curve can be described using the following equation:

$$C_t = -k_1 k_2 \exp\frac{k_3 k_4^2}{RT\left(k_4 - T\right)^2} \exp\frac{k_5}{RT} \tag{4}$$

where C_t is the critical time required to form a specific percentage of a new phase; k_1 is a constant which equals the natural logarithm of the fraction untransformed during quenching (typically 99,5%: ln(0,995)=-0,00501); k_2 is a constant related to the reciprocal of the number of nucleation sites; k_3 is a constant related to the energy required to form a nucleus; k_4 is a constant related to the solvus temperature; k_5 is a constant related to the activation energy for diffusion; R is the universal gas constant, 8,3144 J/ºK*mol; T is the absolute temperature (K).

By decreasing the cooling rate for the effect of casting thickness or by adopting different quenching media (air, warm water or oil), value of Q increases (Figure 24) and, thus, worse tensile properties are achieved as consequence of precipitation during quenching, Figure 25.

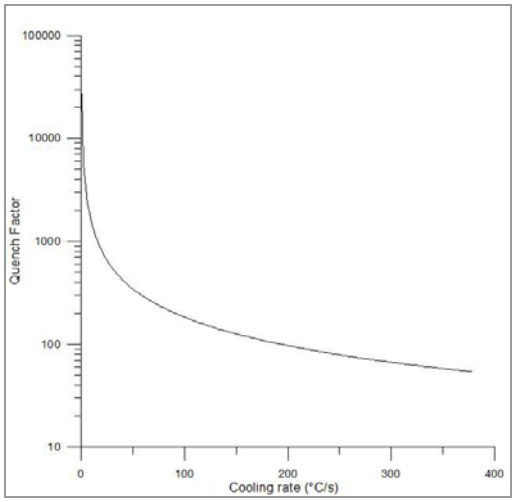

Figure 24. Influence of cooling rate on Quench Factor value **[Article 4]**.

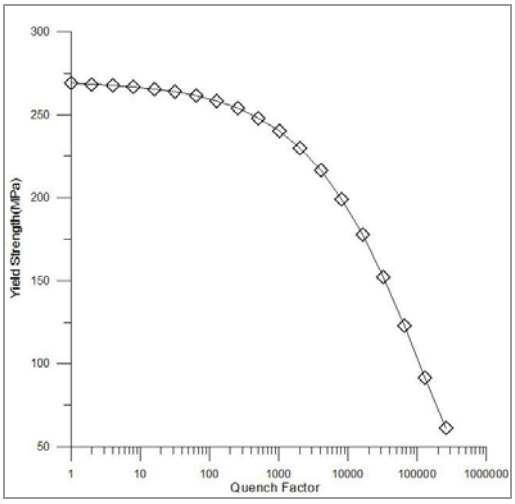

Figure 25. Reduction in Yield Strength in function of Quench factor value **[Article 4]**.

Age hardening model

The Ageing hardening model was developed by Shercliff and Ashby[77] to describe the age-hardening response of the yield strength and hardness of aluminum alloys for 2000- and 6000-series aluminium alloys. Subsequent Rometsch and Schaffer have applied this model to cast Al alloys[78] [X]. The process model can be written as follows:

$$YS_t = YS_i + \Delta YS_{ss} + \Delta YS_{ppt} \quad (5)$$

where YS_t, the final yield strength, it the sum of intrinsic strength, YS_i, including all the contributions not affected by the heat treatment process, of the solid-solution strength, $\Delta YS_{ss,}$, and of the precipitation strength, ΔYS_{ppt}, derived from the kinetics of precipitate formation and growth and from dislocation-precipitate interaction.
Thus, the model is a combination of sub-models to predict yield strength after various ageing treatments as expression of[78]:

- the decrease in solute concentration and growth in volume fraction of precipitates during the early stages of precipitation;
- the effect of ageing temperature on the equilibrium volume fraction of precipitates;
- the precipitate coarsening by Ostwald ripening;
- the strengthening contribution from solute atoms;
- the strengthening contribution from both shearable and non-shearable precipitates.

In Figure 26, the modelled ageing curves for a both PMDC A356 and AlSi7Cu2(Mg) alloys are displayed. It can be noted the ageing curve for the AlSi7Cu2(Mg) shows a double Yield Strength peak, in agreement to the experimental curves reported in Figure 22. A complete description of the model can be read in **Article [4]**, attached in Part 2 of this thesis.

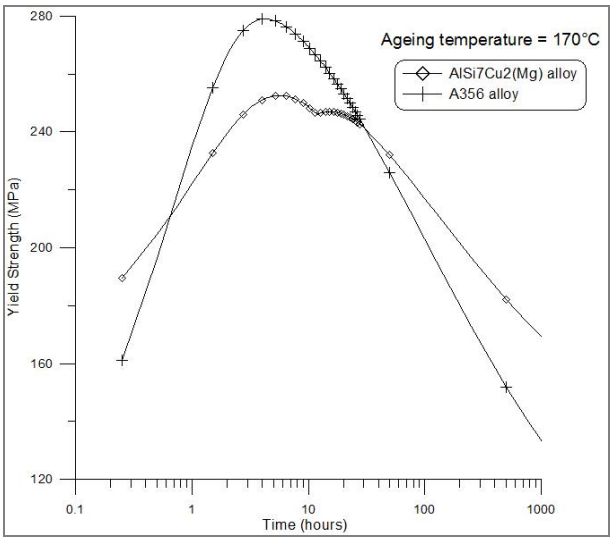

Figure 26. Modelled ageing curve for A356 and AlSi7Cu2(Mg) alloys.

9. INTEGRATED SIMULATION OF CASTING PROCESS

In the previous paragraphs, the interaction process-microstructure-defect in the determination of the final mechanical properties of a casting has been discussed. The importance of a strong control of the evolution of the metal from the melting process to final heat treatment as well as a correct design of the component and the gating system has been also underlined to obtain an improved quality of final component.
This aim is achievable by adopting a "simultaneous engineering" approach to design. Simultaneous engineering, called also "Concurrent engineering" is a systematic approach that integrates the design and the manufactured of a product with the view of optimizing all elements involved in the life cycle of the product.[30]
In this environment, computer simulation is a power tool especially for complex production system, such us casting manufacture, since it allows to evaluate the performance of the product in relation to the process to produce it.[30]
The numerical simulation of casting is mainly based on the solving of the equations:[29]

- in fluid dynamics, such us Navier–Stokes equation, for the filling of the cavity by means of a molten metal;
- in heat transfer, such us Fourier equation, for solidification and cooling of the alloy;
- in physical metallurgy for solid state transformation, related with thermodynamics and kinetics.

Nowadays, the main results provided by simulation code involve filling and solidification processes as well as microstructure and mechanical properties in as-cast and heat treatment temper. The simulation of *filling process* permits to analyse the flow of molten metal in the cavities in terms of temperature and degree of turbulence allowing the study of the susceptibility to incorporate gas, to form oxide inclusions or to produce "splash" or "shotting".
On the other hand, the analysis of temperature during *solidification* allows to detect the presence of "hot spot" due to un-correct solidification gradient.
The possibility to predict the microstructure plays a key role to understand the full potential of the component. As described in Section 6, the fracture mode of the alloy depends on amount, dimension and morphology of primary α-Al or Si phase and eutectic Si particles as well as distribution of Fe-bearing and secondary θ-$CuAl_2$/β-

Mg_2Si phases.[79] Thus, the prediction of microstructural features plays a key role in the analysis of the mechanical behaviour of the component in relation to in-service requirements.

The use of an integrated approach, based on using multi-scale simultaneous engineering tools, for automotive components has been one of the purposes of NADIA project.

As it can be seen in Figure 27, NADIA project is structured in three different levels having different objectives: basic, intermediate and final level.

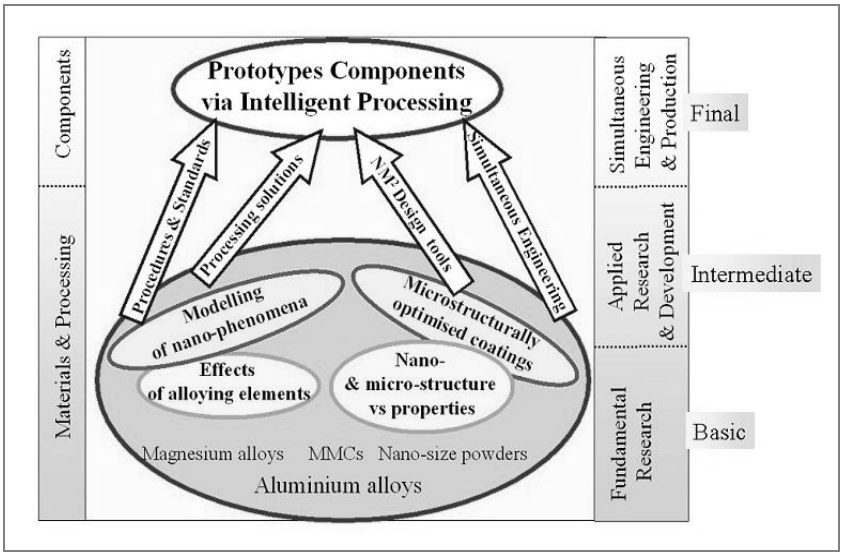

Figure 27. Structure of NADIA project.

In general, in the *Basic Level-Fundamental Research*, nano-scale phenomena and the effect of a wide set of alloying elements on components behaviour have been experimentally investigated and, then, modelled. Thus, the aim of the next level, or, *Intermediate Level-Applied Research and Development*, has been the implementation of the analytical models in engineering tools in order to improve the potential to simultaneous engineering. Finally, these enhanced tools have been applied in *Final Level-Breakthrough Simultaneous Engineering and Production* to produce strategic light alloys cast component prototypes for the European transport industry.

Following this structure, part of the experimental work carried out in this doctoral thesis concerned the development of an LPDC aluminium monocylinder (Figure 28).

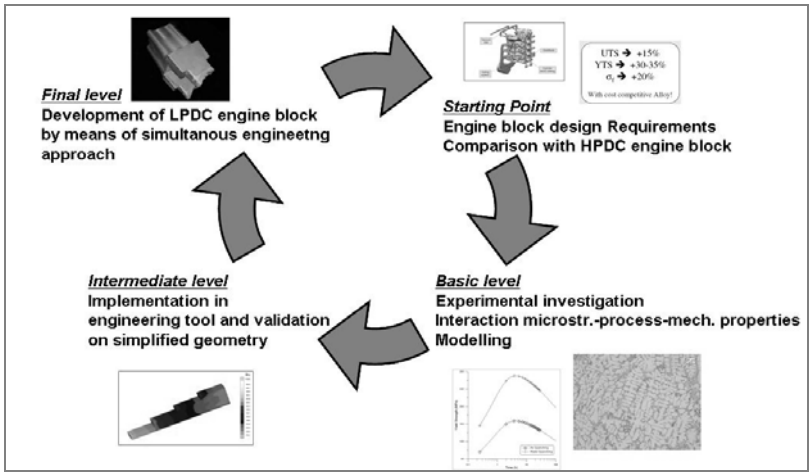

Figure 28. Vertical integration in the development of a monocylinder engine block.

Starting from the comparison with the properties of HPDC engine block **[Article 1, Article 4]** and design requirement for new LPDC cylinder block, the development of an optimized AlSiCu(Mg) alloy **[Article 2]** suitable for LPDC process has been performed in the *Basic Level*. In particular, the influence of composition, casting and heat treatment processes on microstructural and mechanical features has been investigated, leading also to the development and setting up of models. The aim of this models is the mathematical synthesis of the complex interactions between process, microstructure and mechanical properties.

In order to improve the potential of concurrent engineering approach, in *Intermediate level* the implementation of such models in numerical simulation software has been carried out **[Article 3].** To obtain a reliable engineering tool, the validation in term of comparison between numerical and experimental data has been also performed using a simplified geometry component.

Finally, as *Final Level*, simultaneous engineering approach, Figure 29, based on new and exiting tools has been applied in the production of the final engine block demonstrator. An exhaustive description in provided in **Article 5**.

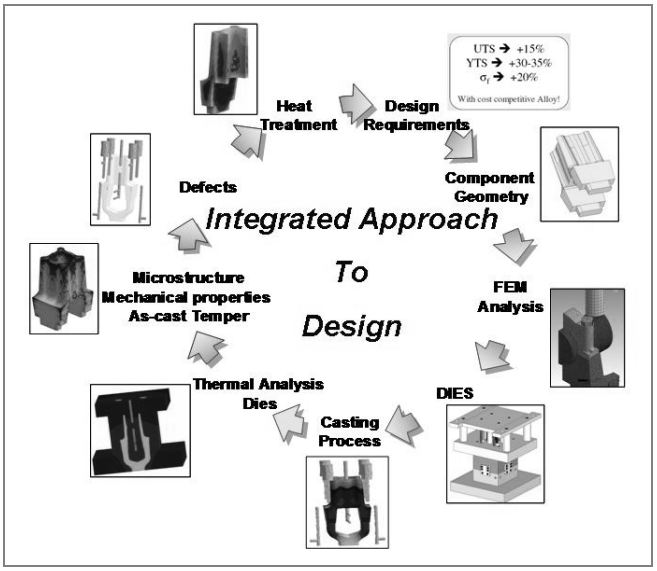

Figure 29. Simultaneous engineering applied to the development of monocylinder engine block.

From the filling process to the Yield Strength after heat treatment, all the interaction between process, microstructure and mechanical properties have been considered in design stage in order to develop a component with high integrity and matching the requirements. Furthermore, it suggests that numerical simulation is a useful tool for the reduction of time and costs in process and product development.

CONCLUSIONS

The following conclusions can be draw from this doctoral thesis work:

1. The microstructure of an aluminium casting depends on the combined effect of casting process, alloy composition and heat treatment:
   - An high solidification time leads to coarser microstructure in terms of grain size, large SDAS, eutectic Si particles with plate-like morphology along with an higher fraction of blocky-like Fe-bearing phase;
   - Coarser Si-particles were also observed in AlSiCu(Mg) alloys by increasing Cu and Ti content. The addition of Cu also increases the grain size while the presence of Ti refines the microstructure;
   - Heat treatment mainly affects eutectic Si roundness: solutioning leads to a morphology evolution resulting in rounder particles.

2. In turn, mechanical properties are influenced by microstructure:
   - High values of UTS and elongation to fracture are obtained for low SDAS values and small and more compact eutectic Si particles.
   - The effect of microstructural features on mechanical properties can be described by correlating UTS and elongation to fracture to the combined effect of SDAS, equivalent diameter and aspect ratio of eutectic Si particles. It was demonstrated that UTS and ductility decrease as the product (*SDAS x Si-Eq. Diameter x Si- Aspect ratio*) increases and that elongation to fracture shows an higher sensitivity on microstructural variation than UTS.
   - The Yield Strength of AlSiCuMg alloys is generally improved by heat treatment due to the precipitation of hardening β'-Mg_2Si and θ'-Al_2Cu phases.
   - The UTS of AlSiCuMg alloys depends mainly on SDAS, heat treatment and Cu content due to their influence on the morphology of silicon particles and on the precipitation of hardening phases.
   - At the same time, the ductility decreases as the Cu content and solidification time increase and the effect of Cu is more evident in grain refined alloys. Heat treatment improves the ductility by changing the morphology of eutectic Si particles.
   - The presence of defects decreased the alloy strength, promoting fracture nucleation and propagation.
3. Developed on step reference casting and validated on low pressure die cast mono-cylinder engine block, heat treatment model provided values close to experimental data suggesting a good reliability.
   A model correlating Quench Factor to cooling rate has also been set up and a good fitting between calculated and modelled values was observed.

4. "Concurrent engineering" approach was adopted in the development of a low pressure die cast mono-cylinder engine block. This approach allowed to obtain a component with high integrity and meeting design requirements. These results were possible thanks to numerical simulation able to reproduce the experimental data with a good accuracy. Therefore, it can be stated that numerical simulation is a useful tool for the reduction of time and costs in the design stage.

OBJECTIVES AND SURVEY OF THE ARTICLES

The aim the **Article 1** was to investigate the microstructural and mechanical properties of high pressure die cast (HPDC) cylinder block. The cylinder block, which is the main contributor to engine mass, offers very good potential to weigh reduction, up to 45% for gasoline engines.
In order to understand the impact of microstructure on mechanical behaviour of the component, in this work, mechanical properties were correlated to microstructural features, such as SDAS, size and the morphology of eutectic Si particles. The material was an EN AC-46000–UNI EN 1706 alloy (European designation, equivalent to the US designation A380), widely used in load-bearing components in automotive field.

The aim of **Article 2** was the optimization of an AlSiCu(Mg) alloy in terms of composition and heat treatment for the production of a low pressure die cast (LPDC) engine block. Thus, the concurring effects of the Cu content, the grain refinement, the solidification rate and the heat treatment on microstructural and mechanical properties were investigated by means of Design of Experiment methodology.

The aim of **Article 3** was to study the evolution of the microstructure (quantitatively evaluated by means of SDAS and Si-related parameters) as a function of the solidification time. Furthermore the correlation between microstructural parameters and the mechanical properties was performed. The experiments were carried out on permanent mould (PMDC) step bar reference casting with a range of thickness going from 5 to 20 mm. EN-AC 46000 and 46100 secondary aluminium alloys have been used. Finally, a comparison between experimental values and those provided by a commercial simulation code in terms of mechanical properties was also analyzed.

The aim of **Article 4** was to set up and validate of a model predicting the Yield Strength of casting from the heat treatment parameters. In detail, the model results from the integration of *Quench Factor Model*, developed by Evacho and Staley, and the *Age Hardening Model* developed by Rometsch and Schaffer. The setting up activities were carried out on permanent mould (PMDC) step bar reference casting using A356 primary aluminium alloy while the validation was performed on low pressure die cast (LPDC) mono-cylinder engine block.

The aim of **Article 5** was the validation of the results provided by the commercial MAGMASOFT® v4.6 software. The study has been carried out in the development of A356 aluminium alloy mono-cylinder engine block, cast by means of Low Pressure Die Casting (LPDC). Thus, the comparison between experimental data and simulation results was carried out in terms of solidification time, porosity and die temperature along with microstructure features and mechanical properties in as-cast state and after heat treatment.

REFERENCES

1. R. H. Bacon: “The car: engine and structure”; 1968, London, Macmillan & Cleaver.

2. W. H. Crouse and D. L. Anglin: “Automotive engines”; 1995, New York, Glencoe/McGraw-Hill.

3. S. Viswanathan, A.J. Duncan, A.S. Sabau, Q. Han, W.D. Porter and B.W. Riemer: AFS Trans., 1998, 106, 411-417.

4. A. Kearney, Kearney & Company, E.L. Rooy: Aluminum Company of America, “Aluminum foundry product”, Introduction to Aluminum and Aluminum Alloy”, Properties and Selection: Non ferrous alloys and Special purpose Materials vol. 2, 123-151; 1993, ASM Metals Handbook.

5. J. E. Gruzleski and B. M. Closset: “The treatment of liquid aluminium-silicon alloys”; 1990, IL, USA, The American Foundrymen's Society.

6. J. Campbell: “Castings”, 2nd edn; 2003, Oxford, Elsevier Butterworth-Heinemann.

7. J. Asensio-Lozano, B. Suárez-Peña: Mater. Charact., 2006, **56**, 169-177.

8. J. E. Eklund: “On the Effects of Impurities on the Solidification and Mechanical Behavior of Primary and Secondary Commercial Purity Aluminum and Aluminum Alloys”, Ph.D. thesis, Helsinki University of Technology, 1991.

9. H.Ye: J. Mater. Eng. Perf., 2003, **12**, 288-297.

10. R.X. Li, R.D. Li, Y.H. Zhao, L.Z. He, C.X. Li, H.R. Guan, Z.Q. Hu: Mater. Lett., 2004, **58**, 2096-2101.

11. Y.J. Li, S. Brusethaug, A. Olsen: Scr. Mater., 2006, **54**, 99-103.

12. A.L. Dons, G. Heiberg, J. Voje, J.S. Mæland, J.O. Løland, A. Prestmo: Mater. Sci. Eng., A, 2005, **413–414**, 561-566.

13. Samuel, F.H., A.M. Samuel, H.W. Doty: AFS Trans., 1996, **104**, 893-901.

14. C.A. Cloutier, P.M. Reeber-Schmanski, J.W. Jones, J.E. Allison: Automotive Alloys 1999, 153-160

15. L. Heusler, W. Schneider: J. Light Met., 2002, 2, 17–26.

16. C.H. Caceres, M.B. Djurdjevic, T.J. Stockwell, J.H. Sokolowski: Scr. Mater., 1999, **40**, 631-637.

17. M. Dash, M. Makhlouf: *J. Light Met.*, 2001, **1**, 251-265.

18. F.J. Tavitas-Medrano, J.E. Gruzleski, F.H. Samuel, S. Valtierra, H.W. Doty: Mater. Sci. Eng., A, 2008, **480**, 356-364.

19. P. Ouellet, F. H. Samuel: J. Mater. Sci., 1999, **34**, 4671-4697.

20. X.P Niu, B.H. Hu, S.W. Hao: J. Mater. Sci. Letters, 1998, **17**, 1727-1729.

21. Z. Ma, A.M. Samuel, F.H. Samuel, H.W. Doty, S. Valtierra: Mater. Sci. Eng., A, 2008, **490**, 36-51.

22. S.Seiffeddine: "Characteristics of cast aluminium–silicon alloys-Microstructures and mechanical properties", Ph. D. Thesis, Linkoping University, 2006.

23. S.G. Shabestari: Mater. Sci. Eng., A, 2004, **383**, 289-298.

24. C. M. Dinnis, J. A. Taylor, A. K. Dahle: Scr. Mater., 2005, **53**, 955-958.

25. G.K. Sigworth, M.M. Guzowaski, AFS Trans., 1985, **93**, 907.

26. P.S. Mohanty, J.E. Gruzleski, Acta Mater., 1996, **44**, 3749.

27. T. Grab, L. Arnberg, Int. J. Cast Metal. Res., 2006, **19**, 201-209.

28. M. Faraji, I . Todd, H. Jones, J. Mater. Sci., 2005, **40**, 6363-6365.

29. F. Bonollo, S. Odorizzi: "Numerical Simulation of Foundry processes", SGE (Italy), 2001.

30. S. Kalpakjian, S. R. Schmid: "Manufacturing Processes for Engineering Materials", Prentice Hall, 2002

31. G. Timelli: "Correlation between processing and quality aluminium alloy castings", Ph.D. thesis, University of Padua, 2008.

32. S. Khan, R. Elliot: Acta Metall. Mater., 1993, **41**, 2433-2439.

33. G.K. Sigworth: AFS Trans., 1983, **66**, 7-16.

34. L.M. Hogan, M. Shamsuzzoh: Mater. Forum, 1987, **10**, 270-277.

35. S.Z. Lu, A. Hellawell: Metall. Mater. Trans. A, 1987, **18A**, 1721-1733.

36. J.E. Gruzleski: AFS Trans., 1992, **164**, 673–683.

37. L. Lua, K. Nogita, A.K. Dahle: Mater. Sci. Eng., A, 2005, **399**, 244–253.

38. M. Tiryakioglu: Mater. Sci. Eng., A, 2008, **A473**, 1-6.

39. G. Chadwick: Prog. Mater. Sci., 1963.

40. R. Elliot: Eutectic Solidification Process, London, Butterworth,1983.

41. A.K. Dahle, K. Nogita, J.W. Zindel, S.D. McDonald, L.M. Hogan: J. Met. Mater. Trans. A, 2001, **32**, 949-960.

42. W. Khalifa, F.H. Samuel, J.E. Grizleski: J. Met. Mater. Trans A, 2003, **34**, 807-825.

43. S. Shankar. Y.W. Riddle, M.M. Makhlouf: Acta Mater., 2004, **52**, 4447-60.

44. K. Nogita, S.D. McDonald, K. Tsujimoto, K.Yasuda, A.K. Dahle: J. Electron. Microsc., 2004, **53**, 361-369.

45. S. Nafisi, R. Ghomashchi, H. Valia: Mater. Charact., 2008, **59**, 1466-1473

46. Hema V. Guthy: Evolution of the Eutectic Microstructure in Chemically Modified and Unmodified Aluminum Silicon Alloys, Ph.D. thesis, Worcester Polytecnic Instiurte, 2002

47. D.R. Hamilton, R.G. Seidensticker: J. Appl. Phy., 1960, **31**, 1165-1168.

48. Shu-zu-lu, A. Hellawell: Met. Trans., 1987, **18A**, 1721-1733.

49. Shu-zu-lu, A. Hellawell: J. Cryst. Growth, 1985, **73**, 316.

50. B.M. Thall, B. Chalmers: J. Inst. Metals., 1949, **78**, 79.

51. J. Asensio-Lozano, B. Suárez-Peña: Mater. Charact., 2006 , **56**, 169-177.

52. L. Backerud, G. Chai, J. Tamminen: "Solidification Characteristic of Aluminum Alloys-Vol.2: Foundry Alloys." American Foundrymen's Society, Inc., IL, USA(1990)

53. S.G. Shabestary, F. Shari: J. Mater. Sci., 2004, **39**, 2023-2032

54. S. Viswanathan, A.J. Duncan, A.S. Sabau, Q. Han, W.D. Porter, B.W. Riemer: AFS Transactions, 1998, **106,** 411-417.

55. V. Rontò, A. Roosz: Int. J. Cast Metals Res., 2001, **13,** 337-342.

56. Warmuzek, M., 2004: "Aluminium-Silicon Casting Alloys: Atlas of Microfractographs, first ed., ASM International".

57. G. Timelli, F. Bonollo: Proc. Int. Conf. Aluminium Two Thousand, Florence (2007), Modena.

58. C.H. Caceres, J.R. Griffiths: Acta Mater., 1996, **44**, 25-33.

59. Q.G. Wang, C.H. Caceres: Mater. Sci. Eng. A, 1998, **241**, 72-82.

60. G. Timelli, F. Bonollo: Metall.. Sci. Technol., 2008, **26**, 2-8.

61. Q.G. Wang, D. Apelian, D.A. Lados: J. Light Met., 2001, **1**, 73-84.

62. M. Avalle, G. Belingardi, M.P. Cavatorta, R. Doglione: Int. J. Fatigue, 2002, **24**, 1-9.

63. F. Faura, J. López, J. Hernández: Int. J. Mach. Tools Manuf., 2001, **41**, 173-191.

64. C.H. Cáceres, B.I. Selling: Mater. Sci. Eng. A, 1996, **220**, 109-116.

65. A.M. Gokhale, G.R. Patel: Scripta Mater., 2005, **52**, 237-241.

66. X. Dai, X. Yang, J. Campbell, J. Wood: Mater. Sci. Eng. A, 2003, **354**, 315-325.

67. A.J. Ardell: Metall. Trans. A, 1985, **16A**, 2131-2165.

68. 15. A.J. Ardell: "Encyclopedia of Materials Science and Engineering", M.B. Bever, ed., Pergamon Press, Oxford, United Kingdom, 1986, 3882.

69. S.C. Weakley-Bollin, W. Donlon, C. Wolverton, J.W. Jones, J.E. Allison: J. Met. Mater. Trans. A, 2004, **35A**, 2407-2418.

70. L. Pedersen, L. Arnberg: Metall. Mater. Trans. A, 2001, **32**, 525-532.

71. D.L. Zhang, L.H. Zheng, D.H. StJohn: J. Light Met., 2002, **2**, 27-36.

72. L. Pedersen: Doctoral Thesis, Norwegian University of Science and Technology, Trondheim, Norway, 1999.

73. D. Zhang, J. Peng, G. Huang. D. Zeng: Mater. Sci. Ed., 2008, **23**, 184-188.

74. W. Evancho, J.T.Stanley: Metall. Trans., 1974, **5**, 43-47.

75. P.A. Rometsch, G.B. Schaffer: Int. J. Cast Metals Res.,2000, **12**, 431-439.

76. P.A. Rometsch, M.J. Starink: Mater. Sci. Eng. A, 2003, **339**, 255-265

77. H.R. Shercliff, M.F. Ashby, Acta Metall. Mater.,1990, **38**, 1789.

78. P.A. Rometsch, G.B. Schaffer: Mater. Sci. Eng. A, 2002, **325**, 424-434.

79. S. Seifeddine, T. Sjögren, I. L. Svensson: Matall. Sci. Technol., 2007, **25**, 12-22.

PART 2

ARTICLES

ARTICLE 1

CORRELATION BETWEEN MICROSTRUCTURE AND MECHANICAL PROPERTIES OF Al-Si DIECAST ENGINE BLOCKS

Fabio Grosselle*, Giulio Timelli*, Franco Bonollo*, Roberto Molina**

* Department of Management and Engineering – DTG
University of Padova
I-36100 Vicenza
ITALY

** Teksid Aluminum,
I-10022 Carmagnola
ITALY

Published in: Metallurgical Science and Technology, 2009.

ABSTRACT

In spite of weight reduction of passenger car, the cylinder block is the heaviest component among many automotive engine parts and plays a key role in fuel efficiency and the drivability of vehicles. In hypoeutectic aluminium alloys, the final mechanical properties are strictly connected to microstructural features such as the distribution, the morphology and dimensions of primary α-Al phase and eutectic Si particles, as well as, type of iron-bearings and defects. The microstructure, in turn, depends on filling process and solidification dynamic. In this work, a HPDC 4-cylinders-in-line cylinder block was exhaustively analysed and mechanical properties were correlated to microstructural features. Mechanical properties are affected by microstructure. The best values of UTS and elongation to fracture are obtained for low secondary dendrite arm spacing (SDAS) values and small and more compact eutectic Si particles. If the combined effect of α-Al phase and eutectic Si particles is taken into account, a linear correlation between UTS and product of SDAS, equivalent diameter and aspect ratio of Si particles is observed, while the elongation to fracture shows an exponential trend, suggesting an high sensitivity on microstructural variation.

KEYWORDS
Aluminium alloys; EN-AC 46000; High-pressure die-casting; SDAS; Eutectic Si; Microstructure; Engine block

1. INTRODUCTION

Aluminium alloy castings are making a significant contribution in the construction of modern passenger cars due to the potential capability in weight and emission reduction. In particular, the application of aluminium alloys to cylinder block, which is the main contributor to engine mass, in replacement of cast-iron offers very good potential to weigh reduction, up to 45% for gasoline engines. The enhancement in power rating owing to the highest thermal conductivity of aluminium alloys, three times better than that of cast iron, allows engines to deliver more power per cylinder size [1] due to a better control of local temperatures.
For mass produced engines, high-pressure die-casting (HPDC) is widely used for the possibility of obtaining net to shape components of complex geometry and thin wall thickness at high production rates, reducing production costs [2-4]. Due to the complexity of the casting shape and variability in process parameters, common defects in industrial HPDC manufactured parts are shrinkage cavities, cold fills, oxide films, dross, entrapped air bubbles [4].
Due to excellent castability along with good mechanical properties achievable and low cost, hypoeutectic secondary Al-Si alloys are normally used for HPDC process. The microstructure expected in components cast with these alloys will be a mixture of pro-eutectic α-Al dendrites surrounded by Al–Si eutectic. The distribution, the morphology and dimension of primary α-Al and eutectic Si particles depend on cooling conditions and solidification history [5-8]. Moving from the wall in contact with the die to the centre line a very fine porosity-free microstructure becomes coarser and defects can easily form as consequence of filling dynamics and high solidification time [9]. The presence of Cu, Mg and tramp elements promotes the formation of other phases [1,10]. Copper and Magnesium lead to the formation of strengthening Al_2Cu and Mg_2Si precipitates [1-11] while iron promotes the formation of various intermetallic phases, the most common of which are needle-like β-Al_5FeSi and angular globules block-like $Al_{15}(Mn,Fe)_3Si_2$ [1-12].
Process parameters, microstructure features and defects contribute to the final mechanical properties of the aluminium alloy. In defect free components, fracture is initiated by cleavage of either brittle intermetallic or eutectic Si particles. Then, fracture propagates mainly along grain boundaries (intergranular mode) for small values of SDAS or along cell boundaries (transgranular mode) for large SDAS [13-15]. However, in presence of defects, mechanical properties decrease monotonically with an increase in the area fraction of defects as consequence of effect on fracture initiation and propagation [4,16-17].
In this work a HPDC engine block was analysed and mechanical properties were correlated to microstructural features, such as SDAS and the size and the morphology of eutectic Si particles. The material was an EN AC-46000–UNI EN 1706 alloy (European designation, equivalent to the US designation A380), widely used in load-bearing components in automotive field.

2. EXPERIMENTAL METHODS

In the present work, a secondary AlSi9Cu3 foundry alloy has been used. The chemical composition, measured on separately poured samples, is shown in Table I. The liquidus temperature of the alloy was determined by means of thermal analysis, T_{liq} = 585°C.

Table I. Chemical composition of the AlSi9Cu3 alloy studied in the present work (wt.%).

Alloy	Al	Si	Cu	Fe	Mg	Mn	Ni	Ti	Zn	Cr
EN-AC 46000	bal.	9.2	3.3	0.89	0.19	0.24	0.06	0.037	0.97	0.031

The Fe content was kept above 0.8 wt.%, to prevent the molten metal from "soldering" to the casting die. The Al–Si–Fe eutectic composition occurs at about 0.8 wt.% Fe. When Fe is alloyed to somewhat above this level, the molten metal has little or no tendency to dissolve die steel while the two materials are in intimate contact. Thus, the higher iron content of the alloy reduces the solution potential for the iron components of the casting machine and die, and for this reason, most aluminium pressure die casters desire that their alloys contain between 0.8 and 1.1 wt.% iron [18-20]. Further, the morphology of iron-rich β-phase, Al_5FeSi, deteriorates the strength and ductility behaviour of the alloy and promotes the initiation of cracks under load [21]. The addition of Manganese and the high solidification rate in die-casting change the morphology of Fe-bearing needles or enhance the precipitation of phases which are less harmful than β-phase. Manganese is also used to provide good ejection behaviour and reduced die soldering [22]. Magnesium, Copper and Zinc determine here the yield strength (YS) and the ultimate tensile strength (UTS).
The castings studied were HPDC 4-cylinders-in-line (L4) cylinder blocks. Figure 1 shows the open-deck geometry of the cylinder block and the location of the gates, runners and overflows. The castings were produced using a cold chamber die-casting machine equipped with the dynamic shot control system and the vacuum system connected to the venting channels.

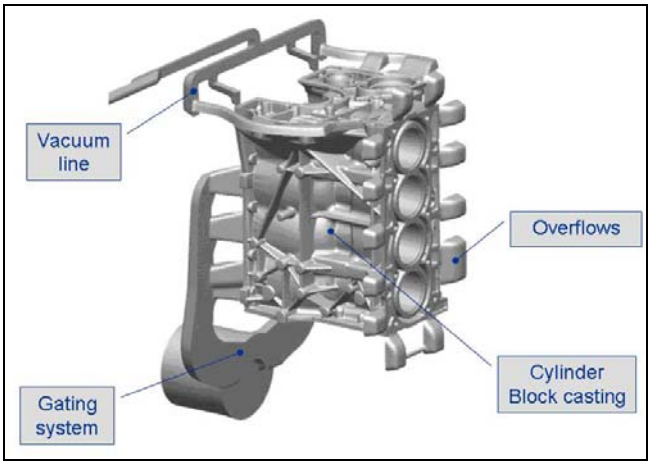

Figure 1. Illustration of engine block with 6 ingates and the vacuum channels.

The engine blocks were cast with grey iron liners that resist the attrition of the moving pistons. Each tubular liner was positioned directly into the die before pouring, remaining as cast-in inserts into the block. The melt was kept at ~690±10°C in the holding furnace and was automatically ladled into the shoot sleeve and injected into the die cavity. Several castings were scrapped after the startup, to reach a quasi-steady-state temperature in the shot chamber and die. Oil circulation channels in the die served to stabilize the temperature. The other best machine parameters including die temperature, injection speed of the melt and lubricant were selected to enable the mass production of the cylinder blocks. By means of a dynamic shot control system

in the HPDC machine, every casting was documented with its shot profile, to monitor the final quality and repeatability.
Radiographic inspection was carried out throughout the castings, in order to detect the presence of macrodefects. The diecast engines were then sectioned and several blocks were drawn from different locations of the castings (Figure 2). Flat tensile test bars with rectangular cross section were machined from each of the blocks.

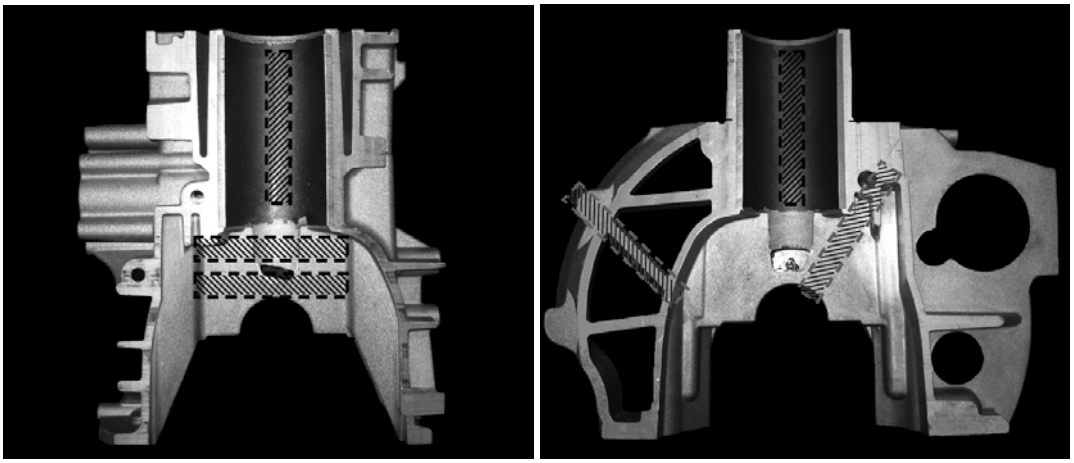

Figure 2. Position from which tensile specimens were machined.

The tensile specimens were 100-mm long, 20-mm wide, and 3-mm thick, with a gage length of 30 mm and a width of 10 mm, according to ASTM-B577.
The tensile tests were done on a computer controlled tensile testing machine MTS 810. The crosshead speed used was 2 mm/min ($\dot{\varepsilon} \sim 10^{-3}$ s^{-1}). The strain was measured using a 25-mm extensometer. Experimental data were collected and processed to provide yield stress (YS, actually 0.2% proof stress), ultimate tensile strength (UTS) and elongation to fracture (s_f). At least three specimens were tested for each zone. When the experimental data differed by more than 5%, another tensile specimen was tested. For the analysis in this paper, the average of the best values were selected in an attempt to minimise any effects arising from casting defects on the fracture data and to maximise the possibility of isolating the effects of microstructural parameters, such as SDAS and eutectic Si parameters. Contrary, casting defects do not generally affect YS values in the same way [16].
Microhardness measurements were performed on ground and polished samples cut from the gage sections of flat test bars. Vickers microhardness measurements were carried out using loads of 0.2 kgf and a 30-second dwell period, according to the standard ASTM E-384. The measurements were done at eight different locations along the cross section of the sample; the typical standard deviation was 5 HV.
The samples cut from the cross section of the gage length were mechanically prepared to a 1-μm finish with diamond paste and, finally, polished with a commercial fine silica slurry for metallographic investigations. Microstructural analysis was carried out using an optical microscope and a scanning electron microscope (SEM) equipped with an energy-dispersive spectrometer (EDS), and quantitatively analyzed using an image analyzer. To quantify the microstructural features, the image analysis was focused on the secondary dendrite arm spacing (SDAS), and on the size and aspect ratio of the eutectic silicon particles. Size is defined as the equivalent circle diameter (d); the aspect ratio (α) is the ratio of the maximum to the minimum Ferets. To obtain a statistical average of the distribution, a series of at least 10 photographs of each specimen were taken; each measurement included more than 1000 particles. The secondary phases, such as the Mg_2Si and

Al_2Cu particles, and the iron-rich intermetallics were excluded from the measurements and further analysis. Average SDAS values were obtained using the linear intercept method, which involves measuring the distances between secondary dendrite arms along a line normal to the dendrite arms.

3. RESULTS AND DISCUSSION

3.1 Radiographic Inspection

The results of radiographic investigation show a good integrity of the castings and the absence of defects/porosities with critical size for mechanical properties. This was assured by the vacuum system reducing the gas quantity and, therefore the gas entrapment within the die. However, a small quantity of macroporosity is mostly detected in circular sections or profiles, as well as, in correspondence of the bulkhead supports and underneath liners, especially close to the vacuum line (Figure 3). The defects seem to result from local die filling conditions, which promote the entrapment and dragging of air bubbles.

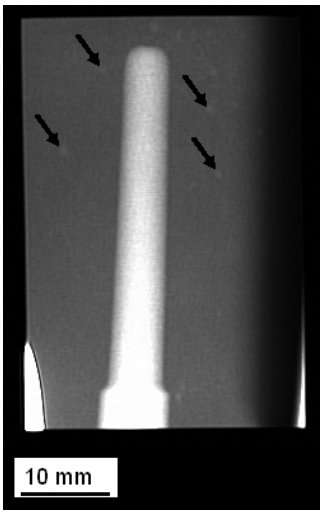

Figure 3. Radiographic image of the bulkhead support showing the presence of porosity.

3.2 Microstructural observations

The microstructure consists of a primary phase, α-Al, solid solution, and an eutectic mixture of aluminium and silicon. Al_2Cu secondary phase and Fe-bearing intermetallic are also observed. Differences in solidification between wall and centre of sections reflect upon dimension and distribution of α-Al phase as well as morphology and distribution of eutectic Si particles (Figure 4).
It is noted that the amount of α-Al phase decreases from the wall to the centre line of the sections. As regards the morphology of the α-Al phase, it shows mainly an equiaxed globular-geometry in wall regions and thin wall thickness area. The α-Al cells are little branching due to an increased undercooling governing the entire solidification process and due to the shift in the equilibrium diagram to lower temperatures [23]. The dimensions of α-Al globules increase from the wall to the centre due to lower solidification rates; here, a clear dendrite morphology is observed.

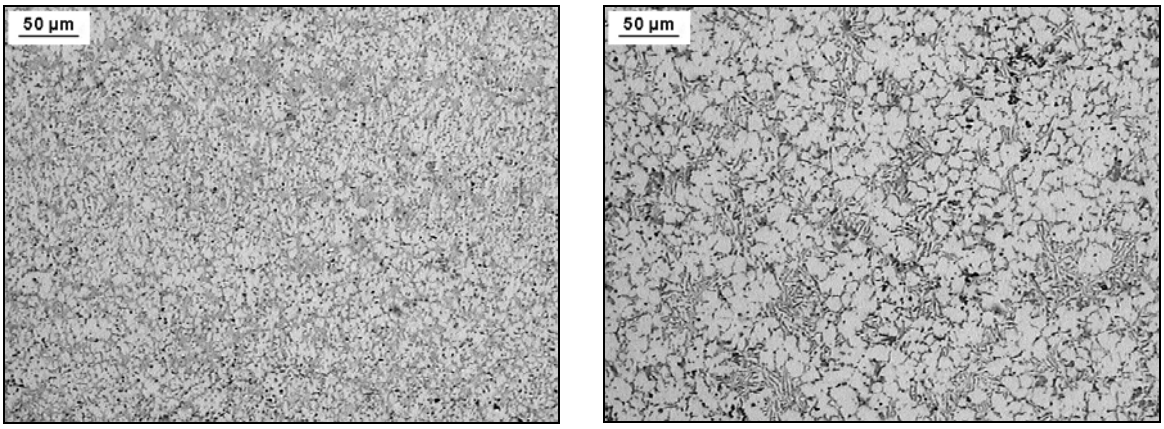

(a) (b)

Figure 4. Microstructure in correspondence of a thick section. It can be noted the changes in the microstructure moving from (a) the wall to (b) the centre of the specimen.

Figure 5 shows the effect of the solidification rate on the dimension and the morphology of eutectic Si particles. Along the wall and in the thin sections, the nucleation prevails on growing mechanism due to an elevated undercooling; therefore, the formation of a fine and fibrous eutectic silicon is promoted (Figure 5a). On the other hand, , the eutectic Si particles shows a typical coarse plate-like morphology in centre of thick sections, typical of un-modified aluminium alloys (Figure 5b).

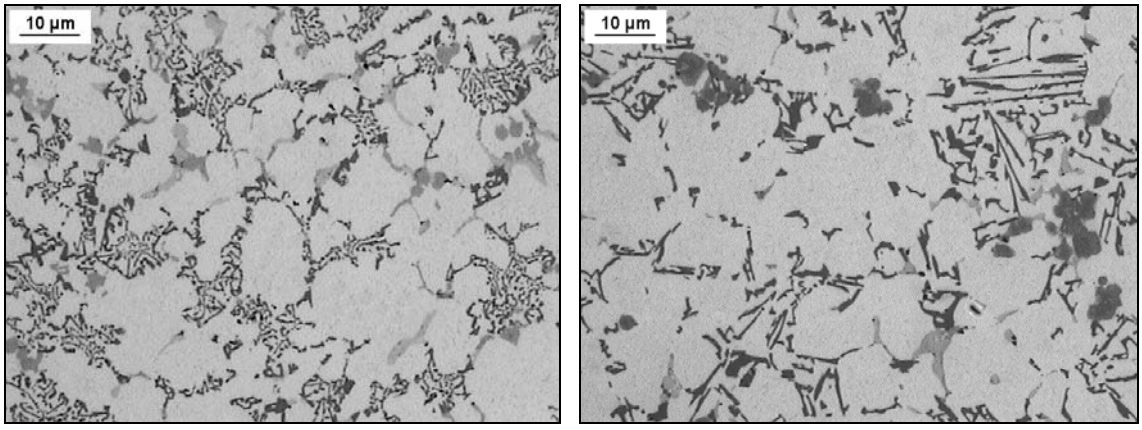

(a) (b)

Figure 5. Eutectic silicon particles with (a) fibrous and (b) lamellar shape in the zones with high and low cooling rates respectively.

This is supported by quantitative measurements of eutectic particle size, in terms of equivalent circle diameter d, and aspect ratio, α. The results are shown in Figure 6 where the mean value of d and α are plotted as function of SDAS. The effect of increasing cooling rate (i.e. the decrease of SDAS) upon the equivalent diameter is quite pronounced: decreasing dimension of dendrite cell size, equivalent diameter varies from 3.1 to 2.4 µm with a linear tendency. Decreasing SDAS from 20 to 8 µm, the aspect ratio of eutectic Si particles also reduces from ~3 to ~2.2.

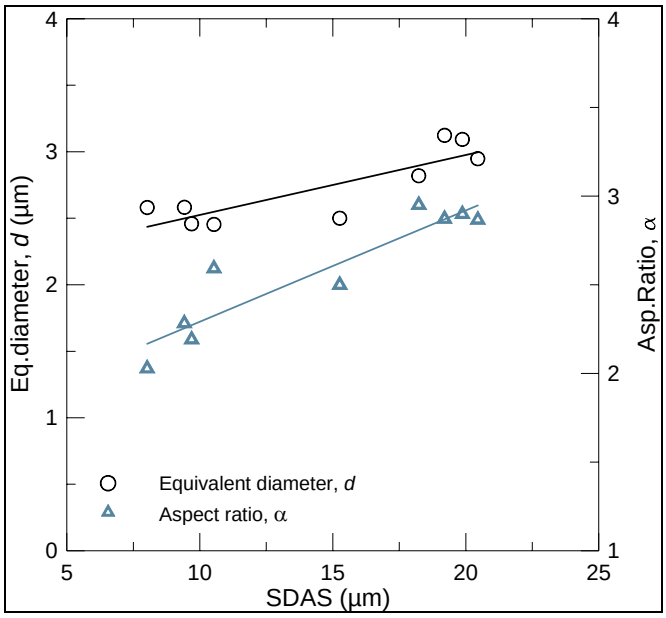

Figure 6. Average diameter and aspect ratio of the eutectic Si particles as a function of SDAS.

In Figure 7, Al_2Cu secondary phase and iron-bearing intermetallics can be also seen. Al_2Cu phase occurs in the form of both pockets of fine eutectic (Al + Al_2Cu) in the interdendritic regions and block-like Al_2Cu particles. The former is due to high cooling rate while the latter is consequence of high fraction of Fe-rich intermetallics, nucleating site for Al_2Cu and resulting from low cooling rate.

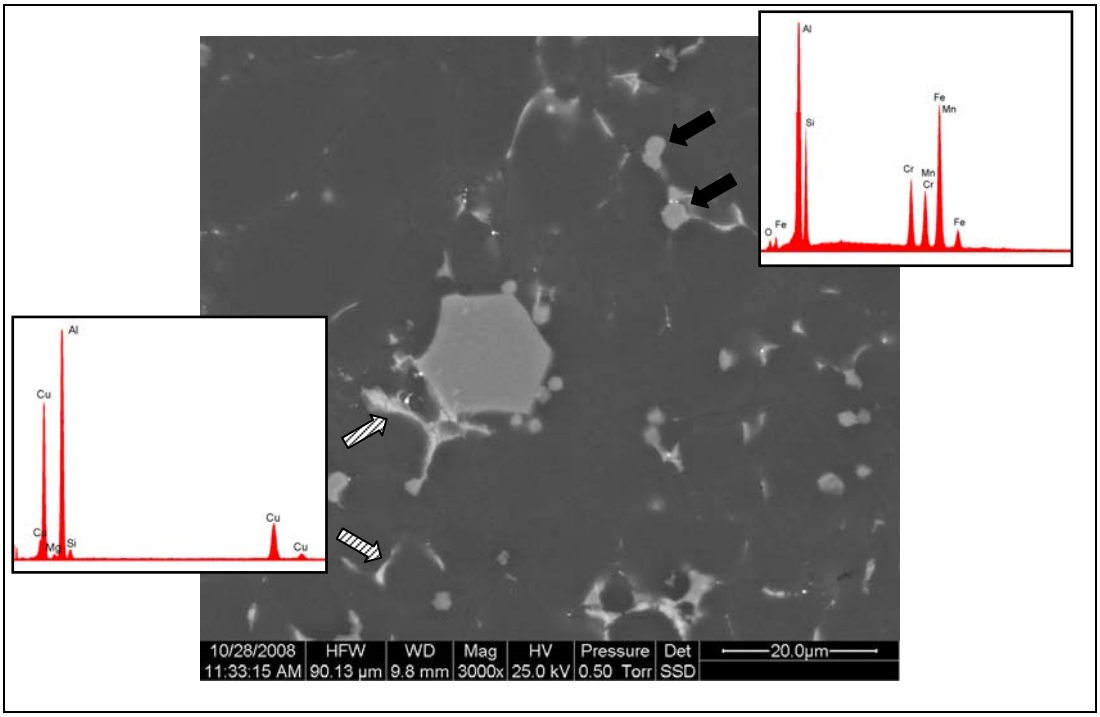

Figure 7. Microstructure of die-cast AlSi9Cu3 engine block. Dashed arrows indicate Al_2Cu particles while solid arrows show α-Al(Mn,Fe,Cr)Si intermetallic particles, as revealed by EDS spectra.

Fe-rich particles are mainly present in the form of fine blocky-like α-Al(Mn,Fe,Cr)Si particles even if acicular β-Al_5FeSi particles are shown in the thickest sections. The form depends upon the combination of Mn and Cr content and the undercooling degree. High cooling rate promotes nucleation of α-phase, while β-phase formation results from low solidification rate [21]. Large blocky-like α-Al(Mn,Fe,Cr)Si particles are also observed in the microstructure (Figure 7). In high silicon alloys, α-Al(Mn,Fe,Cr)Si may be primary, and since its crystals tend to be limited by the (111) faces, it appears as more or less well-formed hexagons [24]. These primary phases or complex intermetallic compounds formed with iron, manganese, and chromium are usually called "sludge".
The different microstructure as function of the distance from the wall reflects upon mechanical properties. It is expected that high properties are associated to a finer microstructure as result of a reduced tension filed around the eutectic Si and Fe-rich particles. A quantitative evaluation of this variation is provided in Figure 8, where the Vickers micro-hardness is plotted as function of increasing distance from the wall. The skin layer is in the range of 250-500 μm width, while the hardness decreases from 100 to 85 HV by increasing the distance from the edge.

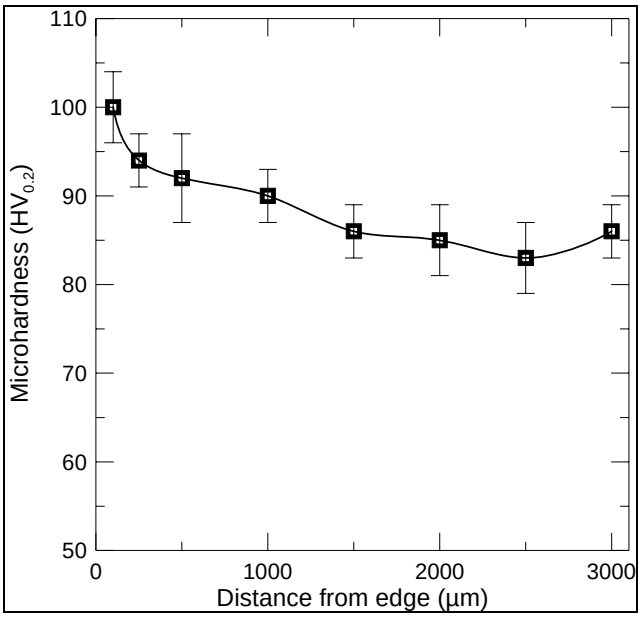

Figure 8. Vickers microharness measured along the cross section of a specimen. Standard deviations are given as error bars.

Common defects of HPDC process, such us oxide films, oxide inclusions, cold shots are observed within the casting, especially underneath liners and in bulkhead supports close to the vacuum line. Some examples are given in Figure 9.

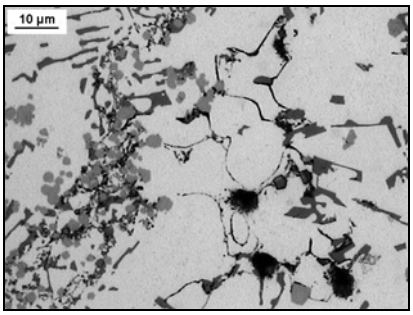

(a)

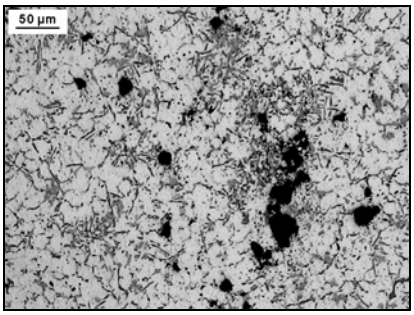

(b)

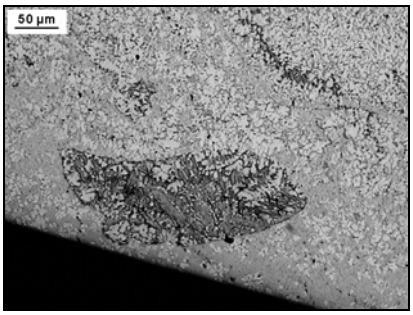

(c)

Figure 9. (a) Oxide inclusions and films, (b) porosities and (c) cold shots observed in diecastings.

Segregation bands were detected in the interface between the aluminium alloy and the cast iron liners, as shown in Figure 10. The formation of segregation bands is due to the local collapse of the dendrite network that causes flow of enriched liquid in that zone. The main factors affecting this mechanism are the heat transfer coefficient, the interior flow velocity and the reduced solidification rate. In location of cast iron liners, due to their thin thickness (~5 mm), an equilibrium temperature between liquid alloy and liner is rapidly reached resulting in a lower heat transfer. Thus, the increased solidification time promotes the collapse of α-Al dendrites and, in turn, the formation of segregation [25].

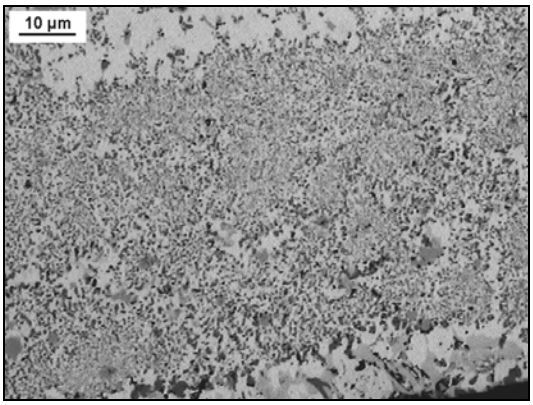

Figure 10. Segregation bands of eutectic silicon in regions with low solidification rate.

In general, a fine microstructure with small α-Al globules, fibrous eutectic Si and blocky-like Fe intermetallic particle is observed in the top part of the engine blocks as consequence of thin sections resulting in high cooling rate. On the other hand, the bottom part (i.e. bulkhead supports) shows a coarser microstructure and defects due to filling process and lower solidification rate.

3.3 Tensile testing

Mechanical properties have been measured in different zones of the engine block. In general, the component shows high mechanical properties suggesting an appropriate setting up of the process parameter that limits the formation of defects.
No sensible variations in the YS values have been obtained; a mean value of 169±8 MPa is measured considering all tensile specimens. This tendency suggests that the effect of the dimension and morphology of α-Al phase and eutectic Si particles is negligible. The best mechanical properties are measured in the regions between cast iron liners. In this case, the mean values and standard deviation of UTS and elongation to fracture are 274±10MPa and 2.5±0.4% respectively. Conversely, the zones underneath the liners and bulk-head support show an average value of 236 MPa as UTS and of 1.4% as elongation to fracture. Lower values are the consequence of thicker sections along with higher quantity of defects decreasing the mechanical strength of the alloy.
The best UTS and s_f values have been correlate to the microstructure in order to estimate the influence of α-Al phase and Si particle on the fracture behaviour of the alloy. Figures 11 and 12 show a general decrease in UTS and s_f values with increasing SDAS or eutectic Si size.

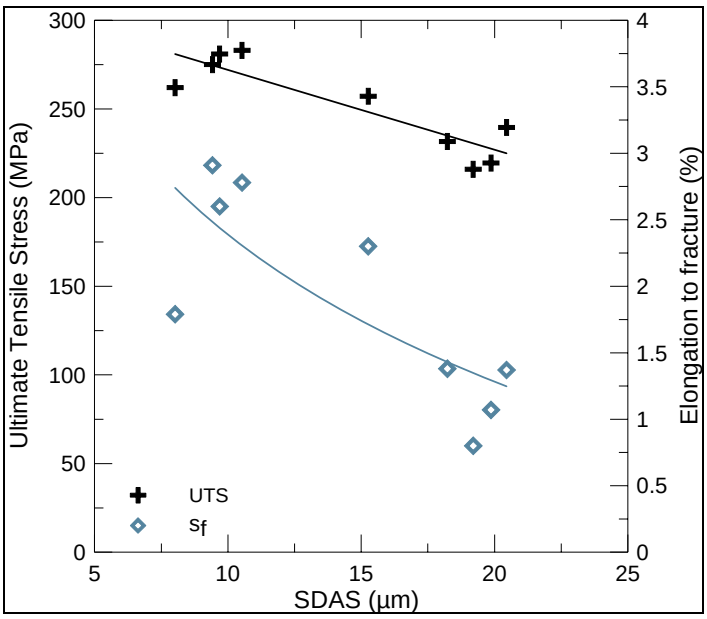

Figure 11. UTS and elongation to fracture as function of SDAS.

An increased dimension of SDAS, from 8 to 20 μm, leads to a reduction of 24% and 70% of UTS and elongation to fracture, respectively. While the decrease of UTS is linear with increasing SDAS values, the elongation to fracture decreases exponentially. The type of correlation has been selected on the base of the highest value of the coefficient of determination R^2 measured for different regression

functions. The coefficient R^2 measures the quality of the least-squares fitting to the original data and it can be written as follows:

$$R^2 = 1 - \frac{\sum_{i=1}^{n}\left(f(x_i) - g(x_i)\right)^2}{\sum_{i=1}^{n}\left(f(x_i) - \overline{f}(x_i)\right)^2} \quad (1)$$

where x_i is the discrete variable, $g(x_i)$ is the corresponding calculated value using the regression function, $f(x_i)$ is the corresponding experimentally measured value, $\overline{f}(x_i)$ is the mean value of experimental data and n is the total number of experimental points. When $R^2 = 1$, the fit is perfect.

For both functions describing the dependence of UTS and elongation to fracture on SDAS, the calculated R^2 is 0.52. The fairly good value of R^2 is consequence of the scatter in experimental data related to the defects which are intrinsic in a HPDC component and, thus, difficult to be completely isolated.

A reduction of the mechanical properties is also observed when the size of eutectic Si particles increases (Figures 12). The UTS varies from 281 to 219 MPa and the elongation to fracture decreases from 2.9% to 0.8%. By increasing the solidification time, coarser Si particles can be observed in the microstructure leading to high tension field around particles. This promotes cleavage mechanism and, thus, fracture can easily propagate. The best fitting lines are similar to that of Figure 11: a linear function with R^2=0.83 and an exponential function with R^2=0.89 describe the variation of UTS and s_f on eutectic Si particles, respectively. This definitively suggests that the elongation to fracture is more sensitive to eutectic Si and SDAS values than the UTS.

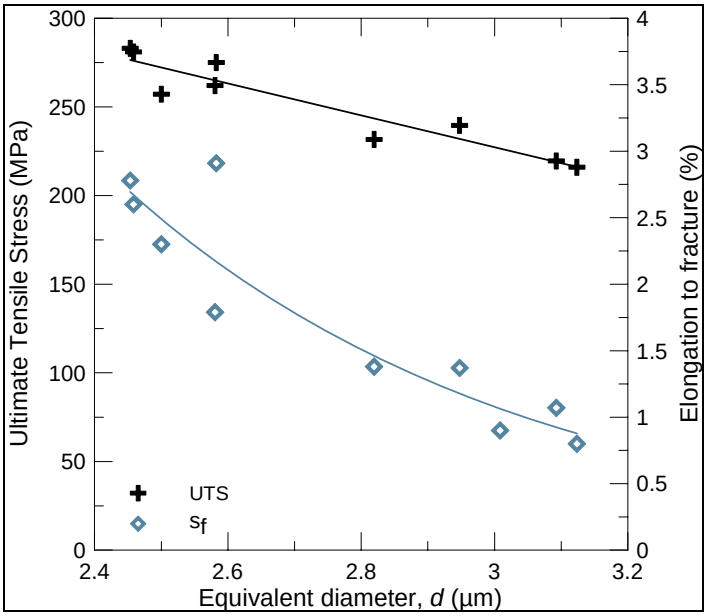

Figure 12. UTS and elongation to fracture as function of equivalent diameter of the eutectic Si particles.

Since the plastic behaviour of cast aluminium alloy is influenced by α-Al phase and eutectic Si particles, it is reasonable to expect that the UTS and the elongation to fracture are controlled by a combined effect of SDAS and eutectic Si features. Figure 13 plots UTS and elongation to fracture as function of the product of SDAS,

equivalent diameter and aspect ratio of eutectic Si particles. An increased value of this product reflects upon a reduction of UTS and s_f values. It can be observed that both UTS and elongation to fracture maintain the tendency shown in the previous plots. The UTS decreases linearly (R^2=0.50) with the product, while the elongation to fracture exponentially (R^2=0.55), mainly for the effect of size and morphology of Si particles.

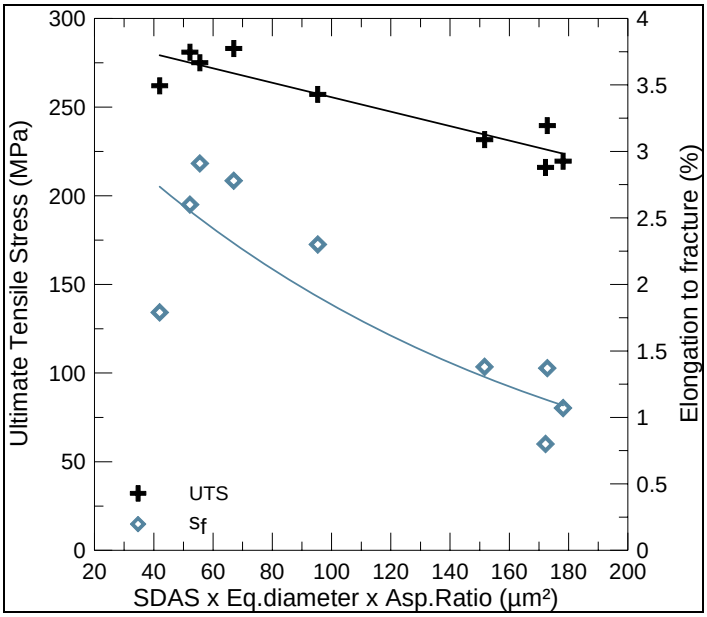

Figure 13. UTS and elongation values as function of the combined parameter SDAS × Equivalent diameter × Aspect ratio of eutectic Si particles.

4. CONCLUSIONS

Microstructure and mechanical properties of a HPDC 4-cylinders-in-line cylinder block have been analyzed. Based on the results obtained in the present study, the following conclusions can be drawn.

1. A fine microstructure is associated to high solidification rates in correspondence of casting wall and thin sections.
2. Higher solidification time leads to coarser microstructure, formed by large SDAS, eutectic Si particles with coarse plate-like morphology, as well as, higher fraction of blocky-like α-Al(Mn,Fe,Cr)Si phase.
3. In general, a low quantity of defects is detected within the castings. A small quantity of macroporosity are mostly detected in correspondence of the bulkhead supports and underneath liners, especially close to the vacuum line.
4. Mechanical properties are affected by microstructure. The best values of UTS and elongation to fracture are obtained for low SDAS values and small and more compact eutectic Si particles.
5. A coarser microstructure along with higher defect amount decreased the alloy strength, promoting fracture nucleation and propagation.
6. If the combined effect of α-Al and eutectic Si is taken into account, a linear correlation between UTS and product of SDAS, equivalent diameter and aspect ratio of Si particles can be observed; while the elongation to fracture shows an exponential trend, suggesting an high sensitivity on microstructural variation.

ACKNOWLEDGEMENTS

The European Project Nadia- New Automotive components Designed for and manufactured by Intelligent processing of light Alloys (NMP-2004-SME 3.4.4.5, contract n.026563-2) is gratefully acknowledged for financial support.

REFERENCES

[1] Colás, R., A. Rodríguez, J. Talamantes, and S. Valtierra. Solidification analysis of aluminium engine block. Int. J. Cast Metals Res., 17 (2004), 332-338.

[2] Verran,G.O., R.P.K. Mendes and M.A. Rossi. Influence of injection parameters on defects formation in die casting Al12Si1,3Cu alloy: experimental results and numeric simulation. J. Mater. Process Technol., 179 (2006), 190–195.

[3] Avalle, M., G. Bellingardi, M.P. Cavatorta and R. Doglione. Casting defects and fatigue strength of a die cast aluminium alloy: a comparison between standard specimens and production components. Int. J. Fatigue 24 (2002), 1-9.

[4] Timelli, G. and F. Bonollo. Quality mapping of aluminium alloy diecastings. Metal. Sci. Tech., 26 (2008), 2-8.

[5] Shabestari, S.G. and F. Shari. Influence of modification, solidification conditions and heat treatment on the microstructure and mechanical properties of A356 aluminum alloy. J. Mater. Sci., 39 (2004), 2023-2032.

[6] Viswanathan, S., A.J. Duncan, S.A. Sabau, Q. Han, W.D. Porter and B.W. Riemer. Modeling of Solidification and Porosity in Aluminum Alloy Castings. AFS Transactions, 98-103 (1998), 411-417.

[7] Rontó, V. and A. Roósz. The effect of the cooling rate or the local solidification time and composition on the secondary dendrite arm spacing during solidification Part II: Al-Mg-Si alloys. Int. J. Cast Metals Res., 13 (2001), 337-342.

[8] Grosselle, F., G. Timelli, F. Bonollo, A. Tiziani and E. Della Corte. Correlation between microstructure and mechanical properties of Al-Si cast alloys. Metall. Ital., 6 (2009), 25-32.

[9] Chen, Z.W. Skin solidification during high pressure die casting of Al-11Si-2Cu-1Fe alloy. Mater. Sci. Eng., A348 (2003), 145-153.

[10] Ye, H. An overview of the development of Al-Si alloy based material for engine applications. J. Mater. Eng. Perf., 12(3) (2003), 288-297.

[11] Samuel, F.H., A.M. Samuel and H.W. Doty. Factors controlling the type and morphology of Cu-containing phases in 319 Al alloy. AFS Trans., 104 (1996), 893-901.

[12] Niu, X.P, B.H. Hu and S.W. Hao. Effect of iron on the microstructure and mechanical properties of Al die-casting alloys. J. Mater. Sci. Letters, 17 (1998), 1727-1729

[13] Wang, Q.G. and C.H. Cáceres. Fracture mode in Al-Si-Mg casting alloys. Mater. Sci. Eng, A241 (1998), 72-82

[14] Wang, Q.G., C.H. Cáceres and J.R. Griffiths. Damage by eutectic particle cracking in aluminum casting alloys A356/357. Metall. Mater. Trans. A, 34 (2003), 2901-2912

[15] Cáceres, C.H. and J.R. Griffiths. Damage by the cracking of silicon particles in an Al-7Si-0.4Mg casting alloy. Acta Mater. 44 (1996), 25-33.

[16] Cáceres, C.H. and B.I. Selling. Casting defects and the tensile properties of an Al-Si-Mg alloy. Mater. Sci. Eng., A220 (1996), 109-116.

[17] Gokhale, A.M. and G.R. Patel. Origins of Variability in the fracture related mechanical properties of a tilt-pour-permanent-mold cast Al-alloy. Scripta Mater., 52 (2004), 237-241.

[18] Shankar, S. and D. Apelian. Die soldering: Mechanism of the interface reaction between molten aluminum alloy and tool steel. Mater. Trans., 33B (2002), 465–476.

[19] Jorstad, J.L. Understanding "Sludge". Die Casting Eng., November/December (1986), 30-36.

[20] Ghomashchi, M.R. Intermetallic compounds in an Al-Si Alloy used in high pressure die-casting. Z. Metallkunde, 78 (1987), 784–787.

[21] Seifeddine, S., T. Sjögren and I.L. Svensson. Variations in microstructure and mechanical properties of cast aluminium EN AC 43100 alloy. Proc. High Tech Die Casting, AIM, (2006), Vicenza.

[22] Zovi, A. and F. Casarotto. Silafont-36, the low iron ductile die casting alloy development and applications. Metall. Ital. 6 (2007), vol.,33–38.

[23] Asensio-Lozano, J. and B. Suárez-Peña. Microstructure-properties correlation of pressure die cast eutectic aluminum-silicon alloys for escalator steps (Part I). Mater. Characterization, 56 (2006), 169-177.

[24] Mondolfo, L.F. Manganese in Aluminum Alloys. The Manganese Center, (1978).

[25] Mo, A., M. M'Handi and H.I. Laukly. Modelling defect bend formation in Al-Si die casting. Proc. High Tech Die Casting, AIM, (2006), Vicenza.

ARTICLE 2

DOE APPLIED TO MICROSTRUCTURAL AND MECHANICAL PROPERTIES OF Al-Si-Cu-Mg CASTING ALLOYS FOR AUTOMOTIVE APPLICATIONS

Fabio Grosselle, Giulio Timelli, Franco Bonollo

Department of Management and Engineering – DTG
University of Padova
I-36100 Vicenza
ITALY

Accepted for publication in: Materials Science & Engineering A, 2009

ABSTRACT

Mechanical properties and microstructural features of an aluminium alloy are affected by several parameters, such us alloy composition, solidification rate and heat treatment. The analysis of the effects of each variable and their reciprocal interaction on the alloy behaviour plays a key role in order to develop a component with improved performance and well-known potentiality. The use of the Design of Experiment (DOE) methodology and the Analysis of Variance (ANOVA) can be a useful instrument to reach the aim. In this study, DOE and ANOVA have been applied to assess the concurring effects of the Cu content, the grain refinement, the solidification rate and the heat treatment on microstructural and mechanical properties of a secondary AlSi7CuMg foundry alloy for engine block application. The results indicate that the size of eutectic Si is controlled by the solidification time and by the interaction between Ti and Cu content, while the eutectic Si morphology depends mainly on the heat treatment process. The grain size is affected by the solidification time, the Ti content and the interaction between Cu and Ti. While the strength of the alloy increases with increasing Cu amount, cooling rate and after a heat treatment, the ductility decreases as the Cu amount and the solidification time increase.

KEYWORDS
Al-Si foundry alloys; design of experiment; microstructural properties; mechanical properties; automotive application

1. INTRODUCTION

Due to the excellent combination among castability, mechanical and technological properties, cast Al-Si alloys are widely used in automotive industry, where there is an increasing demand of light metals.
In particular, the use of cast aluminium alloys in engine components contributes to the enhancement in power rating owing to higher thermal conductivity of aluminium alloys compared to that of cast iron, which allows engines to work at higher temperatures and deliver more power per cylinder size. The addition of alloying elements, such as Mg and Cu, is mandatory for applications where an high strength at high temperature is required and ductility is not of prime importance, *e.g.* cylinder heads, manifolds and engine blocks [1]. The strengthening of these alloys is mainly due to the precipitation of hardening Mg- and Cu-rich phases, during ageing heat treatment [2-3].
In general, thermal treatments play a key role in the determination of the final physical and mechanical properties of aluminium alloys. Solution heat treatment dissolves coarse Mg- and Cu-rich particles, homogenising the microstructure; the spheroidization of eutectic Si particles and morphological changes of Fe-rich phase can also take place [4,5]. Quenching at higher rates after solution treatment preserves the supersaturated solid solution in the matrix at a maximum level, increasing the hardening effect through controlled precipitation in later stages of ageing [6].
Therefore, the final mechanical properties will be given by the interaction between the heat treatment processes and the alloy chemical composition [7-15].
It is easy to understand that the effect of composition and processes on microstructural features and mechanical properties is very difficult to analyze exhaustively due to the interactions among several factors.
Many studies have been carried out in order to investigate the effect of single variables on the properties of cast Al-Si-Cu-Mg alloys [2,7,10,16-21], even if the possible interactions among the variables have not been considered. Statistic tools, such as the Design of Experiments (DOE), have been taken from the exclusive world of the statistician and brought into the world of manufacturing, aiming at determining how different parameters influence the final casting properties [18-19].
The aim of this study is to assess the concurring effects of the Cu content, the grain refinement, the solidification rate and the heat treatment on microstructural and mechanical properties of cast AlSi7CuMg based alloy. An experimental Design of Experiment methodology is used.

2. THEORETICAL ASPECTS AND DESIGN OF EXPERIMENTAL MATRIX

The Design of Experiments (DOE) is a statistic approach to the experimental investigation that allows the analysis of the effect of several independent factors and their interaction on a dependent variable. An experimental matrix is implemented and it is composed of control factors at different levels for each run, that is the intensity assumed by each independent variable in a particular experiment [21-23]. In order to estimate the variance (experimental error) caused by slightly different experimental conditions, multiple experimental runs with the same factor settings are required.
Furthermore, when a factor, or an interaction of factors, can be considered to influence the response, the analysis of variance (ANOVA), based on density values,

should be performed. ANOVA is a statistical methodology, similar to a regression method, that allows to investigate and to model the relationship between a response and one or more predictor variables.

There are several types of ANOVA depending on the number of treatments and the way they are applied to the subjects in the experiments [23]:

- **One-way ANOVA** is used to test for differences among two or more independent groups. The one-way ANOVA is usually used to test for differences among at least three groups, since the two-group case can be covered by a t-test:
- **Factorial ANOVA** is used to analyze the effects of two or more treatment variables. The most commonly used type of factorial ANOVA is the 2×2 matrix, but it can also be multi-level such as 3×3 matrix or higher order;
- **Multivariate analysis of variance (MANOVA)** is used when there is more than one dependent variable.

In particular, the analysis of variance extends the two-sample t-test to test the differences among at least three groups. A hypothesis test is used to determine which statement is best supported by the data. These two statements are called the null hypothesis and the alternative hypotheses. They are always statements about populations attributes, such as the value of a parameter, the difference between corresponding parameters of multiple populations, or the type of distribution that best describes the population. The hypothesis has to be tested. The test calculates the probability of obtaining the observed sample data under the assumption that the null hypothesis is true. If this probability (the p-value) is below a user-defined cut-off point (the α-level), then this assumption is probably wrong. Therefore, the null hypothesis is rejected and the alternative hypothesis is selected. A detailed description of the ANOVA procedure is given elsewhere [23]. Briefly, the main concepts of ANOVA are described as follows [23]:

- **Source**: indicates the Source of variation, either from the factor, the interaction, or the error. The total is a sum of all the sources;
- **DOF:** Degrees of Freedom of each source;
- **SS-value:** Sum of Squares between groups (factor) and the sum of squares within groups (error);
- **MS-value:** Mean Squares are the result of dividing the Sum of Squares by the Degrees of Freedom;
- **F-value:** related to Fisher test, it is calculated by dividing the MS factor with the MS error. This value is then compared with a critical F-value found in the distribution Fisher table. This ratio allows to analyse the dependence between the variables;
- ***p*-value:** used to determine whether a factor is statistical significant; the higher the *p* level the less it is probable that the observed relation between two variables in the single sample is a reliable indicator of the relation between the respective variables in the population. A significant correlation was considered only when the *p* level was less than 0.05, *i.e.* there is a 5% probability that the relation between the variables found in the sample is fortuitous.

The results of the ANOVA procedure are the *main effect* and the *interaction effect* among the variables. A *main effect* is present when different levels of a factor affect the response differently. A main effects plot graphs the response mean for each factor level connected by a line. On the other hand, an interaction between factors occurs when the change in response from the low level to the high level of one factor is not the same as the change in response at the same two-levels of a second factor. The interaction effect can be displayed by means of interaction plot or Pareto chart.

In the interaction plot if the connecting lines are parallel to each other, no interaction is present while if the interaction lines cross each other interactions between factors have an effect on response.
In the Pareto Chart the effects are plotted in decreasing order of the absolute value of the standardized effects and they are compared to a reference line, drown for *p* value of 0.05. Any effect extending over this reference line is significant [23].
On the basis of level of significance, a regression model can be developed describing the relationship between the response and predictor variables. The reliability of the model by means of goodness coefficient R^2. It measures the quality of the least-squares fitting to the original data and it can be written as follows:

$$R^2 = 1 - \frac{\sum_{i=1}^{n} \left(f(x_i) - g(x_i)\right)^2}{\sum_{i=1}^{n} \left(f(x_i) - \overline{f}(x_i)\right)^2} \quad (1)$$

where x_i is the discrete variable, $g(x_i)$ is the corresponding calculated value using the regression function, $f(x_i)$ is the corresponding experimentally measured value, (x_i) is the mean value of experimental data and n is the total number of experimental points. When $R^2 = 1$, the fit is perfect.

In this work, a factorial ANOVA approach was implemented in order to investigate the effects of the cooling rate, the Ti content, the Cu level and the T7 heat treatment (independent variables) on the size and the morphology of eutectic Si particles and on the mechanical properties (dependent variables). The cooling rate has been evaluated by means of secondary dendrite arm spacing (SDAS) measurements.
Each independent variable was analysed at two and three levels. The independent variables, along with their values at selected levels, are given in Table 1. The possible interactions among the variables were studied. With the aim to take into account the highest degree of interaction, a full balanced factorial plan was implemented, as show in Table 2.

Table 1. Process parameters with their different levels of observation.

Parameter destination	Variable	Lower level	Central level	Higher level
A	SDAS (μm)	17	-	34
B	Titanium content (wt.%)	0	-	0.2
C	Copper content (wt.%)	2	3	4
D	T7 Heat treatment	0 (No)	-	1 (Yes)

Table 2. Control factors for each experimental combination.

Runs	SDAS (μm)	Ti content (%)	Cu content (%)	Heat Treatment
P01	17	0	2	0
P02	34	0	2	0
P03	17	0.2	2	0
P04	34	0.2	2	0
P05	17	0	3	0
P06	34	0	3	0
P07	17	0.2	3	0
P08	34	0.2	3	0
P09	17	0	4	0
P10	34	0	4	0
P11	17	0.2	4	0
P12	34	0.2	4	0
P13	17	0	2	1
P14	34	0	2	1
P15	17	0.2	2	1
P16	34	0.2	2	1
P17	17	0	3	1
P18	34	0	3	1
P19	17	0.2	3	1
P20	34	0.2	3	1
P21	17	0	4	1
P22	34	0	4	1
P23	17	0.2	4	1
P24	34	0.2	4	1

3. EXPERIMENTAL METHODS

The geometry of the casting, with the front and side views, is shown in Figure 1. The step casting presented a range of thickness going from 5 to 20 mm and it was gated from the side of the thinnest step, while the riser, over the casting, ensured a good feeding. This configuration allows to obtain a range of solidification rates and consequently different microstructures in the casting, corresponding to about 17, 24, 30 and 34 μm in SDAS [24].

Castings were produced by Teksid Aluminum. The weight of the aluminium alloy casting was 1.4 or 1 kg, including or not the runner system.

The two part die is split along a vertical joint line passing through the pouring basin. To facilitate assembly and mutual location the die halves are hinged. The dimension of the whole die was 310x250x115 mm^3 and the thickness of the two die halves was 45 and 75 mm respectively. The die was made by an AISI H11 tool steel and the weight was around 140 kg.

A semi-permanent layer of coating was spray applied on the die walls at the temperature of about 200°C according to standard practice. Before pouring the melt, the temperature of the die was increased to about 250±10°C. Trough the use of thermocouples the temperatures in different zones of the die were measured in order to evaluate the local temperature and assure a good reproducibility of the tests. The working temperature in the die was in the range of (450-520)±5°C.

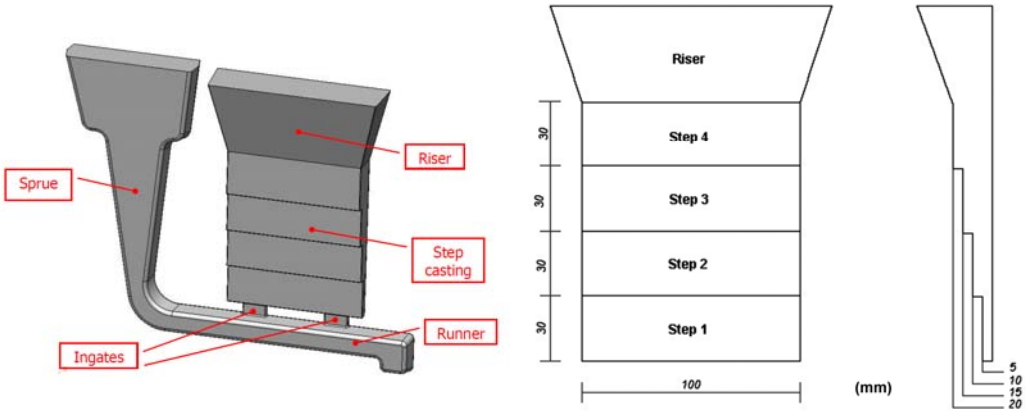

(a) (b)

Figure 1. (a) The step casting CAD geometry with (b) front and side views.

The base AlSi7Cu2Mg secondary alloy was supplied by Raffineria Metalli Capra as commercial ingots, containing 7%Si, 2%Cu, 0.4%Mg, 0.6%Fe, 0.45%Mn and balance Al. The Cu content was increased to ~3% and ~4% respectively by adding pure Cu into the base material during melting. The chemical composition of the alloys used in this work, as obtained by an atomic emission spectrometer, is given in Table 3.

Table 3. Chemical composition of the alloys studied in the present work (wt.%).

Alloy	Al	Si	Cu	Fe	Mg	Mn	Ni	Zn
AlSi7Cu2Mg	bal.	6.77	2.25	0.60	0.46	0.45	0.05	0.64
AlSi7Cu3Mg	bal.	6.89	3.33	0.59	0.45	0.46	0.06	0.70
AlSi7Cu4Mg	bal.	6.45	4.01	0.66	0.50	0.45	0.05	0.66

The material was first melted in an electric-induction furnace set at 720±5°C and then held for alloying and melt treatment. AlTi5 rod type grain refiner was also added to the molten metal when required by the experimental plan. Before pouring, the melt was degassed with an argon-sulphur hexafluoride mixture (Ar/SF_6 0.2%).
When the heat treatment was planned, the castings were subjected to a T7 heat treatment. The step castings were solution heat treated in an electric-resistance heated-air-circulating box-type muffle furnace at 480±1°C for 4 h and immediately quenched in water at room temperature. The temperature of the electric furnace was set; when it was stable for at least 30 minutes, the castings were inserted inside the furnace. The castings were then artificially aged at 220±1°C for 5 h. This is a typical overageing treatment used in the manufacture of engine blocks [25].
Flat tensile specimens were machined from the step of thickness 5 and 20 mm and were 90 mm long, 20 mm wide, and 3 mm thick, with a gage length of 30 mm and a width of 10 mm, according to ASTM-B577. Five specimens were prepared for each combination of alloy composition, SDAS and heat treatment condition (Table 2). Radiographic inspection has been performed on tensile specimens before mechanical testing, in order to assure an acceptable level of soundness.
The tensile tests were done on a computer controlled tensile testing machine. The crosshead speed used was 2 mm/min ($\dot{\varepsilon} \sim 10^{-3}$ s^{-1}). The strain was measured using a 25-mm extensometer. Experimental data were collected and processed to provide yield stress (YS, actually 0.2% proof stress), ultimate tensile strength (UTS) and elongation to fracture (s_f).

For the analysis in this paper, the average of the best two values (out of five) of UTS, s_f for each condition were used. The best values in terms of quality index, Q [26], were selected in an attempt to minimise any effects arising from casting defects on the fracture data and mechanism [27-30] and to maximise the chance of isolating the effects of alloy composition, SDAS and heat treatment.
The samples from each run were cut from the cross section of the gage length and mechanically prepared to a 3-μm finish with diamond paste and, finally, polished with a commercial fine silica slurry for metallographic investigations. Microstructural analysis was carried out using an optical microscope and quantitatively analyzed using an image analyzer. The image analysis was focused on the size, aspect ratio and roundness of the eutectic silicon particles. Size is defined as the equivalent circle diameter (d); the aspect ratio (α) is the ratio of the maximum to the minimum Ferets; the roundness (r) is defined as:

$$r = \frac{p^2}{4 \times \pi \times A} \tag{2}$$

where p and A are the perimeter and the area of the particle respectively.
To obtain a statistical average of the distribution, a series of at least 10 photographs of each specimen were taken; each measurement included more than 600 particles. The secondary phases, such as the Mg_2Si, $CuAl_2$ particles, and the iron-rich intermetallics were excluded from the measurements on the base of particles morphology and colour.
Average SDAS values were obtained using the linear intercept method, which involves measuring the distances (spacing) between secondary dendrite arms along a line normal to the dendrite arms.
To quantitatively calculate the grain size in the tensile specimens, the polished specimens were etched in a Keller etchant (7.5 mL HNO_3, 5 mL HCl, 2.5 mL HF and 35 mL H_2O) [31]. The grain size was measured using the intercept method, according to the ASTM-E112.
The ANOVA was performed on step sizes of thickness 5 and 20 mm, according to the DOE matrix of Table 1. In order to apply the analysis, the total number of measurements was divided into three subsets and the average value and the distribution were calculated for each one. The hypothesis of a normal distribution of the data has been verified.

4. RESULTS AND DISCUSSION

4.1 Microstructural observations

The microstructure consists of a primary phase, α-Al solid solution, and an eutectic mixture of aluminium and silicon. α-Al precipitates from the liquid as the primary phase in the form of dendrites. The scale of microstructure in different zones of the step castings analysed is characterized by means of SDAS measurements and then correlated with mechanical properties. The coarseness of the microstructure varied inversely with the casting thickness, *i.e.* the solidification rate. No significant variation among the alloys was noted in SDAS measurements made at equivalent positions in the castings.
Typical microstructures of the as-cast step castings are shown in Figure 2, referred to the step-1 and step-3, corresponding to ~17 and ~34 μm in SDAS respectively. The eutectic Si particles show a lamellar morphology and the amount of Al_2Cu phases increases by increasing the Cu content up to 4 wt.%. The Fe-rich intermetallics are

observed in the microstructure both in the form of coarse α-Al(FeMnSi) particles and needle shape β-Al_5FeSi.

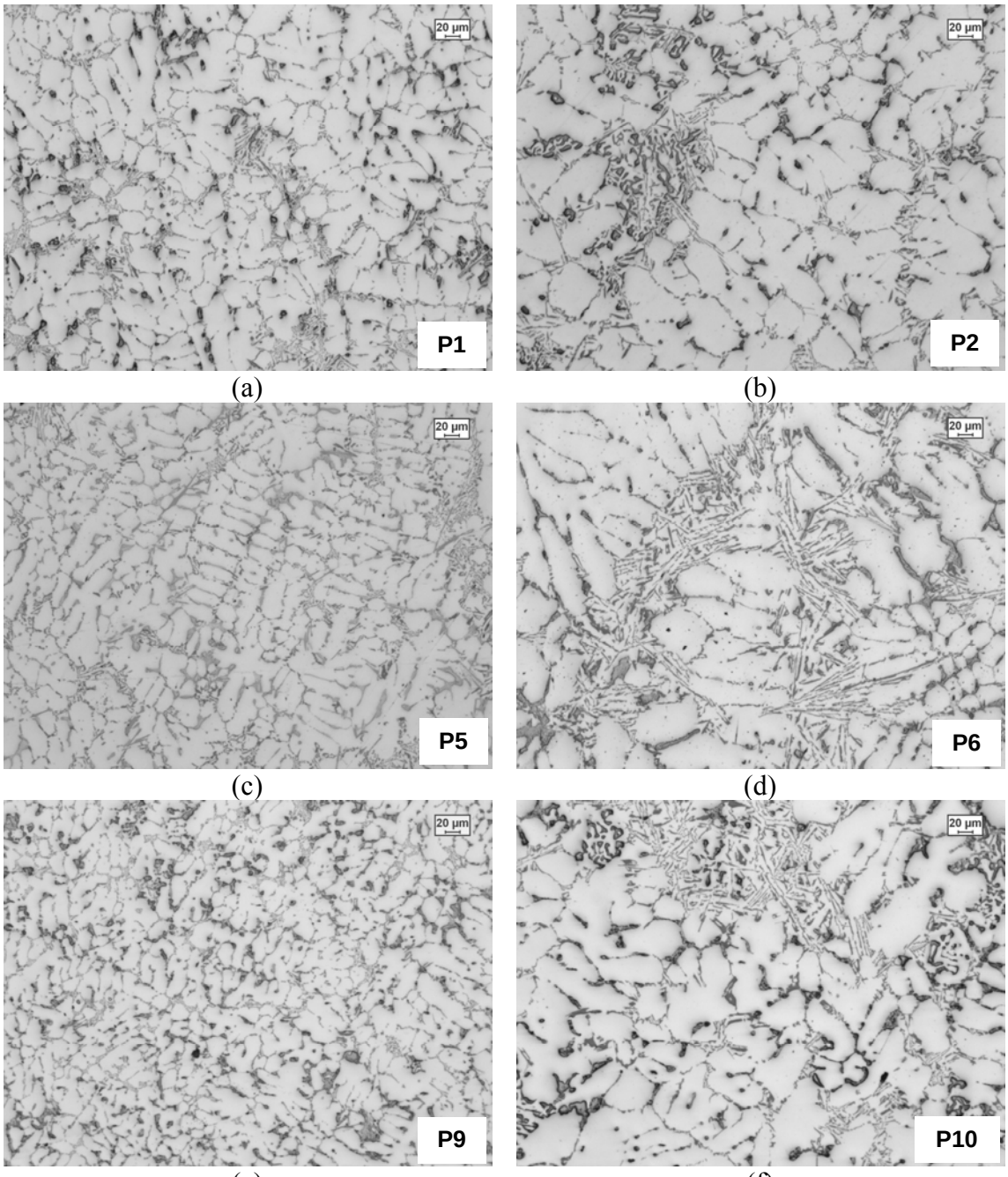

Figure 2. Microstructure of as-cast samples where a), c) and e) correspond to SDAS of 17 µm with 2, 3 and 4 wt.% Cu respectively; the microstructure of as-cast samples corresponding to SDAS of 34 µm is presented in the same manner in b), d) and f).

The microstructural features of the analysed alloys in the T7 heat treated conditions are shown in Figure 3. The micrographs show that the silicon particles have undergone some changes due to the heat treatment, independently from the Cu content. The shape is altered from lamellar to spherical morphology and this behaviour is more pronounced in the samples with SDAS of 17 µm than for the 34 µm SDAS where the silicon is more elongated. These findings are in agreement with the results reported in References [12,32-35].

Un-dissolved θ-$CuAl_2$ particles can be also noted in the interdentric regions and at grain boundaries, especially in sample with high Cu content and high SDAS. An increased Cu and SDAS value along with low solutioning temperature reduce dissolution rate and, thus, lead to remaining θ phase even after solutioning treatment [36-37].

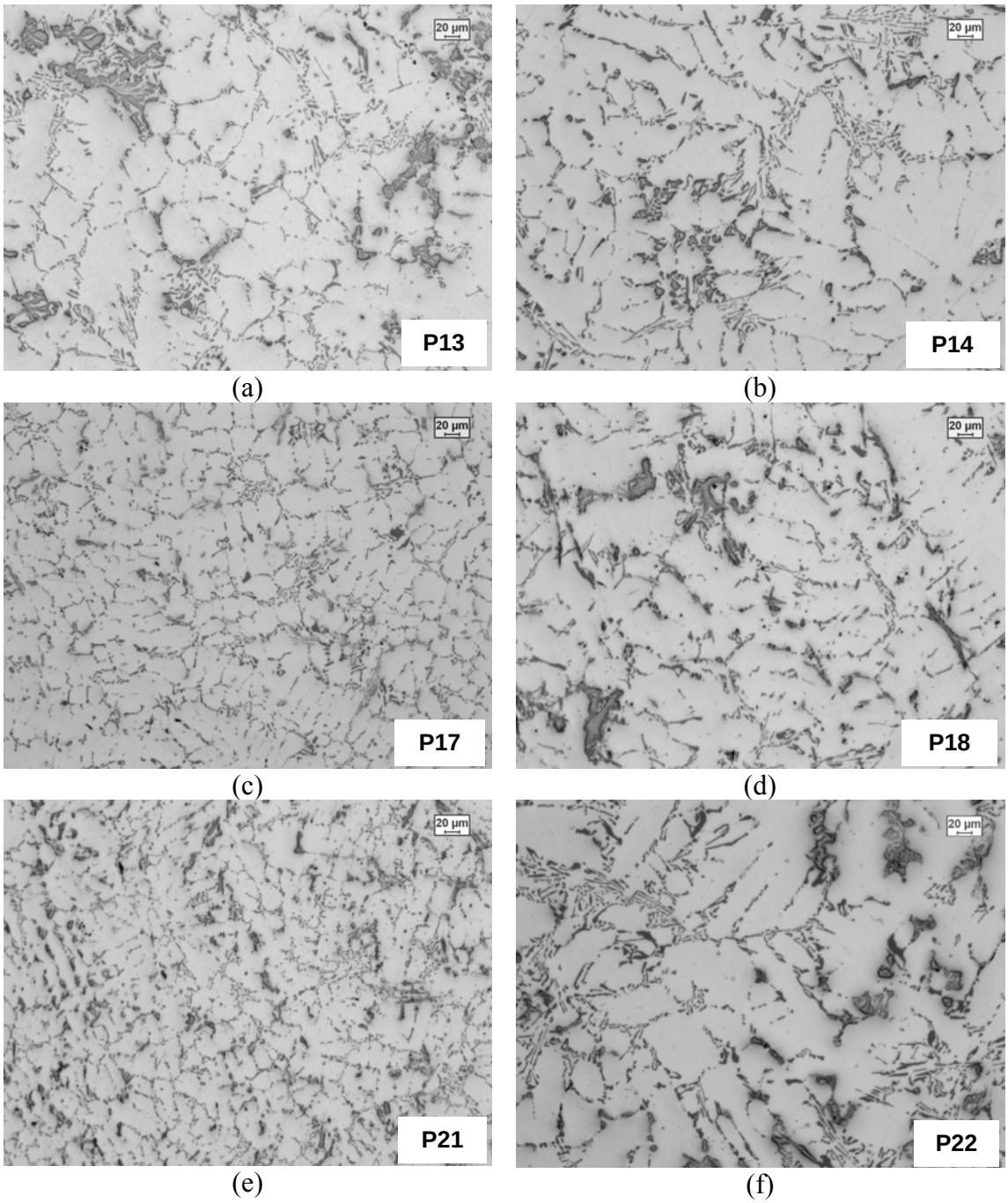

Figure 3. Microstructure of T7 heat treated samples where a), c) and e) correspond to SDAS of 17 µm with 2, 3 and 4 wt.% Cu respectively; the microstructure of T7 heat treated samples corresponding to SDAS of 34 µm is presented in the same manner in b), d) and f).

Table 4 collects the average values and the standard deviation of the eutectic Si features. In general, it can be stated that the runs with SDAS of 17 μm show the lowest values of equivalent diameter and roundness; higher cooling rates promote faster nucleation and growth, resulting therefore to finer eutectic Si particles [12].
In addition, the T7 heat treatment plays a key role on the eutectic Si morphology. The solution heat treatment affects the morphology of the particles making them rounder. It has been reported that solution heat treatment changes the morphology of eutectic silicon from a polyhedral to a globular structure and that the kinetics of spheroidization and coarsening processes occur much more rapidly in a modified structure [32-33,38]. Rayleigh instability [39] occurs; silicon particles undergo necking and are broken down into fragments. Due to the instability of the interfaces between the two different phases and a reduction in the total interface energy, spheroidization and coarsening processes occur. Because the coarsening and spheroidization are diffusion-controlled processes, they are directly proportional to the solution temperature and time. In the present work, the low solution temperature and the short solutioning time are insufficient to promote a complete coarsening of the unmodified Si particles during the heat treatment. This leads to a slightly effect on the eutectic Si dimensions. In unmodified alloys, the Si crystals are coarse and relatively unaffected by the solution heat treatment. However, after short times of heat treatment, small silicon crystals may fragment and the edges of the particles become more rounded [32]. The iron-rich intermetallic particles are not significantly affected by the solution heat treatment used in the present work, in accordance with Reference 40.

Table 4. Average diameter (*d*) and roundness (*r*) of eutectic Si particles for each of the experimental combinations (Standard deviation in parentheses).

Runs	Equivalent diameter, *d* (μm)	Roundness, *r*	Runs	Equivalent diameter, *d* (μm)	Roundness, *r*
P01	2.3 (1.1)	4.1 (2.9)	*P13*	2.9 (1.2)	1.7 (0.9)
P02	4.6 (3.5)	5.4 (5.2)	*P14*	4.2 (2.2)	2.9 (2.0)
P03	2.9 (1.7)	4.3 (3.3)	*P15*	3.5 (1.8)	2.3 (1.4)
P04	4.8 (3.6)	4.7 (4.6)	*P16*	5.3 (2.9)	3.5 (2.9)
P05	3.3 (1.9)	5.1 (4.9)	*P17*	2.8 (1.8)	2.0 (1.1)
P06	4.5 (2.9)	5.2 (4.5)	*P18*	4.1 (2.7)	2.5 (1.7)
P07	4.4 (2.7)	6.6 (5.8)	*P19*	4.2 (2.1)	2.5 (1.7)
P08	6.3 (4.0)	6.3 (5.0)	*P20*	5.4 (4.2)	2.5 (2.9)
P09	2.7 (1.4)	3.9 (3.1)	*P21*	2.6 (1.6)	1.7 (1.1)
P10	4.5 (3.0)	5.4 (4.8)	*P22*	3.7 (2.2)	2.5 (1.7)
P11	4.3 (2.5)	3.9 (3.1)	P23	4.0 (2.0)	2.5 (1.7)
P12	7.5 (4.0)	7.1 (7.3)	*P24*	5.7 (2.6)	2.6 (1.8)

4.1.1 Equivalent diameter of eutectic Si particles

The subsequent analysis of the data by means of ANOVA reveals a complete and more exhaustive evaluation of the relationship between the average size of the eutectic Si particles and the independent variables, such as SDAS, Cu content, Ti addition and T7 heat treatment. The *main effects* as well as the interactions are displayed in Figure 4a and 4b.

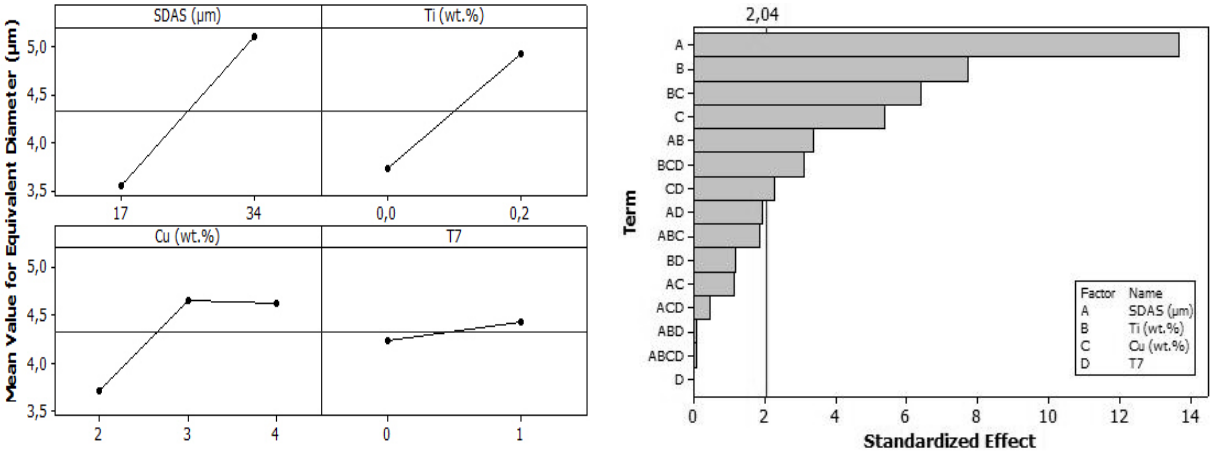

(a) (b)

Figure 4. (a) Main effects chart displaying the influence of SDAS, Cu content, Ti addition and T7 heat treatment (independent variables) on the equivalent eutectic Si diameter (dependent variables); (b) the Pareto chart evaluates the possible interactions among the variables.

While the main factor affecting Si size is the solidification condition, the effect of Ti and Cu content and their interaction can not be neglected. In particular, decreasing SDAS from 34 to 17 µm the equivalent diameter of eutectic Si particles decreases from ~5.1 to ~3.6 µm as a consequence of a faster cooling rate that promotes the nucleation [12,15,41]. An increased value of the average Si diameter is observed by increasing Ti content up to 0.2 wt.%; the average diameter increases from 3.7 µm in non-grain refined alloy to 4.9 µm in the grain refined alloy. In agreement with hypothesis of Nafisi *et al.* [42] the eutectic reaction can be thought as starting with the formation of Al-rich spikes nucleating on the primary Al dendrites. The consequence of such morphological development is the formation of localized Si enrichment within interdendritic liquid and eventual segregation of numerous small silicon particles. Thus, some of these small Si particles act, in the same manner as the impurity based particles of β-AlFeSi or AlP, as nucleation sites for the eutectic Si [43-44]. Consequently, the presence of Ti, promoting the nucleation of α-Al dendrites, reduces the interdentritic spaces; a liquid enriched in Silicon is obtained and coarser eutectic Si particles are formed. The results obtained in the present work seem to be in contrast with the work of Grab *et al.* [15] where the presence TiB_2 particles reduces the size and changes the morphology of eutectic Si particles.
In addition to SDAS and Ti amount, the Cu content and its interaction with the Ti addition seem to have an effect on the dimension of eutectic Si particles. In particular, increasing the Cu content from 2 up to 3 wt.%, the size of Si particles increases from ~3.7 to ~4.6 µm and it is steady with further Cu addition. Heusler *et al.* [45] stated that the introduction of Cu into Al–Si alloys results in an eutectic modification. In particular, an addition exceeding 1.2 wt.% Cu leads to regions with coarser eutectic suggesting a certain overmodification. In the present work, this effect is more evident in grain refined alloy as shown in Figure 5.

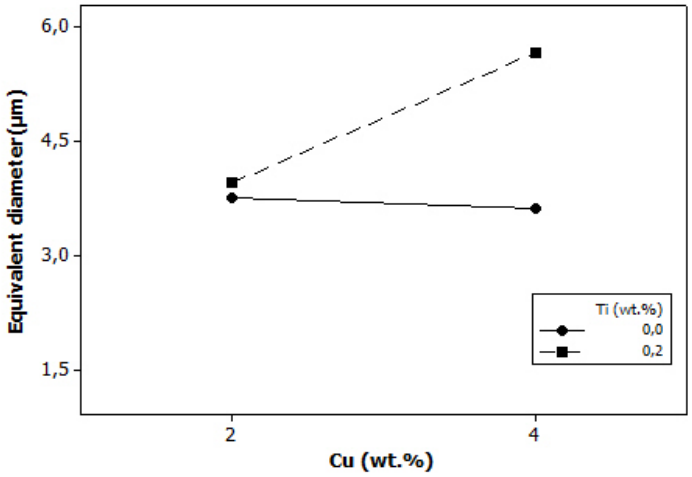

Figure 5. Interaction effect of Cu and Ti on the equivalent eutectic Si diameter.

Increasing the Cu content from 2 to 4 wt.%, the average dimension *d* of the eutectic Si particles grows from 3.9 up to 5.6 µm in the grain refined alloys, while it remains constant at about 3.7 µm in the un-refined alloys (Figure 5).
No references for the combined effect of Cu and Ti addition on the size of eutectic Si particles were found in literature to allow for a useful comparison. Thus, a full explanation of the phenomena requires further analysis.
In the considered range of data, the average eutectic Si diameter can be described by the following model with R^2=0.82:

$$d = 0.93+(0.12 \times \text{SDAS})-(8.28 \times \text{Ti})-(0.073 \times \text{Cu})+(4.62 \times \text{Ti} \times \text{Cu}) \qquad (3)$$

where SDAS is in µm, while the Ti and Cu content are in wt.%.

4.1.2 Roundness of eutectic Si particles

The effects of SDAS, Cu content, grain refinement and T7 heat treatment on the roundness of eutectic Si particles are shown in Figure 6a and 6b as analysed by ANOVA.

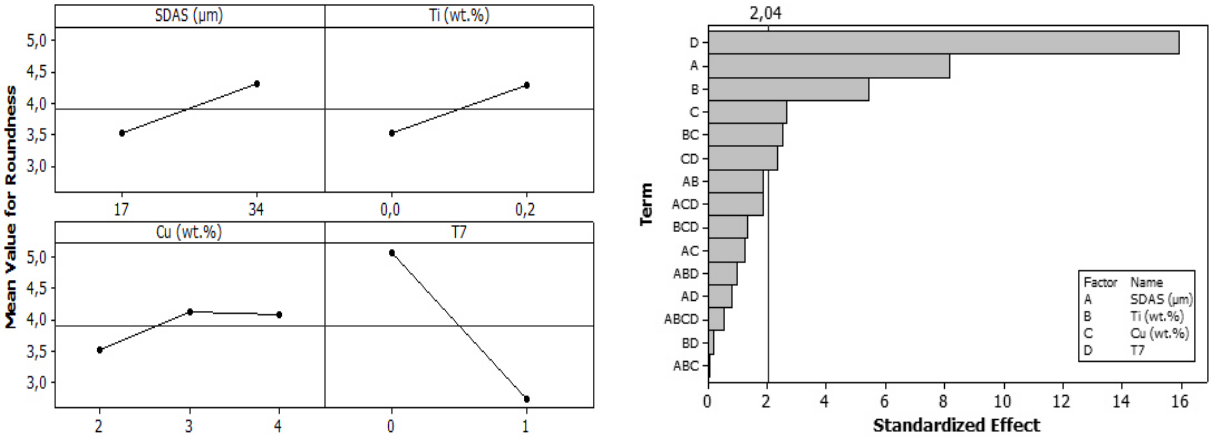

Figure 6. (a) Main effects chart displaying the influence of SDAS, Cu content, Ti addition and T7 heat treatment (independent variables) on the roundness of eutectic Si particles (dependent variables); (b) the Pareto chart evaluates the possible interactions among the variables.

The role of heat treatment in spheroidizing the eutectic Si is confirmed by ANOVA results. In *main effects* diagrams it can be noted that T7 heat treatment allows to reduce the roundness to a value of 2.8, about 45% less than the as-cast specimens.
The solidification time and the Ti content influence significantly the eutectic Si morphology, while the Cu amount doesn't show any effect.
The decreasing SDAS from 34 to 17 µm, the roundness decreases from 4.3 to 3.5 as a consequence of a faster solidification rate, which changes the eutectic Si shape in a similar way to chemically modified eutectic Si [46-48].
Figure 6 shows that the morphology of the Si particles is also influenced by the Ti content. In the grain refined alloys the average roundness value is ~5, which is 28% higher than in the un-refined alloys. This behaviour can be attributed to the growing mechanism of eutectic Si particles as previously described [43-44].
In the considered range of data, the average Si roundness can be described according to the following equation:

$$r = 1.64+(0.07 \times \text{SDAS})+(3.99 \times \text{Ti})-(1.17 \times \text{T7}) \quad (4)$$

where SDAS is in µm, Ti in wt.% and the variable T7 assumes value 0 or 1 for as-cast and heat treated temper, respectively. In this case, the goodness coefficient R^2 is 0.87.

4.1.3 Grain Size

The effects of SDAS, Cu content, grain refinement, T7 heat treatment, and their interactions on the grain size have been investigated by ANOVA. In Figure 7a the results of *main effects* are reported while the effect of interaction between Cu and Ti is shown in Figure 7b.

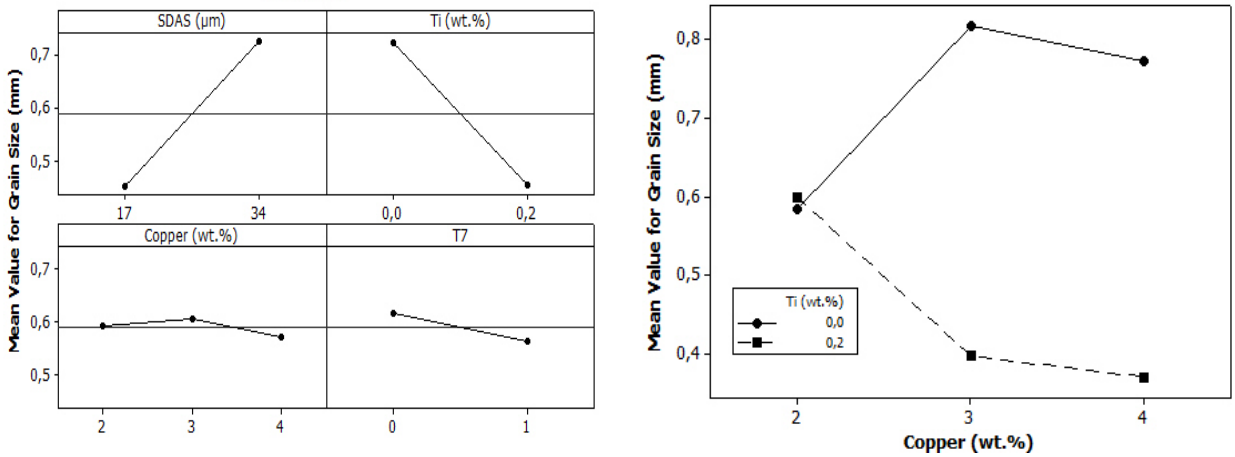

(a) (b)

Figure 7. (a) Main effects chart displaying the influence of SDAS, Cu content, Ti addition and T7 heat treatment (independent variables) on the grain size (dependent variables); (b) the effect of the interaction between Cu and Ti content on the grain size.

As expected, the main factors affecting the dimension of grain are the solidification time and the Ti addition. A faster solidification rate allows to reduce the grain from about 0.7 to 0.4 mm. The same variation can be observed considering the only effect of the grain refiner. The $TiAl_3$ particles act as nucleants in cast aluminium alloys,

increasing the sites for nucleation of α-Al phases, and consequently, producing a finer microstructure [46].
Figure 6b evidences the interaction between Ti and Cu as affecting the grain size. In the un-refined alloys, the addition of Cu leads to coarser grains. Increasing the Cu content up to 3 wt.%, the grain size grows up to 0.8 mm (~37%). A further addition of Cu seems to be un-affecting. On the other side, in the grain refined alloys, an higher quantity of Cu reflects upon a variation of the grain size, which decreases from 0.5 a 0.3 mm as consequence of the Ti addition. No references for the combined effect of Cu and Ti content on the grain size were found in literature to allow for a useful comparison. Further analysis will be needed to explain the results.

4.2 Tensile testing

The mean values and the standard deviation of YS, UTS and elongation to fracture are collected in Table 5. Some preliminary considerations can be done about the effect of SDAS, Cu and Ti content and heat treatment on mechanical properties. It can be noted that an increased Cu content reflects upon enhanced strengthening both in as-cast and heat treated samples. The strengthening is also improved by heat treatment leading to much higher values of YS and UTS. The effect of SDAS is more evident in ductility: an increased solidification time reduces the elongation to fracture.
In some runs, an expected high value of standard deviation can be observed as consequence of difficulties to completely isolate the impact of defect on mechanical properties.

Table 5. Average YS, UTS and s_f values for each of the experimental combinations (Standard deviation in parentheses).

Runs	YS (MPa)	UTS (MPa)	s_f (%)	Runs	YS (MPa)	UTS (MPa)	s_f (%)
P01	159 (3)	210 (17)	1.3 (0.4)	*P13*	255 (1)	292 (1)	1.4 (0.1)
P02	161 (7)	204 (1)	1.1 (0.1)	*P14*	244 (4)	272 (11)	1.1 (0.3)
P03	137 (11)	209 (8)	1.7 (0.1)	*P15*	261 (1)	308 (5)	1.7 (0.3)
P04	161 (1)	214 (7)	1.3 (0.1)	*P16*	258 (1)	278 (4)	0.9 (0.1)
P05	160 (12)	212 (11)	1.1 (0.1)	*P17*	268 (9)	305 (2)	1.2 (0.1)
P06	172 (10)	210 (11)	0.9 (0.1)	*P18*	266 (6)	289 (2)	1.0 (0.1)
P07	171 (5)	213 (13)	0.5 (0.5)	*P19*	260 (2)	309 (23)	1.6 (0.6)
P08	182 (3)	225 (6)	1.1 (0.1)	*P20*	263 (1)	296 (2)	1.1 (0.0)
P09	169 (2)	242 (12)	1.4 (0.3)	*P21*	256 (1)	316 (4)	1.7 (0.1)
P10	182 (8)	218 (2)	0.9 (0.1)	*P22*	256 (1)	284 (1)	1.0 (0.1)
P11	187 (6)	227 (2)	0.9 (0.1)	P23	279 (4)	321 (4)	1.2 (0.1)
P12	187 (2)	207 (3)	0.7 (0.1)	*P24*	267 (1)	289 (12)	0.9 (0.2)

The subsequent analysis of the data by means of ANOVA reveals a complete and more exhaustive evaluation of the relationship between independent and dependent variables.
In Figure 8, the main effect diagrams and the Pareto charts summarize the effects of the independent variables on the YS of the analysed alloys.

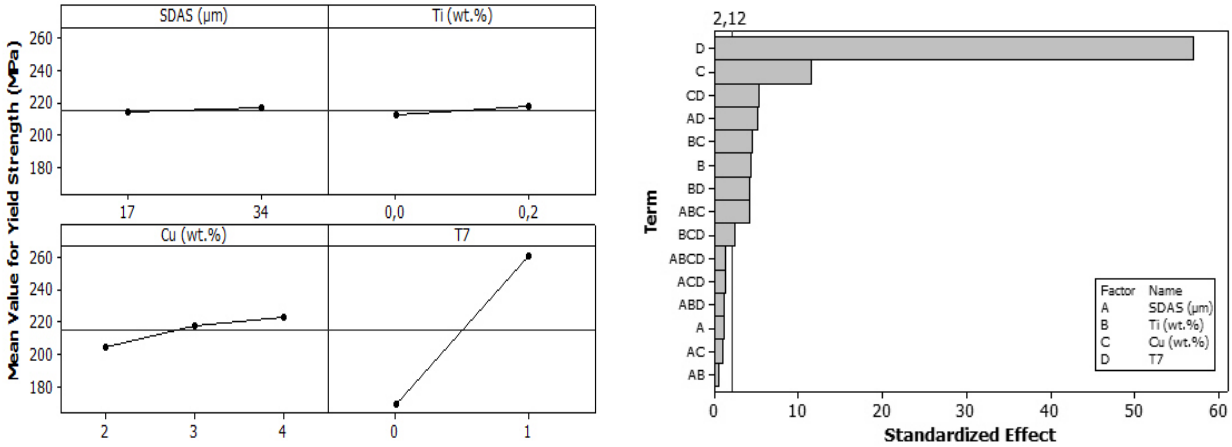

(a) (b)

Figure 8. (a) Main effects chart displaying the effects of SDAS, Cu content, Ti addition and T7 heat treatment (independent variables) on YS (dependent variable) of the analysed alloys; (b) the Pareto chart evaluates the possible interactions among the variables.

It can be observed that the T7 heat treatment plays a key role in the determination of YS. In the T7 specimens, the mean value is 267 MPa, 41% higher than the as-cast specimens. The reason for the increase in strength during T7 heat treatment is primarily due to the precipitation of metastable phases from the supersaturated solid solution. The reason is the formation of a high density of β'/β-Mg_2Si and θ'/θ-$AlCu_2$ precipitates obstructing the movement of dislocations.

Considering *main effect* graph, it can be stated that the strength is also enhanced by the Cu content as consequence of its influence in the precipitation of θ and β precipitates [3,49]. In detail, YS varies linearly from 223 MPa for the alloy with 4 wt.% of Cu to 204 MPa in the case of 2 wt.% of Cu.

No other factor or interactions seem to affect the YS. In the considered range of data, the YS can be described according to the following regression model (R^2=0.95):

$$YS=186.2+(9.2 \times Cu)+(45.8 \times T7) \quad (5)$$

where Cu is in wt.% and the variable T7 assumes value 0 or 1 for as-cast and heat treated temper, respectively

In Figure 9 the results of ANOVA for UTS are shown. The main factors are the T7 heat treatment, the Cu content and the SDAS values.

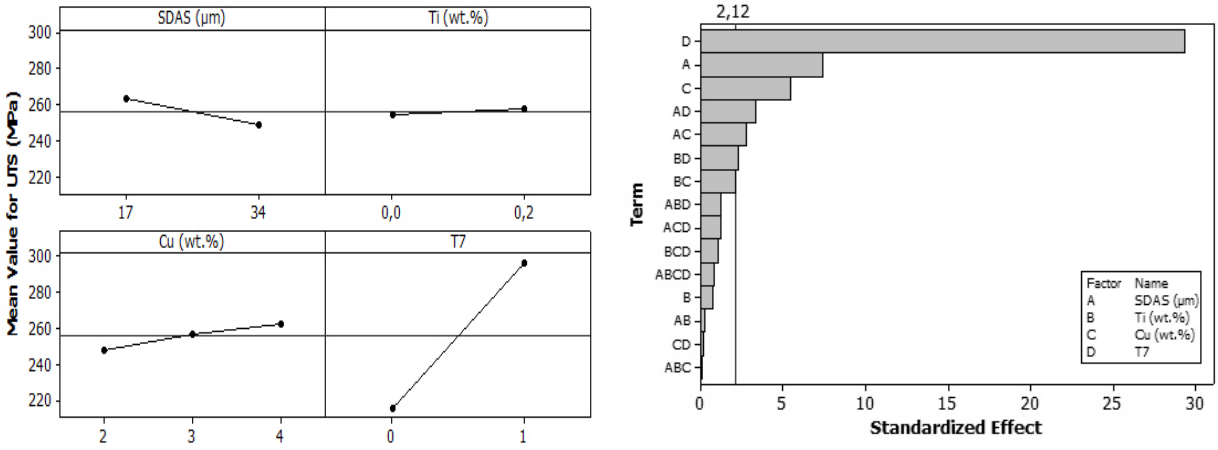

(a) (b)

Figure 9. (a) Main effects chart displaying the effects of SDAS, Cu content, Ti addition and T7 heat treatment (independent variables) on UTS (dependent variable) of the analysed alloys; (b) the Pareto chart evaluates the possible interactions among the variables.

Considering the solidification rate, the UTS decreases from 270 to 240 MPa as SDAS increases from 17 to 34 µm. As previously said, by increasing the solidification time, coarser and longer eutectic Si particles are observed in the microstructure. During plastic deformation, the tension field around the particles is thus increased promoting cleavage mechanism; low strain values are then associated to transition from intergranular to transgranular fracture.[50-52].

The morphology evolution of eutectic Si particles during the solution heat treatment along with the precipitation of hardening phases reflect upon higher UTS values. As result, the mean value of UTS increases from ~215MPa for as-cast samples to ~293 MPa, obtained for heat treated specimens.

Improved mechanical properties are also observed for increased Cu content. As Cu varies from 2 up to 4 wt.%, UTS increases linearly from 248 to 263 MPa due to an high quantity of Al_2Cu precipitates. In the considered range of data, the UTS can be described according to the following regression model:

$$UTS=263-(1.2 \times SDAS)+(7.3 \times Cu)+(39.3 \times T7) \quad (6)$$

where the variables have been previously described and R^2 is 0.95.

The effect of Ti addition on the YS and UTS is negligible in the range of data of the present work. Generally, in Al-Si alloys, the improvements carried out by grain refiners are mainly due to better porosity distribution rather than to any decrease in grain size [46]. Remember that, in this study, the best samples in terms of quality index Q were selected with the aim to minimise the effects of casting defects and, thus, among with the porosities.

In Figure 10 the results of ANOVA for the elongation to fracture are shown.

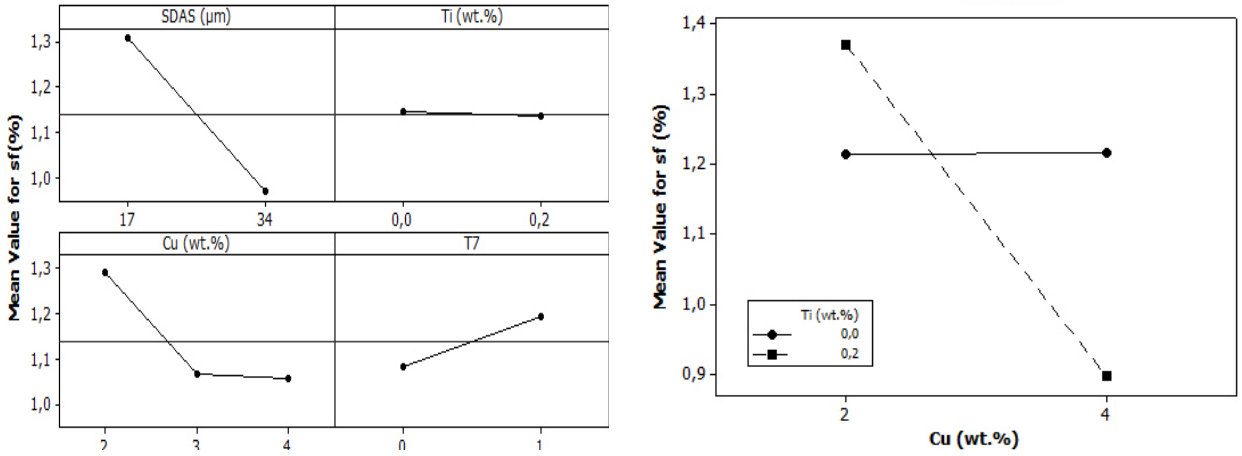

(a) (b)

Figure 10. Main effects chart displaying the effects of SDAS, Cu content, Ti addition and T7 heat treatment (independent variables) on elongation to fracture (dependent variable) of the analysed alloys; (b) the effect of the interaction between Cu and Ti content on the elongation to fracture.

The elongation to fracture is mainly affected by SDAS, Cu content and T7 heat treatment. Increasing the solidification time, the subsequent transition from intergranular to transgranular fracture mode leads to a reduction in ductility which is moreover influenced by the size and morphology of eutectic Si [40]; thus, the elongation to fracture decreases from 1.3 to 0.96% by increasing the SDAS from 17 to 34 µm.

The increase of mechanical strength due to higher Cu amount is accompanied by a higher density of hardening precipitates, thereby increasing the micro stresses, resulting in a reduction of matrix deformation and thus decreasing ductility [1,49]. Increasing the Cu content from 2 to 4 wt.%, the elongation to fracture exponentially decreases from 1.3% to 1.15% (~19%). The effect of Cu is moreover significant in presence of Ti as seen in Figure 10b. In the alloys with 2 wt.% Cu, the addition of Ti slightly enhances the ductility (~13%); with further additions of Cu up to 4 wt.%, the elongation to fracture is steady at ~1.2% in the un-refined alloys, while it decreases from 1.3% to 0.9% in refined alloys as a consequence of coarser eutectic Si particles, as observed in Figure 4

The T7 heat treatment slightly affects the ductility about 1.2% (Figure 10). This observation suggests a mismatch between an increase in strength and the improvement of the features of the silicon particles brought about by the solution treatment. While in the solution treatment changed the silicon particles size and morphology, the highest density of β'-Mg_2Si and θ'-Al_2Cu precipitates with their needle-like shapes and brittle behaviour, increased the micro-stresses; as showed by Zhang *et al.* [36], this resulted in the reduction of α-Al matrix deformation, thus decreasing ductility. These precipitates are brittle and may fracture at very low strains during deformation, accelerating the growth of the crack.

In the considered range of data, the elongation to fracture can be described according to the following regression model with R^2=0.67:

$$s_f = 1.83 - (0.0242 \times SDAS) + (0.0013 \times Cu) - (1.19 \times Cu \times Ti) + (0.0404 \times T7) \quad (7)$$

where each variable has been previously described.

5. CONCLUSIONS

The DOE and ANOVA approaches have been implemented to assess the concurring effects of the Cu content, the Ti addition, the solidification rate and the T7 heat treatment on microstructural and mechanical properties of cast AlSi7CuMg based alloy for engine block application. The following conclusions can be drawn from this work.

1. The eutectic Si size is affected by both the solidification process and the alloy composition. The size increases by increasing SDAS and Cu content. The effect of Cu is more evident in presence of Ti; the combined effect of Cu and Ti leads to a coarser microstructure.
2. The eutectic Si roundness depends mainly on the T7 heat treatment; the solution heat treatment leads to a morphology evolution resulting in rounder particles. The effect of SDAS and Ti content is also evident: as the solidification time and Ti content increase, a coarser morphology is obtained.
3. The solidification time, the Ti addition and the interaction between Cu and Ti are the main factors influencing the grain size. A faster solidification rate and Ti addition allow to reduce the average dimension of grains, while increasing the Cu content, coarser grains are observed in un-refined alloys.
4. The YS is improved by the T7 heat treatment due to the precipitation of hardening β'-Mg_2Si and θ'-Al_2Cu phases. The strengthening is also enhanced by increasing the Cu content.
5. The UTS depends on SDAS, T7 heat treatment and Cu content due to their influence on the morphology of silicon particles and on the precipitation of hardening phases.
6. The ductility of the analysed alloys decreases as the Cu content and solidification time increase and the effect of Cu is more evident in grain refined alloys. The T7 heat treatment improves the ductility by changing the morphology of eutectic Si particles.

ACKNOWLEDGEMENT

This work was developed with the financial support of The European Project NADIA (New Automotive components Designed for and manufactured by Intelligent processing of light Alloys, NMP-2004-SME 3.4.4.5, contract n.026563-2)

REFERENCES

[1] C.H. Caceres, I.L. Svensson, J.A. Taylor, Int. J. Cast Metal. Res. 15 (2003) 531-543.

[2] M. Tash, F.H. Samuel, F. Mucciardi, H.W. Doty, Mater. Sci. Eng. A 443 (2007) 185–201

[3] Y.J. Li, S. Brusethaug, A. Olsen, Scr. Mater. 54 (2006) 99–103.

[4] L. Anantha Narayanan, F.H. Samuel, and J.E. Gruzleski, Metall. Mater. Trans. A 26A (1995) 2161–74.

[5] Murat Tiryakioglu, Mater. Sci. Eng. A 473 (2008) 1–6

[6] S. Seiffedine, G. Timelli, I.L. Svensson, Int. Foundry Res. 59 (2007) 2-10.

[7] L. Heusler, W. Schneider, J. Light Met. 2 (2002) 17–26.

[8] A. T. Joenoes, J. E. Gruzleski, Cast Met. 4 (1991) 62-71.

[9] A. L. Dons, G. Heiberg, J. Voje, J. S. Mæland, J.O. Løland, A. Prestmo, Mater. Sci. Eng. A 413–414 (2005) 561–566.

[10] D. A. Ganger, R. Elliot in: Solidification of Eutectic Alloys, Metals Handbook, 9th ed., Vol. 15, p. 159.

[11] B. Closset and J.E. Gruzleski, Tans. AFS 90 (1982) 453.

[12] S. G. Shabestari, F. Shahri, J. Mater. Sci. 39 (2004) 2023 – 2032.

[13] H. Li, Y. Sun, G. Sun, Mater. Sci. Eng. A 335 (2002) 62.

[14] T.Grab, L. Arnberg, Int. J. Cast Metal. Res. 19 (2006) 201-209.

[15] S.G. Shabestari, H. Moemeni, J. Mater. Process. Technol. 153–154 (2004) 193–198.

[16] P. Ouellet, F. H. Samuel, J. Mater. Sci. 34 (1999) 4671 – 4697.

[17] F.J. Tavitas-Medrano, J.E. Gruzleski, F.H. Samuel, S. Valtierra, H.W. Doty, Mater. Sci. Eng. A 480 (2008) 356–364

[18] G. García-García, J. Espinoza-Cuadra, H. Mancha-Molinar, Mater. Des. 28 (2007) 428–433.

[19] K.G. Basavakumar, P.G. Mukunda, M. Chakraborty, Mater. Charact. 59 (2008) 283–289.

[20] Z. Li, A.M. Samuel, F.H. Samuel, C. Ravindran, S. Valtierra, H.W. Doty, Mater. Sci. Eng. A 367 (2004) 96–110.

[21] G. Berti, M. Monti, L. Salmaso, Introduzione alla metodologia DOE nella sperimentazione meccanica. Disegno sperimentale e superfici di risposta, Ed. Cleup, 2002.

[22] G.O. Verran, R.P.K. Mendes, L.V.O. Dalla Valentina, J. Mater. Process. Technol. 200 (2008) 120–125

[23] Minitab Tutorials, Minitab® 15.1.1.0.

[24] F. Grosselle, G. Timelli, F. Bonollo, A. Tiziani, E. Della Corte, Metall. Ital. 6 (2009) 25-32.

[25] K.Moizumi, K.Mine, H. Tezuka, T.Sato, Mater. Sci. Forum 396-402 (2002) 1371-1376.

[26] M. Drouzy, S. Jacob, M. RichardAFS Int. Cast Met. J. 5 (1980) 43-50.

[27] John A. Francis, G.M. Delphine Cantin, Mater. Sci. Eng. A 407 (2005) 322–329

[28] B. Zhang, S.L. Cockcroft, D.M. Maijer, J.D. Zhu, and A.B. Phillion, , JOM (2005) 36-43.

[29] T. Kobayashi, Mater. Sci. Eng. A 286 (2000) 333–341.

[30] C.H. Caceres, B.I. Selling, Mater. Sci. Eng. A 220 (1996) 109-116.

[31] G.F. Vander Voort, Metallography Principles and Practise, McGraw-Hill, New York, NY, 1984, p. 612.

[32] L. Pedersen, L. Arnberg, Metall. Mater. Trans. A, 32 (2001) 525-532.

[33] D.L. Zhang, L.H. Zheng, D.H. StJohn, J. Light Met. 2 (2002) 27–36

[34] M. Panušková, E. Tillová, M. Chalupová, Strength Mater. 40 (2008) 90-101

[35] Li Run et al. , Trans. Nonferrous Met. Soc. China 14 496-500.

[36] D. Zhang, J. Peng, G. Huang. D. Zeng, J. Wuhan University of Technology-Mater. Sci. Ed. 23 (2008) 184-188.

[37] J. H. Sokolowski, M. B. Djurdjevic, C. A. Kierkus, D. O. Northwood, J. Mater. Process. Technol. 109 (2001) 174-180

[38] S. Shivkumar, S. Ricci, C. Keller, D. Apelian, J. Heat. Treat. 8 (1990) 63–70.

[39] L. Pedersen, Doctoral Thesis, Norwegian University of Science and Technology, Trondheim, Norway, 1999.

[40] L. A. Narayanan, F.H. Samuel, J.E. Gruzleski, Metall. Mater. Trans. A 26A (1995) 2161–74.

[41] G.Q. Wang, Metall. Mater. Trans. A 34A (2003) 2887-2899.

[42] S. Nafisi, R. Ghomashchi, H. Valia, Mater. Charact. 59 (2008) 1466-1473.

[43] K. Nogita, S. McDonald, K. Tsujimoto , K. Yasuda, A.K. Dahle, J Electron Microsc. 53 (2004) 361-9.

[44] S. Shankar, Y.W. Riddle, M.M. Makhlouf, Acta Mater. 52 (2004) 4447-60.

[45] L. Heusler, W. Schneider, J. Light Met. 2 (2002) 17–26

[46] J.E. Gruzleski, B.M. Closset, The treatment of liquid Aluminum-Silicon alloys, American Foundrymen's society Inc., IL (1990).

[47] M.M. Makhlouf, H.V. Guthy, J. Light Met 1 (2001) 199-218.

[48] A. Manente, G. Timelli, Metall. Ital. 10 (2008) 37-50.

[49] G. Timelli, O. Lohne, L. Arnberg H.I. Laukli, Metall. Mater. Trans. A 39A (2008), 1747-1758.

[50] Q.G. Wang, C.H. Caceres, Mater. Sci. Eng. A A241 (1998) 72-82.

[51] Q.G. Wang, C.H. Caceres, J.R. Griffiths, Metall. Mater. Trans. A 34 (2003) 2901-2912.

[52] C. H. Caceres, J. R. Griffiths, Acta Mater. 44 (1996) 25-33.

ARTICLE 3

CORRELATION BETWEEN MICROSTRUCTURE AND MECHANICAL PROPERTIES OF Al-Si CAST ALLOYS

Fabio Grosselle*, Giulio Timelli*, Franco Bonollo*, Alberto Tiziani*,
Emilia Della Corte**

* Department of Management and Engineering – DTG
University of Padova
I-36100 Vicenza
ITALY

** Enginsoft Spa
I-35129 Padova,
ITALY

Published in: Metallurgical Science and Technology, 2009.

ABSTRACT
The influence of microstructure and process history on mechanical behaviour of cast Al-Si alloys is reported. In the present work, the EN-AC 46000 and 46100 aluminium alloys have been gravity cast using a step-bar permanent mould, with a range of thickness going from 5 to 20 mm.. Metallographic and image analysis techniques have been used to quantitatively examine the microstructural parameters of the α-Al phase and eutectic Silicon. Microstructure has been also correlated with the results coming from the numerical simulation of the casting process. The results show that SDAS and length of eutectic silicon particles increase with section thickness, and consequently mechanical properties decrease.

KEYWORDS
Aluminium alloys; EN-AC 46000; EN-AC 46100; SDAS; Eutectic Si; Microstructure; Numerical Simulation; Permanent Mould Casting

1. INTRODUCTION

Mechanical properties of Al-Si cast alloys depend on several microstructural parameters. Grain size, secondary dendrite arm spacing (SDAS), distribution of phases, the presence of secondary phases or intermetallic compounds, the morphology of silicon particles (size, shape and distribution) and, finally, defects play a key role in the determination of the elastic and plastic behaviour of aluminium alloys [1-3].
In general, castings having a finer microstructure (quantitatively described by low SDAS values), induced by high solidification rate, show better mechanical properties. Many correlations between mechanical behaviour (UTS, YS, elongation) and SDAS can be found in literature [3-4]. It is worth mentioning that, on industrial production, the control of solidification rate (and therefore the SDAS values) is quite difficult to achieve [5], as consequence of the geometrical complexity and of the different wall thickness in the real-shaped casting. For this reason, reference castings are frequently employed when the solidification rate has to be accurately controlled and different microstructures have to be achieved. Therefore, in these castings, the solidification conditions can be set up by varying the thickness and the material of the mould, as well as the sample size [3,6]. In this way, the factors affecting SDAS, the relationship between SDAS and mechanical properties of cast aluminium alloys can be easily better assessed and these information can be subsequently transferred to real-shaped casting.
On the other hand, it is well known that SDAS is not the only factor affecting the mechanical behaviour of an alloy. For instance, the deformation behaviour of cast aluminium alloys is also affected by eutectic Si particles and intermetallic compounds which determine the initiation and the evolution of fracture [7-8]. In particular, for defect free castings, tensile fracture is initiated by cleavage of either brittle intermetallic particles or eutectic Si particles. The cleavage cracks are mainly perpendicular to the macroscopic principal strain, regardless of the particle orientation. Platelet particles with their length perpendicular to the tensile direction break because of cleavage along their length [9-10]. Therefore, it is easy to hypothesize that the fracture mechanism depends on the size and shape of Si or Fe-rich brittle phases. In detail, large and acicular particles are deleterious for mechanical properties reducing elongation to fracture and ultimate tensile strength [9].
In un-modified Al–Si cast alloys, the eutectic Si particles have a coarse, acicular and polyhedral morphology and the final mechanical properties of an alloy is characterized by their distribution in the microstructure. It was established that the size distribution of eutectic Si particles follows the lognormal distribution [8]. The probability density function of the three-parameters lognormal distribution can be written as:

$$f(d) = \frac{1}{(d-\tau)\sigma\sqrt{2\pi}} \exp\left[\frac{-(\ln(d-\tau)-\mu)^2}{2\sigma^2}\right] \quad (1)$$

where d is the diameter of Si particles, τ the threshold, σ the shape and μ is the scale parameter.
The aim of this work is to investigate the evolution of the microstructure (quantitatively evaluated by means of SDAS and Si-related parameters) as a function of the solidification time and to correlate microstructural parameters with the

mechanical properties of a stepwise reference casting. The experiments considered cast thickness ranging from 5 to 20 mm.

2. EXPERIMENTAL PROCEDURE

2.1 Materials and experimental methods

The geometry of the die is shown in Fig. 1. The two part die is split along a vertical joint line passing through the pouring basin. To facilitate assembly and mutual location the die halves are hinged. The dimension of the whole die was 310x250x115 mm^3 and the thickness of the two die halves was 45 and 75 mm respectively. The die was made by an AISI H11 tool steel and the weight was around 140 kg. The casting, with the front and side views, is shown in Fig. 2. The step casting presented a range of thickness going from 5 to 20 mm and it was gated from the side of the thinnest step, while the riser, over the casting, ensured a good feeding. This configuration allows to obtain a range of solidification rates and consequently different microstructures in the casting. The weight of the aluminium alloy casting was 1.4 or 1 kg, including or not the runner system.

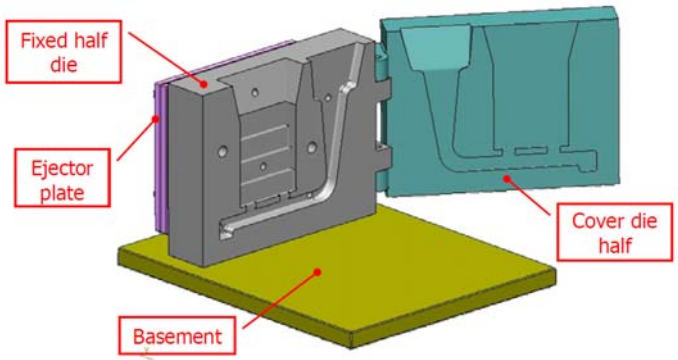

Fig. 1. Permanent mould die used in the present work

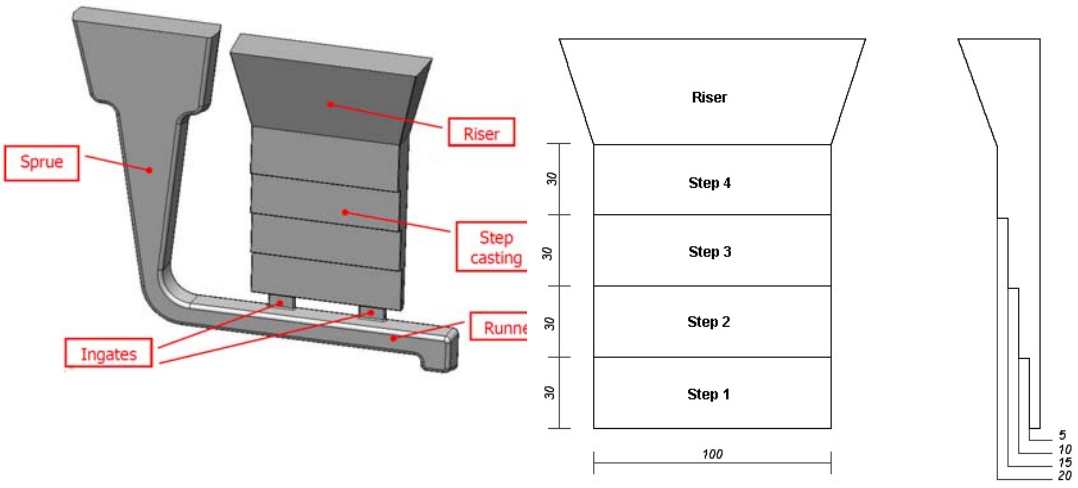

(a) (b)

Fig. 2. (a) The step casting CAD geometry with (b) front and side views. All the measures are in mm.

The step castings were produced with EN-AC 46000 and EN-AC 46100 alloys, two hypoeutectic aluminium–silicon alloys, in the form of ingots, whose composition is indicated in Tab. 1. The material was melted in an electric-induction furnace setup at 720±5°C. Before pouring, the melt was degassed with an argon-sulphur hexafluoride mixture (Ar/SF_6 0.2%).
A semi-permanent layer of DYCOTE® F34 coating was spray applied on the die walls at the temperature of about 200°C according to standard practice [11].
Before pouring the melt, the temperature of the die was increased to about 250±10°C. Trough the use of thermocouples, the temperatures in different zones of the die were measured in order to evaluate the local temperature and assure a good reproducibility of the tests. The temperature in the die was in the range of (450–520)±3°C.

Tab. 1: Chemical composition of the alloys studied in the present work (wt.%).

Alloy	Al	Si	Cu	Fe	Mg	Mn	Ni	Ti	Zn	Others
EN-AC 46000	Bal.	8.8	3.0	0.8	0.21	0.26	0.087	0.039	0.90	0.05
EN-AC 46100	Bal.	10.8	1.8	0.8	0.13	0.18	0.089	0.046	1.29	0.05

The castings were then sectioned and samples were drawn from each step. Radiographic inspection was carried out on tensile specimens before mechanical testing, in order to detect the presence of macrodefects.
Flat tensile test bars with rectangular cross section were obtained from the step castings (Fig. 3), in the middle and external zones of the castings. In this way it was possible to study the effect of the local temperature and the heat transfer on the solidification rate and, thus, on the microstructure and mechanical properties.
The tensile specimens were 100-mm long, 20-mm wide, and 3-mm thick, with a gage length of 30 mm and a width of 10 mm, according to ASTM-B577.
The tensile tests were done on a computer controlled tensile testing machine. The crosshead speed used was 2 mm/min ($\dot{\varepsilon} \sim 10^{-3}$ s^{-1}). The strain was measured using a 25-mm extensometer. At least three specimens were tested for each zone. When the experimental data differed by more than 5 pct, another tensile specimen was tested.

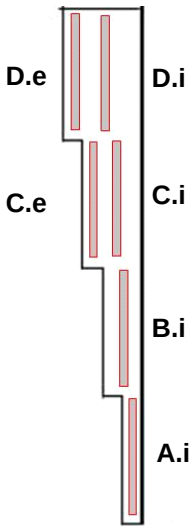

Fig. 3. Side view of the step casting showing sectioning scheme.

The samples cut from the cross section of the gage length were mechanically prepared to a 1-μm finish with diamond paste and, finally, polished with a commercial fine silica slurry for metallographic investigations. Microstructural analysis was carried out using an optical microscope and quantitatively analyzed using an image analyzer. To quantify the microstructural features, the image analysis was focused on the secondary dendrite arm spacing (SDAS), and on the size and aspect ratio of the eutectic silicon particles. Size is defined as the equivalent circle diameter (d); the aspect ratio (α) is the ratio of the maximum to the minimum Ferets. To obtain a statistical average of the distribution, a series of at least 10 photographs of each specimen were taken; each measurement included more than 1000 particles. The secondary phases, such as the Mg_2Si and $CuAl_2$ particles, and the iron-rich intermetallics were excluded from the measurements and further analysis. Average SDAS values were obtained using the linear intercept method, which involves measuring the distances between secondary dendrite arms along a line normal to the dendrite arms.

2.2 Casting simulation

The MAGMASOFT® v4.6 (2007) commercial software, with its module for gravity die casting, was used for numerically simulating the filling and solidification behaviour of analysed wheels. The characteristics of the software used in this study are as follows:

- ease of physical interpretation of various steps of algorithms;
- conservation of physical properties;
- reduction of solving time.

Basic governing equations of the software are continuity equation, Navier–Stoke's equation, energy equation and volume of fluid (VoF) method for the free surface movement during the die filling. The numerical code employs the finite volume approach to convert differential equations into algebraic ones and solve them on a rectangular grid. The CAD model of the step casting was drawn and imported in the simulation software where a controlled volume mesh of 132000 cells for the die cavity was automatically generated by the software. The initial conditions for numerical simulation were defined to reproduce the casting parameters. The pouring temperature was set at 720°C, while, for the die, the temperature for the first cycle was assumed to be at a uniform temperature of 250°C. In the subsequent cycles, the initial temperature in the die is taken to be the predicted temperature distribution at the end of the previous cycle. A number of 10–15 cycles were taken after the start up to reach a quasi-steady-state temperature in the die. The thermal conductivity of the die varied in the range of 33.4–31.5 W/mK, in the working temperature range of 450–520°C. The other physical constants and properties of the die and the alloys, and their evolution with temperature, were chosen among those present in the software database, as well as the heat transfer coefficients (HTC), taking into account affecting parameters, like the type and thickness of coating, and the pouring temperature. To define the whole set of boundary conditions in the model, the process parameters (e.g. regarding the filling and cooling cycle) and the cycle time, acquired from the casting process, were imported in the software, increasing the reliability of numerical simulation. Virtual thermocouples were inserted in the different zones of the die in order to control the temperature profiles and to compare these values with the real ones. Solidification time was assessed via numerical simulation code in order to predict the final microstructure of the casting. The

mechanical properties of the aluminium cast alloy were predicted by using the newly developed add-on module to the simulation software [12].

3. RESULTS AND DISCUSSION

In Fig. 4, typical microstructures of the step castings are reported with reference to the different step, which varies in a range of thickness between 5 to 20 mm. While Fig. 4a shows the as-cast microstructure of EN-AC 46000 alloy, in Fig. 4b the microstructure of EN-AC 46100 alloy is presented. The microstructure of the step castings analysed consists of a primary phase, α-Al solid solution, which precipitates from the liquid as the primary phase in the form of dendrites. The as-cast Al–9Si–3Cu alloy (EN-AC 46000) shows primary α-Al grains in the matrix of the eutectic structure (Fig. 4a). The eutectic structure is a mixture of the α-Al and eutectic silicon phase. The eutectic silicon can be seen in the interdendritic regions. The Al–11Si–2Cu alloy (EN-AC 46100) shows the mixed structure of the α-Al grains and eutectic (Fig. 4b). Moreover, the addition of silicon increased the fraction of the eutectic in the interdendritic region. Intermetallics compounds, such as Fe- and Cu-rich intermetallics, were also observed. A low level of microdefects, in the form of microshrinkage, was found in the specimens analysed.
The scale of microstructure in different zones of the castings was characterized by means of SDAS measurements and then correlated with mechanical properties. These data are further described.

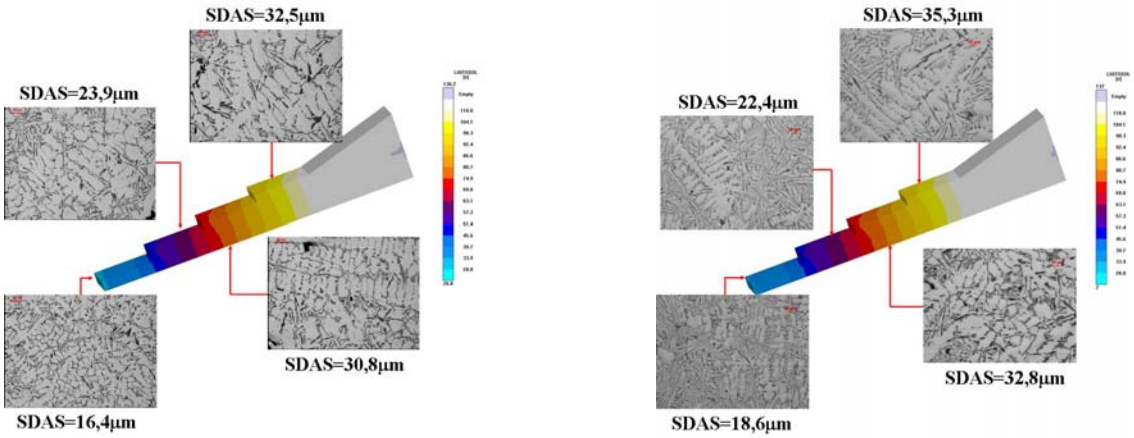

Fig. 4. Calculated solidification times with corresponding microstructure within step castings of (a) EN-AC 46000 and (b) 46100 alloys.

Fig. 4 presents calculated solidification times, from numerical simulation, with the corresponding microstructure within step castings of EN-AC 46000 and 46100 alloys. A general coarsening of microstructure occurs in thicker regions, quantified by SDAS values, as the result of the increased solidification time in both alloys. For every section thickness, the SDAS values were higher in the samples extracted from the inner section than the specimens from the external one.
Similar values of SDAS and solidification time for the two alloys were obtained as consequence of similar thermal properties.
Solidification times were also estimated by means of SDAS measurements using equation [13]:

$$SDAS = 6.4\, t_s^{0.36} \quad (2)$$

developed for aluminium casting alloys with high Si content [12].
A comparison between calculated and estimated solidification times was carried out, indicating a good relationship and testifying the ability of numerical simulation codes to predict the local solidification conditions and the characteristics of casting components.
In Tab. 2, the average values of SDAS, calculated solidification times, and size and morphology of eutectic silicon particles (*i.e.* equivalent diameter, *d*, and aspect ratio, α) are summarized.

Tab. 2. Average values of SDAS, equivalent diameter and aspect ratio of eutectic silicon particles obtained from different sections of the step castings (standard deviation in parentheses); solidification times, calculated with a numerical simulation approach, are also reported. Data refer to EN-AC 46000 and 46100 alloys.

Alloy	Section	SDAS (μm)	Calculated solidification time (s)	Equivalent Diameter, *d* (μm)	Aspect Ratio, α
EN-AC 46000	A.i	16.4 (0.8)	14	5.3 (1.8)	3.0 (1.5)
	B.i	23.9 (1.8)	40	6.4 (3.0)	2.9 (1.6)
	C.e	23.5 (1.0)	38	6.4 (2.7)	2.9 (1.3)
	C.i	30.8 (0.9)	82	6.8 (3.1)	2.7 (1.4)
	D.e	25.0 (1.3)	46	7.4 (3.8)	3.0 (1.5)
	D.i	32.5 (1.9)	95	6.8 (3.3)	3.1 (1.4)
EN-AC 46100	A.i	18.6 (2.4)	20	5.5 (1.8)	4.0 (2.0)
	B.i	22.4 (1.6)	33	6.2 (2.6)	3.7 (2.0)
	C.e	26.8 (1.8)	55	6.7 (2.9)	3.6 (1.8)
	C.i	32.8 (1.3)	98	7.6 (3.8)	3.1 (1.7)
	D.e	26.9 (1.9)	56	6.7 (2.9)	4.0 (2.0)
	D.i	35.3 (2.1)	120	6.8 (3.0)	4.1 (2.3)

Three-parameters lognormal distributions were fitted to eutectic Si particles diameter and aspect ratio data for the different sections of step casting. The results for EN-AC 46000 alloy are shown in Fig. 5. The coefficient of the determination R^2 was used to evaluate the quality of the fitting. When R^2 is equal to 1, the fit is perfect. In the present work, the coefficient R^2 is 0.99, suggesting a good agreement of particle distribution with the three-parameters lognormal distribution adopted. These findings are in agreement with the results reported in Reference 8. By increasing the solidification time, *i.e.* the section thickness of the step, the distribution of the eutectic Si equivalent diameter becomes more spread (Fig. 5a). The equivalent diameter of eutectic Si particles with the maximum frequency shifts toward right and the absolute value of the maximum frequency decreases. In particular, this behaviour is appreciable in A.i and B.i sections.
Therefore, it can be established that by reducing the cooling rate, the microstructure is characterised by coarse eutectic Si particles, while by reducing the solidification time the formation of a high number of fine silicon particles is predominant.
Similar behaviour of the eutectic Si size was observed in the EN-AC 46100 alloy.
The impact of the solidification time on the aspect ratio of eutectic Si particles is negligible, as shown in Fig. 5b. Every step shows similar distributions of the aspect ratio of the eutectic Si particles. The irregular growth mechanism of un-modified eutectic Si particles confirms to be independent from the solidification rate, at least for the range of solidification rate investigated [14].

Generally, the distributions of the aspect ratio of the eutectic Si particles in EN-AC 46100 alloy show similar behaviour.

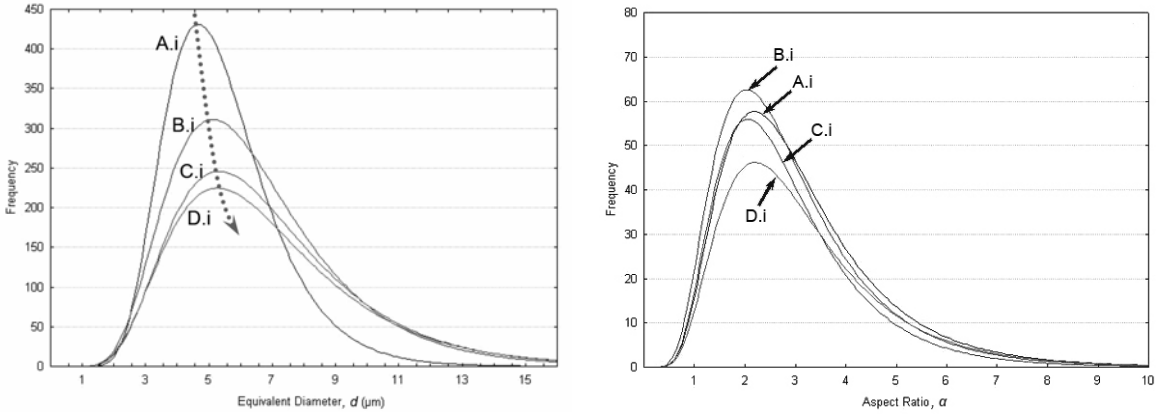

(a) (b)

Fig. 5. Three-parameters lognormal distributions for equivalent diameter, *d*, and aspect ratio, *α*, of eutectic Si particles obtained from different sections of the step castings. Data refer to EN-AC 46000 alloy.

The correlation between solidification time and Si particles parameters is reported in Fig. 6. For both alloys, the average diameter increases significantly by increasing the solidification time from 20 to 40 seconds, while for longer times the values are steady in the range of 6.5 to 7 μm (Fig. 6a). On the other side, the aspect ratio seems to be independent from the solidification time (Fig. 6b), as previously demonstrated by means of the distribution plots in Fig. 5b.

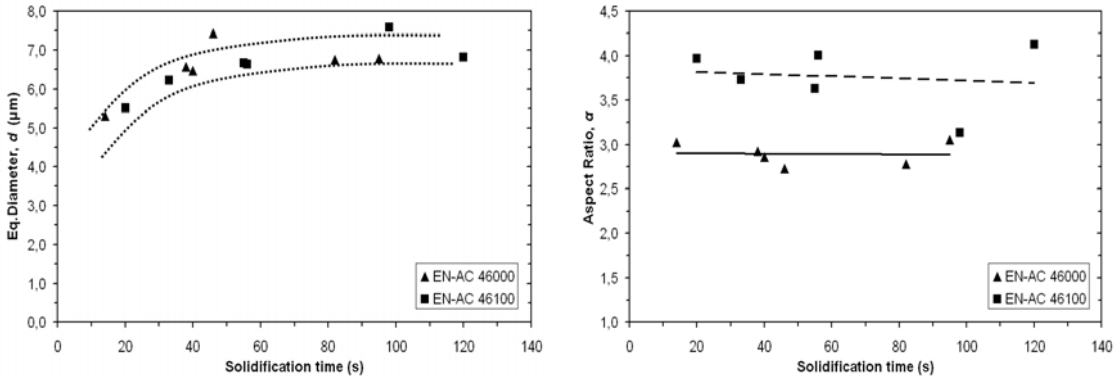

(a) (b)

Fig. 6. Variation in (a) equivalent diameter and (b) aspect ratio of eutectic silicon particles as function of solidification time.

Contrary, a relationship can be found between the aspect ratio and the Si content. If the Si amount is increased from 9 wt.% in the EN-AC 46000 alloy to 11 wt.% and EN-AC 46100 alloy, the aspect ratio of eutectic Si particles increases, indicating a more intense growing along the main axis direction of the Si particles.
In Tab. 3, the results of the mechanical investigation are shown. The values of the standard deviation confirm the presence of a low amount of microdefects, which affect the mechanical properties. However, no macrodefects were observed through the X-ray investigation.

Tab. 3. Average mechanical properties obtained from different sections of the step castings (standard deviation in parentheses). Data refer to EN-AC 46000 and 46100 alloys.

	EN-AC 46000			EN-AC 46100		
Section	YS (MPa)	UTS (MPa)	Elongation to fracture (%)	YS (MPa)	UTS (MPa)	Elongation to fracture (%)
A.i	143 (5)	218 (11)	1.4 (0.16)	120 (7)	188 (7)	1.3 (0.09)
B.i	149 (3)	189 (8)	0.8 (0.16)	132 (4)	188 (9)	1.0 (0.10)
C.e	146 (2)	208 (3)	1.1 (0.11)	131 (5)	170 (4)	0.8 (0.08)
C.i	152 (2)	176 (8)	0.7 (0.10)	129 (8)	166 (11)	0.7 (0.09)
D.e	142 (7)	205 (6)	1.0 (0.04)	119 (6)	174 (3)	1.0 (0.09)
D.i	153 (6)	147 (10)	0.4 (0.02)	122 (7)	160 (7)	0.6 (0.22)

If A.i and D.i sections are considered and compared, a reduction of 23 and 15% in UTS and 71 and 54% in elongation to fracture is observed for the EN-AC 46000 and 46100 alloys respectively, as a consequence of the different microstructure scale. In the EN-AC 46000 alloy, the UTS varies from 167 to 218 MPa and the elongation to fracture from 0.4 to 1.4%, while the change is in the range of 160 to 188 MPa for UTS and from 0.6 to 1.3% for elongation to fracture, in the EN-AC 46100 alloy. On the other hand, the solidification time seems to not affect the YS of the alloys. In the EN-AC 46000 alloy, the mean YS is about 147 MPa independently from the step thickness, while the mean YS is 125 MPa in the EN-AC 46100 alloy.

In addition, the difference of the YS and UTS of the two alloys can be mainly associated to the different Cu content that improves the mechanical properties even in the as-cast temper, due to the precipitation of strengthening Al_2Cu secondary phase, and to the different Si content, which decreases the ductility [15].

In order to evaluate the influence of the microstructure on the mechanical properties, the UTS and the elongation to fracture of the specimens are plotted in Figs. 7 and 8 as a function of SDAS and of the product of SDAS and aspect ratio respectively. As reported in literature [3-4], it can be observed that by increasing the SDAS values, the UTS and the elongation to fracture decrease in both alloys (Fig. 7). However, since SDAS values are similar, other microstructural parameters control the fracture mechanism of these alloys and should be taken into account to explain the existing differences in mechanical behaviour. Since the eutectic Si particles diameter is independent from the alloy type, as previously demonstrated, the aspect ratio was considered as parameter to be correlated. Fig. 8 shows the UTS and the elongation to fracture as a function of the product of SDAS and aspect ratio, showing with more evidence the different behaviour of the analysed alloys. The highest aspect ratio (~4) and Si content (~11 wt.%) in the EN-AC 46100 alloy induces probably higher tension field around eutectic Si particles, originating cracks at inferior loads [1,16].

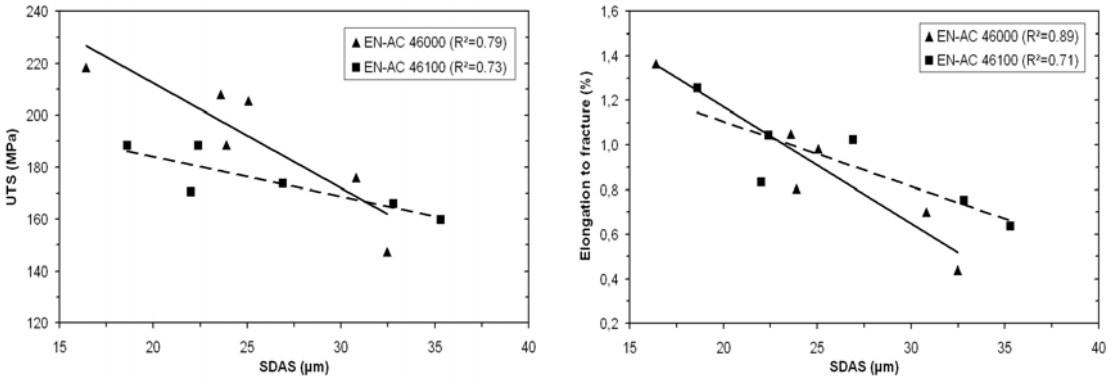

(a) (b)

Fig. 7. Average (a) UTS and (b) elongation to fracture as a function of SDAS; coefficient of determination, R^2, are given. Data refer to EN-AC 46000 and 46100 alloys.

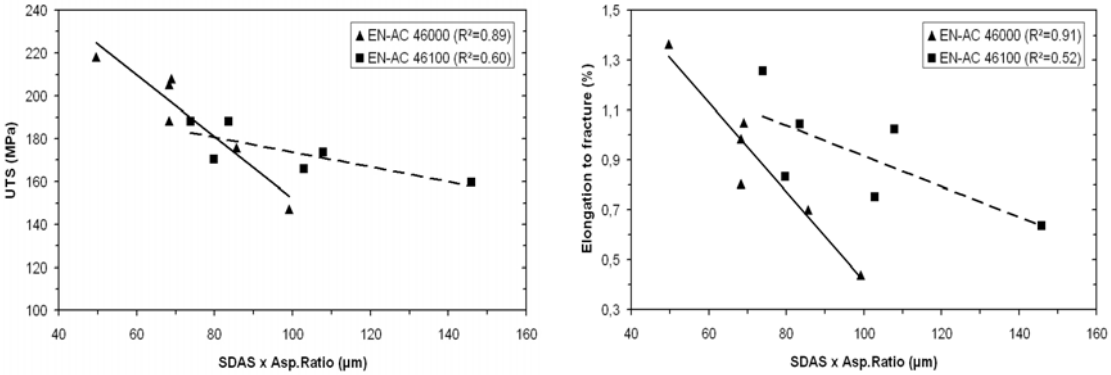

Fig. 8. Average (a) UTS and (b) elongation to fracture as a function of the combined parameter SDAS x Aspect ratio; coefficient of determination, R^2, are given. Data refer to EN-AC 46000 and 46100 alloys.

In Figs. 9 and 10, a comparison between experimental and simulated values in terms of mechanical properties of EN-AC 46000 and 46100 alloys is shown.

In the EN-AC 46000 step castings, the YS shows a difference of about 15% between experimental and simulated values (Fig. 9a). While an average forecast values of 130 MPa is provided by the simulation code, the experimental YS is about 149 MPa, *i.e.* the numerical simulation underestimates the YS values. The difference between experimental and simulated values is reduced considering the UTS and the elongation to fracture. In general, the UTS values in D.i and C.i sections differ of about 4%, while in the remaining sections the simulated values are about 13% lower than the experimental ones (Fig. 9b). As it is possible to observe the relationship is good for the elongation to fracture (Fig. 9c).

If the EN-AC 46100 step castings are considered, it was demonstrated that the experimental and simulated values are similar: the YS, UTS and elongation to fracture differ up to 5% (Fig. 10).

It can be suggested that numerical simulation is an useful tool in the design stage, allowing the optimization of the geometry of casting components, dies and process parameters, thereby, making the design and development process more time and cost efficient. It should be mentioned that this simulation tool is still under development and comprises only a restricted range of alloying elements [12].

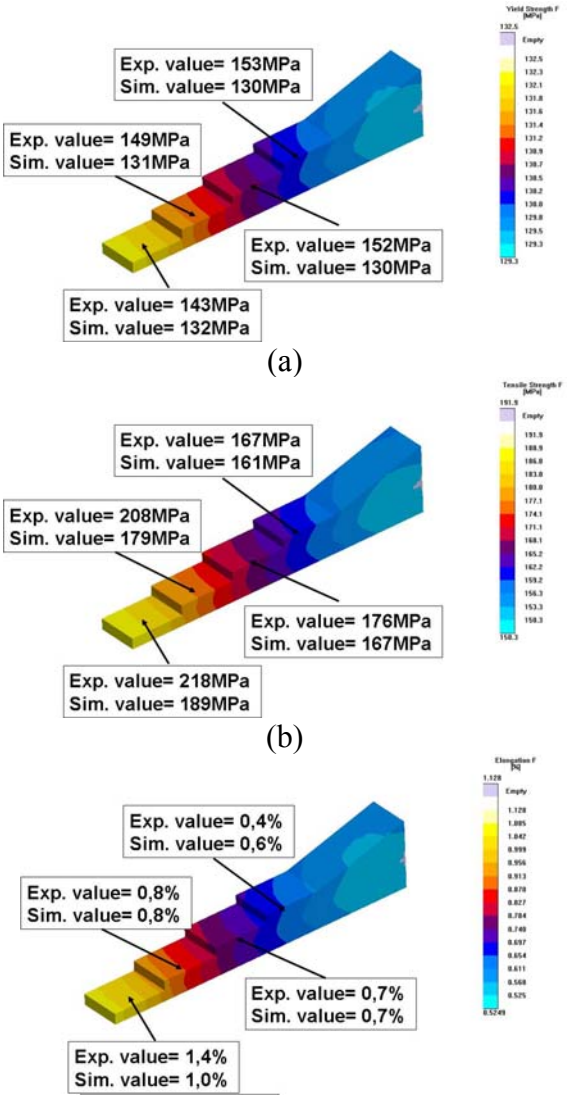

Fig. 9. Comparison between experimental and simulated mechanical properties in EN-AC 46000 step casting. The images refer to (a) YS, (b) UTS and (c) elongation to fracture.

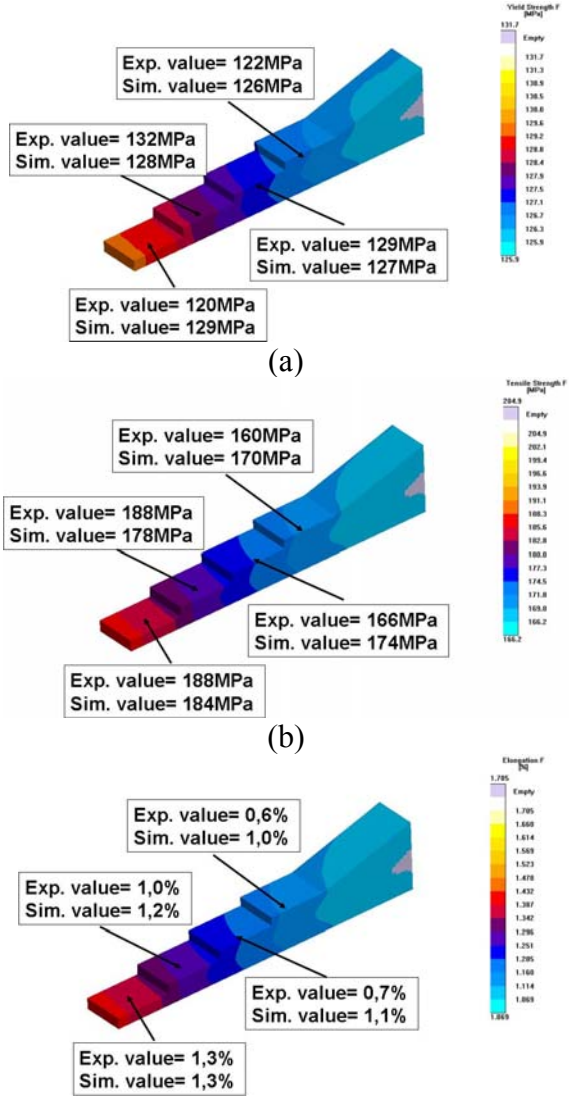

Fig. 10. Comparison between experimental and simulated mechanical properties in EN-AC 46100 step casting. The images refer to (a) YS, (b) UTS and (c) elongation to fracture.

4. CONCLUSIONS

The effects of microstructural parameters such as SDAS, size and morphology of eutectic silicon particles on mechanical properties of EN-AC 46000 and 46100 alloys have been investigated. In addition, the validation of the results provided by a numerical simulation approach has been performed. Based on the results obtained in the present study, the following conclusions can be drawn.

- The equivalent diameter and the aspect ratio of eutectic Si particles follow three-parameter lognormal distributions.
- While the distribution of the equivalent diameter depends on solidification time, the distribution of the aspect ratio is less sensible, indicating the irregular growing mechanism of un-modified eutectic silicon.

- The average size of eutectic silicon particles is similar in both EN-AC 46000 and 46100 alloys, while the aspect ratio of EN-AC 46100 is higher, probably due to higher Si content.
- The mechanical properties, *i.e.* the UTS and elongation to fracture, depend on SDAS and on the aspect ratio of the eutectic Si particles, which seems an alloy-related parameters. Increasing the SDAS and the aspect ratio values, the UTS and the elongation to fracture decrease.
- The difference in the mechanical properties of the two alloys is the consequence of different chemical composition. Higher Cu and Mg contents in the EN-AC 46000 alloy allows to increase the YS, while a lower Si amount permits to enhance the ductility, reaching higher UTS and elongation to fracture values than the EN-AC 46100 alloy.
- Since numerical simulation results reproduce the experimental data with a good accuracy, it can be stated that numerical simulation is a useful tool for the reduction of time and costs in the design stage.
- The present investigation has been carried out on un-modified gravity cast alloys; in the case of higher cooling rate, modification or heat treatment, attention should be also paid to the size of eutectic Si particle, as a parameter affecting the mechanical behaviour.

ACKNOWLEDGMENTS

The European Project NADIA- New Automotive components Designed for and manufactured by Intelligent processing of light Alloys (NMP-2004-SME 3.4.4.5, contract n.026563-2) is gratefully acknowledged for financial support. Many thanks are due to dr. R. Molina (Teksid Aluminum), dr. G.F. Capra and dr. L. Capra (Raffineria Metalli Capra), and dr. G. Valente (DTG) for their contribution to the experimental work.

REFERENCES

1) S.G. SHABESTARY, F. SHAHRI, J. Mater. Sci. 39, (2004), pp.2023-2032

2) S. VISWANATHAN, A.J. DUNCAN, A.S. SABAU, Q. HAN, W.D. PORTER, B.W. RIEMER, AFS Transactions 106, (1998), pp.411-417.

3) V. RONTÓ and A. ROÓSZ, Int. J. Cast Metals Res. 13, (2001), pp.337-342.

4) F. BONOLLO, G. TIMELLI, N. GRAMEGNA, B. MOLINAS, Proc. 3rd Int. Conf. High Tech Die Casting, Vicenza (2006), AIM, Milano, paper 67.

5) F. BONOLLO, G. TIMELLI, G. MAZZACAVALLO, R. MOLINA, Proc. 30th Convegno Nazionale AIM, Vicenza (2004), AIM, Milano, paper 137.

6) S.T. McCLAIN, J.T. BERRY and B. DAWSEY, AFS Transactions 111, (2003), pp.147-158.

7) G. TIMELLI, F. BONOLLO, Proc. Int. Conf. Aluminium Two Thousand, Florence (2007), Interall, Modena.

8) M. TIRYAKIOGLU, Mater. Sci. Eng. A 473, (2008), pp.1-6.

9) C.H. CÁCERES, J.R. GRIFFITHS, Acta Mater. 44, (1996), pp.25-33

10) Q.G. WANG, C.H. CÁCERES, Mater. Sci. Eng. A 241, (1998), pp.72-82.

11) FOSECO, Dycote® Manual – Coatings for non-ferrous metal die-casting, pp.1-28.

12) S. SEIFEDDINE, M. WESSEN, I.L. SVESSON, Metallurgical Science and Technology 24, (2006), pp. 26-32.

13) 1L.BACKERUD, G.CHAI, J.TAMMINEN, Solidification Characteristic of Aluminum Alloys-Vol.2: Foundry Alloys. American Foundrymen's Society, Inc., IL, USA(1990).

14) W. KURZ and D.J. FISHER, Fundamentals of solidification, Cap.5. Trans. Tech. Publications, Switzerland (1998).

15) C.H. CACERES, I.L. SVENSSON, J.A. TAYLOR, International Journal Cast Metals Res., 2003,15, 531-543

16) Q.G. WANG, C.H. CACERES, J.R. GRIFFITHS, Metallurgical and Materials Transaction A, Volume 34A, December 2003, 2901-2912

ARTICLE 4

FINAL CORRELATION & MODELS ABOUT THE EFFECT OF MICROSTRUCTURE OF HEAT TREATED AL ALLOYS ON MECHANICAL BEHAVIOUR

Fabio Grosselle, Franco Bonollo

Department of Management and Engineering – DTG
University of Padova
I-36100 Vicenza
ITALY

Deliverable of European NADIA Project

SIXTH FRAMEWORK PROGRAMME

PRIORITY 3 – NMP

Nanotechnologies and nanosciences, knowledge based multifunctional materials, new production processes and devices

Contract for:

INTEGRATED PROJECT - SMEs

Deliverable – D3.6
Final correlation & models about the effect of microstructure of heat treated Al alloys on mechanical behaviour
(Resp. F.Bonollo,DTG)

Project acronym: **NADIA**

Project full title: **New Automotive components Designed for and manufactured by Intelligent processing of light Alloys**

Contract no.: **026563-2**

Date of emission: December 5, 2008
Revision: 0

Start date of contract: May 1st, 2006
Duration of the project: 48 months

Project coordinator name: Stefano Odorizzi
Project coordinator organisation name: ENGINSOFT S.p.A

1. INTRODUCTION

The possibility of performing heat treatment is a key issue to improve mechanical properties in some Aluminium based alloys. In recent years, in the field of casting alloys especially in the automotive industry, there has been an increasing trend to use Al–Si–Mg casting alloys, specifically A356 (Al–7Si–0.3Mg), due to their excellent castability, corrosion resistance and good mechanical properties [1]. In particular it is well-known that the AlSiMg family is suitable to be reinforced by precipitation hardening by means of the T6 treatment (solution, quenching and artificial ageing), leading to a uniform distribution of Mg_2Si coherent precipitates.
Solutioning and aging time and temperature, as well as quench rate are the factors that influence the mechanical properties of casting at the end of the process. This influence has been widely studied by several authors [2-7].
In particular, the diffusion process, active during artificial ageing, is strictly dependent on the amount of solute in α-Al matrix at the end of the quenching stage. Such an amount is correlated to the cooling rate induced by the quenching medium adopted. At rising cooling rates the amount of solute at room temperature increases, leading to a more efficient precipitation and improved mechanical properties after ageing.
The correlation between cooling rate and mechanical properties was initially investigated by Evacho and Staley [8]; subsequently, some reviews have been performed [9,10].
The quench factor is typically calculated superimposing the cooling curve on the C-curve. The C-curve describes the time required, at different temperatures, for the precipitation of a constant quantity of solute; it was defined by Evancho and Staley as the reciprocal of the nucleation rate equation [8-14]. The curve can be described using the following equation:

$$C_t = -k_1 k_2 \exp\frac{k_3 k_4^2}{RT\left(k_4 - T\right)^2} \exp\frac{k_5}{RT} \qquad (1)$$

where C_t is the critical time required to form a specific percentage of a new phase; k_1 is a constant which equals the natural logarithm of the fraction untransformed during quenching (typically 99,5%: ln(0,995)=-0,00501); k_2 is a constant related to the reciprocal of the number of nucleation sites; k_3 is a constant related to the energy required to form a nucleus; k_4 is a constant related to the solvus temperature; k_5 is a constant related to the activation energy for diffusion; R is the universal gas constant, 8,3144 J/ºK*mol; T is the absolute temperature (K). Figure 1 shows an example of C-curves related to A356 and A357 casting alloys for two different precipitation quantities while Table 1 lists the values of the above mentioned constants adopted for the model reported here.

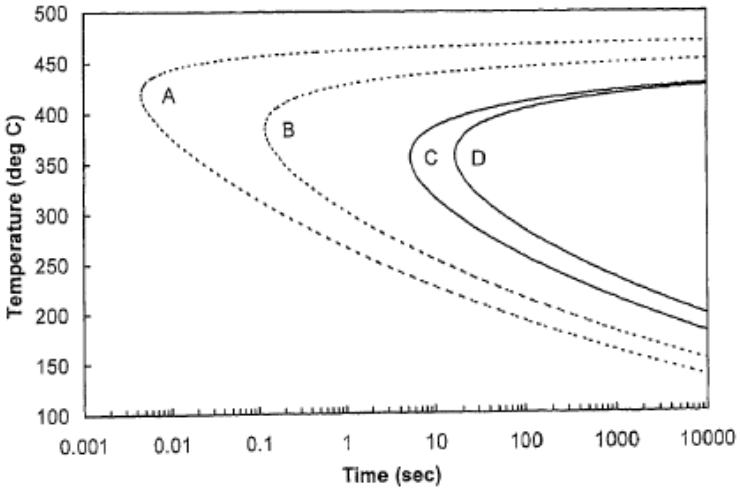

Figure 1: Modelled C curves for alloy A356 (A and C) and A357 (B and D) for 99.5% (dotted curves) and 90% (solid curves) of YS_{max} [9].

Table 1: Value of the constants in the C-curve for two different aluminium alloys [9].

Alloy	**k_1**	**k_2**	**k_3(J/MOL)**	**k_4(K)**	**k_5(J/MOL)**
A356-T6	-0,00501	$3{,}0\times10^{-11}$	64	764	130000
A357-T6	-0,00501	$1{,}1\times10^{-11}$	154	750	131000

A detailed description of the procedure to set up the C-curve for an alloy is provided in Annex A. Based on the additive property of the model, the Quench Factor is calculated as the sum of incremental quench factors, q_i. Each incremental quench factor q_i represents the ratio of the hold time at a particular temperature divided by the time required for a specific amount of transformation [11,14].

$$q_i = \frac{\Delta t_i}{C_{t,i}} \tag{2}$$

The incremental quench factors are summed up over the entire transformation range to produce the cumulative quench factor Q, as shown in Figure 2.

$$Q = \sum_{i=1}^{n} q_i = \int_{t_0}^{t_f} \frac{dt}{C_t} \approx \sum_{i=1}^{n} \frac{dt_i}{C_{t,i}} \tag{3}$$

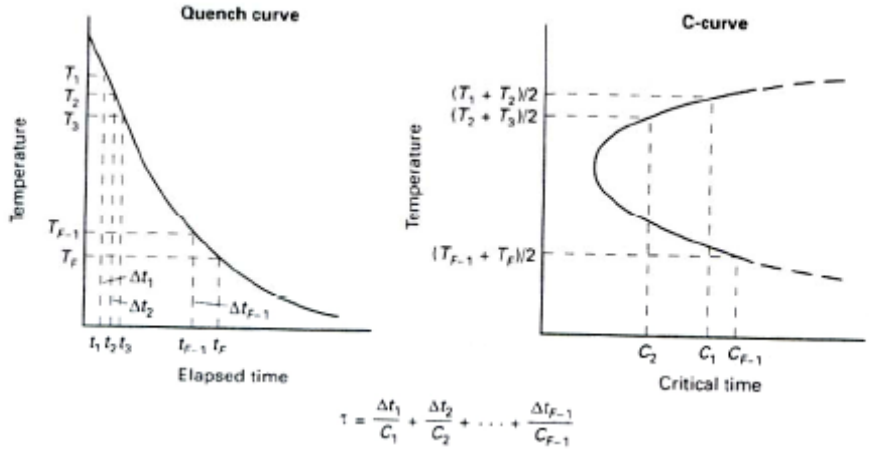

Figure 2: Schematic illustration of the methodology for the calculation of Quench Factor.

With the calculated quench factor Q, the strength can be predicted using the following classical quench factor model [8,9]:

$$\frac{YS - YS_{\min}}{YS_{\max} - YS_{\min}} = \exp\left(k_1 Q^n\right) \tag{4}$$

where *YS* is the yield strength achieved after quenching; k_1 is equal to 0,00501; YS_{min} is the minimum yield strength (achievable by furnace cooling), YS_{max} is the maximum yield strength (achievable by water quenching and aging at 170°C for 8 hours). Since for high performance alloys YS_{min} may be ignored, Eq. (4) can be rewritten as:

$$\frac{YS}{YS_{\max}} = \exp\left(k_1 Q^n\right) \tag{5}$$

Based on the classical quench factor model shown in Eq. (5), improvements have been made to justify the assumptions of quench factor analysis, including Avrami exponent and the relation between strength and solute concentration [10,11].
The Avrami exponent was ignored by Evancho and Stanley [8,9] as the authors have found that the slopes of the plots ln(YS/YSmax) vs time relative to experimental interrupted quench data were equal to 1.
On the contrary, Rometch and Schaffer [9] proposed a value of 0,45 as the best results of correlation between $\ln\left[\left(\frac{1}{k_1}\right)\times\ln\left(\frac{YS - YS_{\min}}{YS_{\max} - YS_{\min}}\right)\right]$ *vs ln(Q).*
If a square root dependency of yield strength on volume fraction of precipitates is taken, similar prediction accuracies of T6 strength/hardness but more realistically positioned C-curves are achieved. Thus, Eq. (5) can be re-written as the following improved formula:

$$YS = YS_{max}(\exp(K_1 Q^{0,45}))^{1/2} \tag{6}$$

In general it can be stated that Eq. (5) and (6) represent the variation of the yield strength due to the changes in quenching rate with respect to the optimal one (i.e. the quenching rate that promotes the achievement of the maximum yield strength; this value is conventionally associated to water quenching at a temperature of 25°C, followed by a 8h ageing treatment at 170°C).

The artificial ageing stage for casting aluminium alloys has been modelled by means of the following formula developed by Shercliff and Ashby and revised by Rometsch and Schaffer for casting aluminium alloys [15,16]:

$$YS_t = YS_i + \Delta YS_{ss,Mg} + \Delta YS_{ppt,Mg\text{-}Si} \quad (7)$$

where YS_t is the total yield strength, YS_i is the yield strength of the material (including all the contributions not affected by the heat treatment process, i.e. the contributions of eutectic Si particles, eutectic Fe-phase particles, and Si in solid solution), $\Delta YS_{ss,Mg}$ is the contribution to yield strength due to Mg in solid solution and, finally, $\Delta YS_{ppt,Mg\text{-}Si}$ is the contribution to the yield strength due to Mg_2Si precipitates.

In Figure 3, the contribution of the different terms to the total Yield Stress and a comparison between the model and experimental data are shown.

It is important to underline that Eq. (7) is a combination of sub-models to predict yield strength (YS) or hardness values after various ageing treatments as expression of [15,16]:

- the decrease in solute concentration and growth in volume fraction of precipitates during the early stages of precipitation;
- the effect of ageing temperature on the equilibrium volume fraction of precipitates;
- the precipitate coarsening by Ostwald ripening;
- the strengthening contribution from solute atoms;
- the strengthening contribution from both shearable and non-shearable precipitates.

By substituting the term YS_{max} in Eq. (5)-(6) with YS_t shown in Eq. (7), an improved heat treatment model is obtained, predicting the mechanical properties of a casting as a function both of quenching rates and ageing conditions.

In detail, the term YS_t describes the yield strength values associated to different ageing conditions following an optimal quenching treatment, while the term exp (K_1Q^n), describes the effect of quenching rate on the super saturation degree of the matrix (which is controlling the degree of formation of strengthening precipitates).

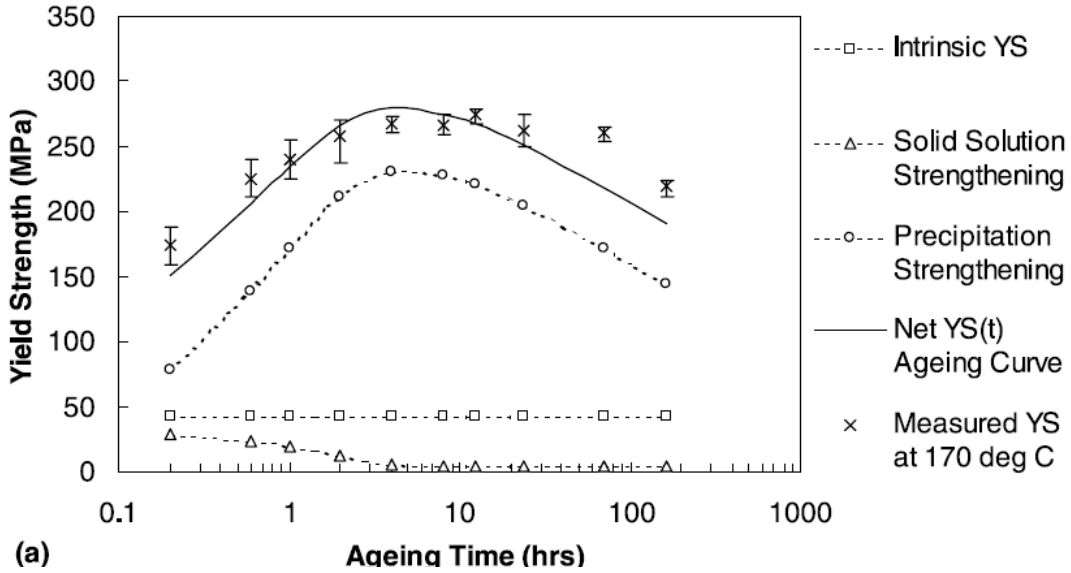

Figure 3: Results of "Age Hardening Model" proposed by Rometsch and Schaffer [15].

2. VALIDATION OF THE MODEL

The validation of the models resulting from the integration of Quench Factor Model and the Age Hardening Model was performed. In particular the models that have been analyzed can be written as follows:

$$YS = YS_{ageing}(exp(k_1 Q^{0,45}) \quad (8)$$

$$YS = YS_{ageing}(exp(K_1 Q^{0,45}))^{1/2} \quad (9)$$

where the term YS_{ageing} depends on age hardening parameters after an ideal quenching (water at 25°C) and YS is the result of the integration.

Due to the simple geometry and the possibility to have a wide range of thickness, the validation has been performed considering a step casting, Figure 4. Thus, the different thicknesses (from 5 to 20mm) of casting made the study of impact of local temperatures and the heat transfer during the treatment on the mechanical properties possible. Step castings were produced using a commercial AlSi7Mg (A356) unmodified alloy melted in a resistance furnace and cast in a steel permanent mold. The composition of the alloy is reported in Table 2.

Table 2: Composition of A356 alloys used for the study.

Composition of A356 alloy (wt%)					
Al	91.1 - 93.3	Fe	<0,15	Zn	<0,05
Si	6,50 - 7,50	Cu	<0,03	Ti	0.10 – 0,15
Mg	<0,05	Mn	<0,05	Cr	<0,01
Ni	<0,05	Ca	<0,003	Co	<0,02
Na	<0,002	P	<0,002	Pb	<0,05
Sb	<0,001	Sn	<0,05	Sr	<0,016

After a solutioning at 540°C for 4 hours, different quenching and ageing treatments were performed. In particular the specimens were subjected to water or air quenching, followed by ageing at 170°C for 3 or 9 hours. Three castings for each condition were treated. The tensile specimens, from the middle section of the different steps of castings were machined according to ASTM-B577. The tensile tests were carried out on a computer controlled testing

machine at a constant cross head speed of 2 mm/min. A strain gauge extensometer (gauge length of 25 mm) was used to measure the deformation.
In addition some virtual thermocouples have been inserted in the casting in correspondence of the middle section where tensile specimens were obtained in order to reproduce the evolution of temperature during quenching.

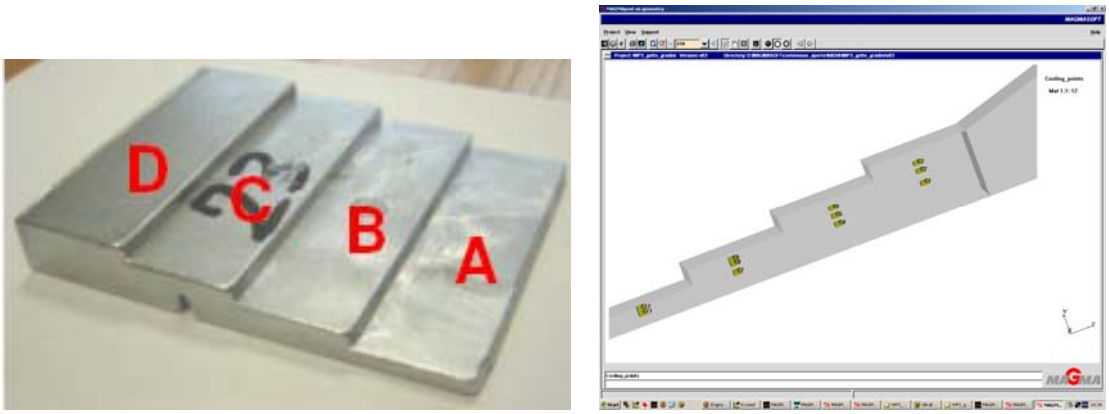

Figure 4: On the left, the reference step casting is shown while, on the right, it is illustrated the position of virtual thermocouples

The validation of models followed different steps, consisting in

- elaboration of literature data (Table 3) to make more flexible the model with respect to working conditions;
- evaluation of quench factor;
- elaboration of data achieved from experimental investigations;
- final comparison between experimental data and model output.

Table 3: Age hardening model parameters suggested by Rometsch and Schaffer [15].

Temperature (°C)	Time to peak, t_p (s)	Peak HB	Peak YS (MPa)	Initial S_0 (MPa)	P_p(x10^{-14}) (sK^{-1})
150	263090	117	272	213	4.90
170	39156	115	268	208	3.71
190	5188	117	271	212	2.17
210	1630	110	256	197	2.66
230	699	103	239	180	3.98
250	268	89	207	148	4.83

Particular attention was paid to the time for hardness to peak (t_p) and to parameter P_p, describing the diffusion mechanism. Data interpolation was used to correlate these parameters to the process temperature (T); the results are shown in Figure 5 and 6.
The influence of process temperature on time to peak and on term P_p can be adequately described by means of Eq. (10) and Eq. (11) respectively:

$$t_p = 5 \cdot 10^{34} T^{-13,496} \quad (10)$$

$$Pp = -5 \cdot 10^{-06} T^3 + 0{,}0039 T^2 - 0{,}9586 T + 77{,}878 \quad (11)$$

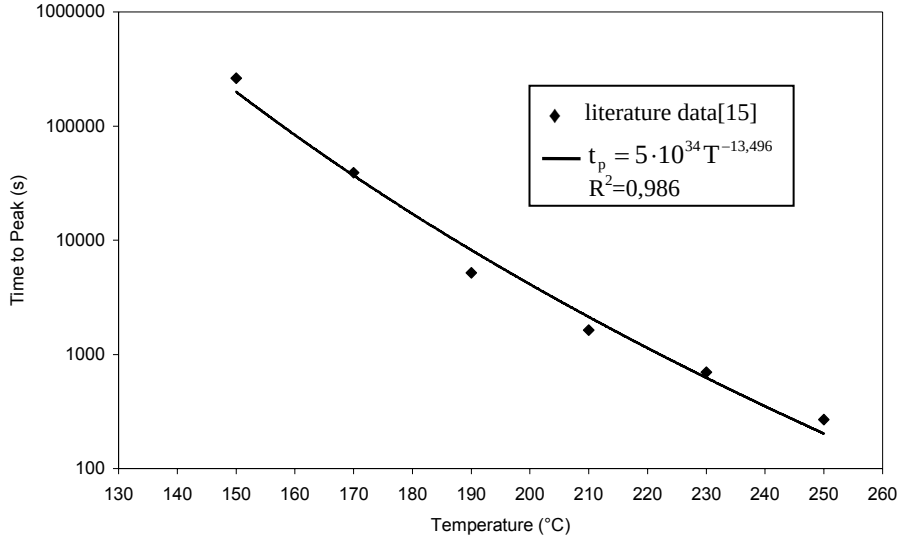

Figure 5: Variation of time to peak, t_p, as a function of different aging temperatures.

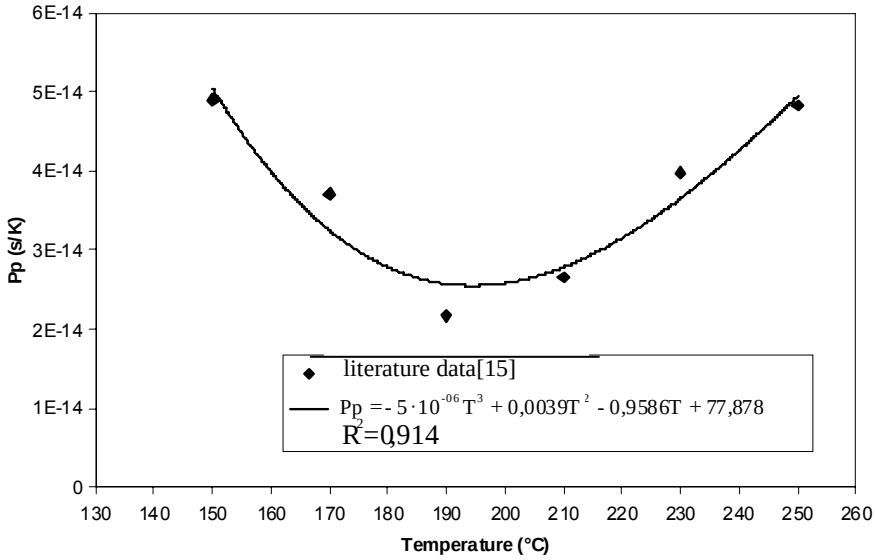

Figure 6: Variation of P_p as a function of different aging temperatures.

The Quench Factor has been determined superimposing the C-curves on the cooling curves (describing the temperature change of the component as a function of processing). The cooling curves were calculated by means of Heat Treatment module of MAGMASOFT (V4.4) [17]. In order to achieve numerical results close to real cooling treatment, special attention to boundary conditions was paid.
Table 4 summarizes the values obtained for both water and air quenching. The Quench Factor has been evaluated using Eq. (3) in the interval time during that C-curve and cooling curve are superimposed.

Table 4. Values of Quench Factor for air and water quenching.

		Quench Factor	
Sample	**Thickness(mm)**	**Water Quenching(25°C)**	**Air Quenching**
A	5	51,6	25692,9
B	10	97,7	26642,5
C	15	153,0	27349,2
D	20	197,9	27712,0

As it can be seen from Table 4, the value of Quench Factor for Air Quenching is one order of magnitude higher than those obtained for Water Quenching. The reason of this difference can be appreciated observing Figure 7 that shows the cooling curve for thermocouple in section A: in case of Air Quenching, the sample is hold, for each temperature, especially for vapour blanket phase, for a longer time as consequence of lower quenching rate. In general it can be established that the massive regions of the casting, being characterised by a lower cooling rate, display higher values of the quench factor. In addition, for Air quenching a more uniform cooling in the different sections has been achieved (the values of Quench Factor are close one to each other) while the different thickness of casting is more evident for water quenching.

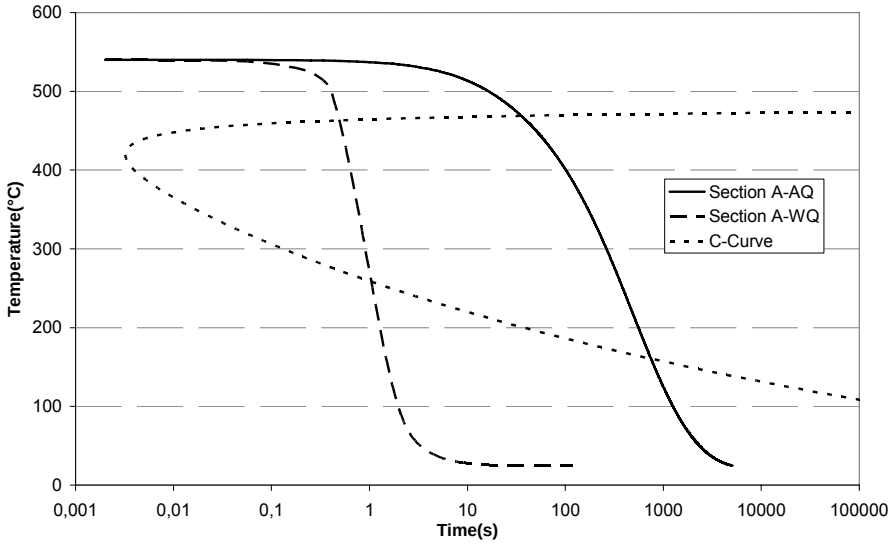

Figure 7: Comparison between water and air quenching curves for Section A

The dependence of Quench Factor from the Cooling Rate, plotted in Figure 8, can be explained by the power relation with an optimum R^2 value:

$$QuenchFactor=12930(CoolingRate)^{-0,9159} \quad (12)$$

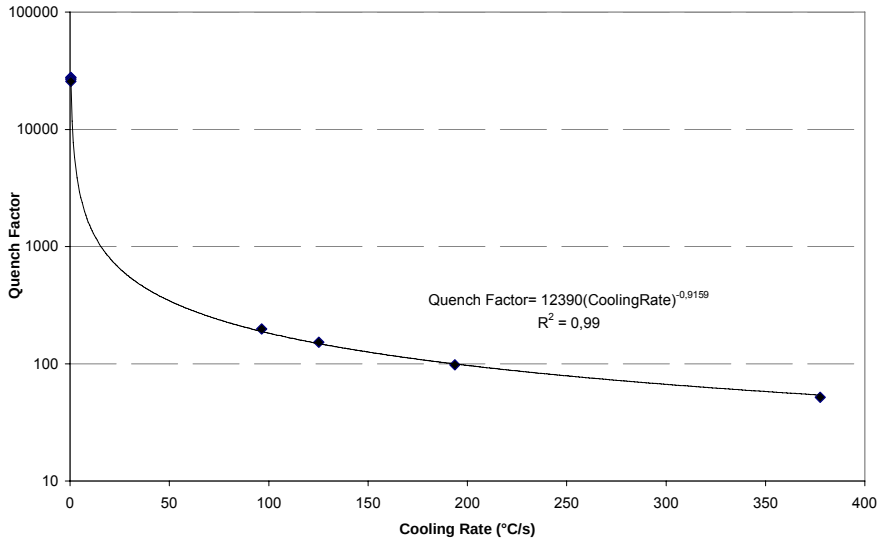

Figure 8: Dependence of Quench factor on Cooling Rate.

Table 5 displays the comparison for Yield Stress values between experimental data and those obtained using Eq. (8) and (9).
In addition, the Equation:

$$YS=YS_{ageing}(exp(K_1Q^{0,456}) \quad (13)$$

has been taken in consideration where square root dependency between strength and solute concentration is not taken into account and Avrami coefficient has been calculated minimizing mean square error between experimental and modelled YS values.

Table 5: Comparison between experimental and modelled YS values for the different treatments conditions.

	Quenching	Ageing Time (T=170°C)	Experimental data	$YS=YS_{ageing}(exp(K_1Q^{0,45}))$		$YS=YS_{ageing}(exp(K_1Q^{0,45}))^{1/2}$		$YS=YS_{ageing}(exp(K_1Q^{0,456}))$	
				Yield Stress (MPa)	Error (%)	Yield Stress (MPa)	Error (%)	Yield Stress (MPa)	Error (%)
Step A	Water	3h	254±5,2	269	5,6	272	6,8	268	5,4
	Air		148±4,6	170	12,8	217	31,8	165	10,4
	Water	9h	276±5,6	263	-4,8	267	-3,1	263	-4,7
	Air		178±0,7	167	-6,3	213	16,7	162	-9,4
Step B	Water	3h	258±3,4	266	2,9	271	4,7	266	2,7
	Air		145±1,9	169	14,4	216	33,0	164	11,7
	Water	9h	284±3,6	261	-9,0	266	-6,8	261	-9,1
	Air		179±1,8	166	-7,7	212	15,7	161	-11,1
Step C	Water	3h	254±1,4	264	3,7	270	6,0	263	3,5
	Air		147±1,2	168	12,6	216	31,9	163	9,8
	Water	9h	278±5,7	259	-7,6	265	-5,1	258	-7,8
	Air		178±2,3	165	-7,8	212	15,9	160	-11,3
Step D	Water	3h	248±1,0	263	5,9	269	8,0	262	5,3
	Air		146±1,9	168	13,1	215	32,1	162	10,2
	Water	9h	277±1,5	257	-7,9	264	-5,1	252	-8,1
	Air		178±0,7	165	-7,6	211	15,8	159	-11,4

If Eq. (9) is considered, a good agreement between experimental and modelled data for water quenching can be observed: in case of an ageing for 3 hours the YS values are overestimated of an average value of 6,3% while in case of 9 hours the YS is underestimated of about 5%. However, the model shows a poor reliability for air quenching where the error assumes values up to 30%.
Better results have been achieved if Eq. (8) or Eq. (13) are considered. In general it can be noted that the models tend to overestimate the mechanical properties in case of ageing for 3h while underestimate the values for a longer treatment with an error lower then those obtained with previous Equation.

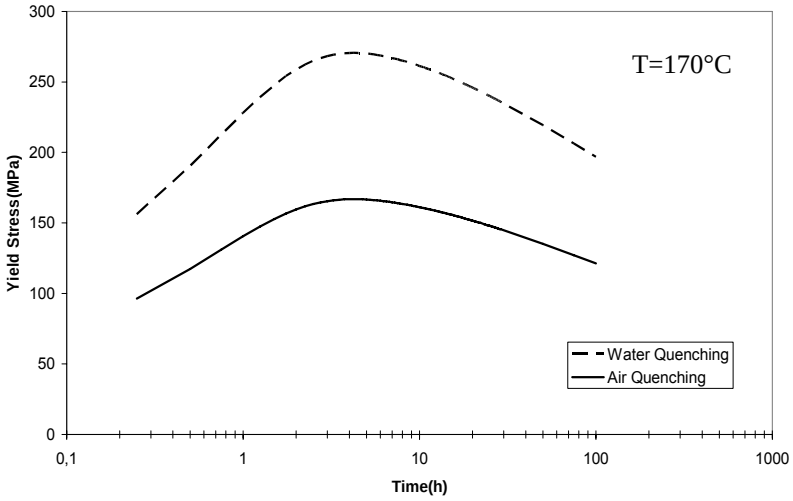

Figure 9: Modelled ageing curve using Eq. (12) for water and air quenching.

In particular, for the Eq. (8), the mean error is about 4,5% for water quenching and ageing at 170°C for 3h and 13% in case of same ageing conditions and air quenching. These values became, for the same condition, equal to 4,2% and 10,5% if Eq. (13) is considered. This Eq. allows to achieved an average value of -7,4% and -10,8% in the case of ageing of 9h and water or air quenching respectively.
Figure 9 displays the two curves associated to the Eq. (13) for the two conditions of quenching and ageing at 170°C. A lower quenching rate reflects upon a decreasing of mechanical properties as consequence of a lower quantity of solute available for precipitation during ageing.

3. APPLICATION OF MODEL

In order to evaluate the influence of a more complex geometry on the reliability of the model, a further validation has been performed on TKAL mono-cylinder. The components were low pressure die cast using A356 alloy. Eight different thermocouples were inserted into samples in order to record the cooling curves during quenching, Figure 10. Thus, after a solutioning at 540°C for 4 hours, different quenching and ageing treatments were performed. In particular the castings were subjected to water or air quenching, followed by ageing at 170°C for 9, in the first case, and 3 hours in the second one

Figure 10: On the left, TKAL low pressure die casting mono-cylinder is shown while, on the right, it is illustrated the position of thermocouples.

The results of quenching monitoring are shown in Figure 11. As expected, the cooling rate in the case of water quenching is much higher than for air quenching. This reflects upon Quench Factor values. In the first case the value is in the interval between about 50 and 245, while in the second case the values are from 79000 and 83000, in dependence of the thickness of the sections. If these values are compared to those calculated for step reference casting it can seen that the different geometry and thicknesses lead to increase the value of Quench Factor; in the case of step reference casting the value of Quench Factor is about 25000 rather than 83000. On other hand, the different is not evident if water quenching is considered. In addition, it can be seen that the air quenching allows to achieve a more uniformity between the sections: the difference between the higher and lowest values is in the order of 5% while for water quenching is about 70%.

Table 6: Values of Quench Factor.

Thermocouples	Quench Factor	
	Water	Air
T1	75,4	79929,8
T2	82	78015,8
T3	53,1	82868,8
T4	111,5	82975,5
T5	65,4	83811,6
T6	244,1	81426,3
T7	63,9	81928,7

Consequently, the amount of solute that can precipitate during the treatment increases and the mechanical properties after ageing decrease.

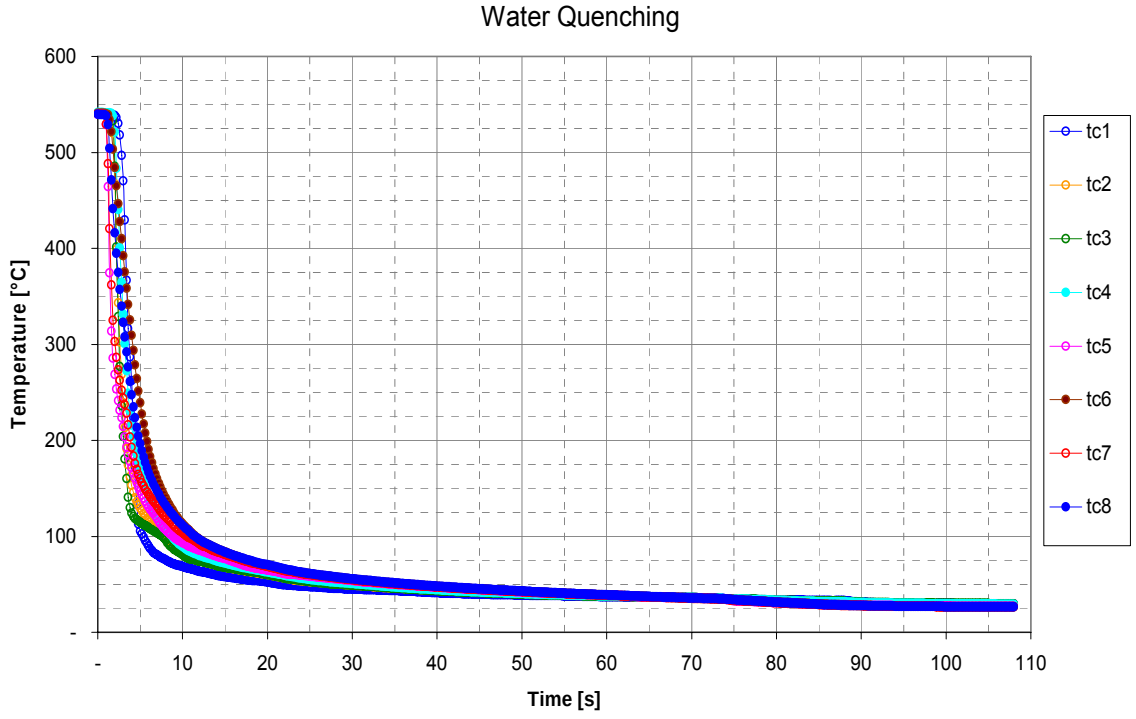

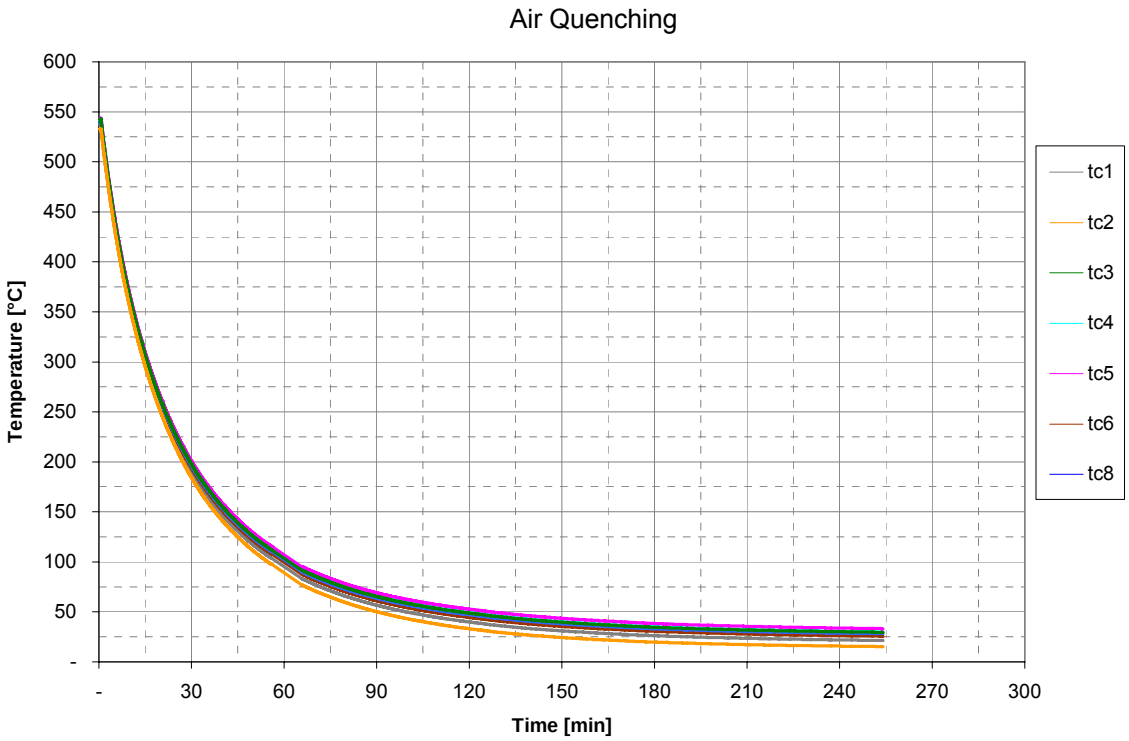

Figure 11: Monitored cooling curves for water and air quenching.

In Figure 12, the comparison between Quench Factor calculated by means of Eq.(12) or the procedure illustrated in paragraph 1 is shown. A good agreement can be noted. This suggests the possibility to calculate the values of Quench Factor directly from cooling rate, simplifying the procedure.

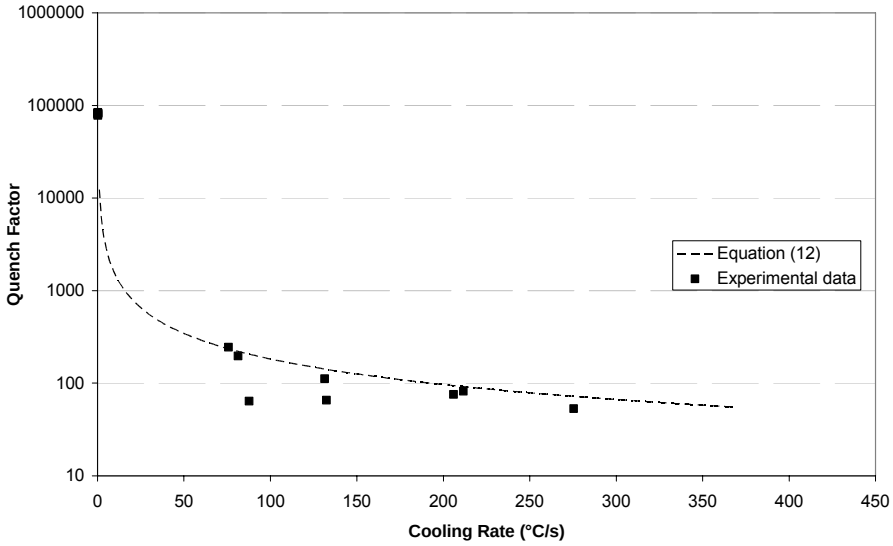

Figure 12: Comparison between calculated and modelled Quench factor values.

The mechanical properties, in particular yield stress, were obtained by means of static tensile test, carried out on specimens, machined from different zones. In particular, three cylindrical specimens were achieved for the columns in the top part of the casting (in correspondence of T4) and other two plate samples from bulkhead supports (in correspondence of T7 and T8), Figure 13.

The test procedure was the same described in paragraph 2. The values of Yield Stress were compared to those obtained implementing the model. The results are shown in Table 7. From the Table, a good agreement between experimental and modelled data in the both treatment conditions can be observed. In the case of water quenching, the average error value is 0,98% (the error of 11,5% is due to defects in casting that decreased the properties) while for air quenching the value is 5,8%.

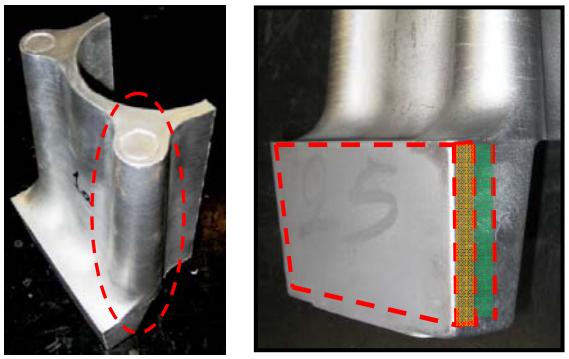

Figure 13: Zones of the monocylinder where the samples for tenile test have been obtained.

Table 7: Comparison between experimental and modelled data.

Treatment Conditions	Experimental Data (MPa)	$YS=YS_{ageing}(exp(K_1Q^{0,456})$ (MPa)	Error (%)
Quenching water **Ageing** 9h at170°C	258,6	262,4	1,47
	257,5	256,6	-0,33
	264,4	261,4	-1,16
	230,0	259,9	11,50
	-	261,4	-
Quenching air **Ageing** 3h at170°C	117,4	115,7	-1,46
	114,4	115,6	1,05
	107,1	117,9	9,19
	103,7	115,1	9,90
	109,4	117,9	7,24

.

4. CONCLUSIONS

Three models integrating quenching and age hardening parameters have been developed and analysed. The results are summarised as followed.

- The quench factor values depend on a geometry factor, on a thickness factor and on the heat thermal coefficient. All these aspects increase the time of intersection between C-curves and cooling curves, thus increasing the quench factor values.
- A model that correlates the Quench Factor to cooling rate has also been provided. The model has been developed on step reference casting and validated on low pressure die cast monocylinder. A good fitting between calculated and modelled values could be noted.
- The results of the model based on Eq. (13), developed on step reference casting and validated on low pressure die cast monocylinder, are in good agreement with the experimental data. This model doesn't incorporate a square-root dependency of the yield strength on the precipitate volume fraction and assumes an Avrami coefficient equal to 0,456, minimizing the mean square error between experimental and modelled YS values. Note that this value is close to 0,45, proposed by Rometch and Schaffer from the fitting between $\ln\left[\left(\frac{1}{k_1}\right)\times\ln\left(\frac{YS-YS_{\min}}{YS_{\max}-YS_{\min}}\right)\right]$ vs ln(Q). Thus, this result can be related to the beginning state of precipitation through a diffusion mechanism at the dislocation sites.

ANNEX A. PROCEURE TO DETERMINE C-CURVE

The C-curve describes the time required, at different temperatures, for the precipitation of a constant quantity of solute; it was defined by Evancho and Staley [8] as the reciprocal of the nucleation rate equation. The curve can be described using the following equation:

$$C_t = -k_1 k_2 \exp\frac{k_3 k_4^2}{RT(k_4 - T)^2} \exp\frac{k_5}{RT} \qquad (14)$$

where C_t is the critical time required to form a specific percentage of a new phase; k_1 is a constant which equals the natural logarithm of the fraction untransformed during quenching (typically 99,5%: ln(0,995)=-0,00501; k_2 is a constant related to the reciprocal of the number of nucleation sites; k_3 is a constant related to the energy required to form a nucleus; k_4 is a constant related to the solvus temperature; k_5 is a constant related to the activation energy for diffusion; R is the universal gas constant, 8,3144 J/°K*mol; T is the absolute temperature (K).
The characteristic shape of the C-curve can be explained as follows; at temperatures just below the solution heat treatment temperature it takes a considerable amount of time for precipitation to occur because the driving force for transformation is low due to small undercooling. With increased undercooling, the driving force for precipitation is high, and the time required for precipitation is low. This temperature region is commonly known as the critical temperature range as the time spent in this region will have a major impact on the mechanical properties of the alloy. At lower temperatures, the time required for precipitation increases again as the driving force for precipitation is high but the solid-state diffusion rates are low. [18]
In order to determine the C-curve, the procedure developed by Fink and Willey [19] who used interrupted quenching technique can be considered. As illustrated in Fig. 14(a), to construct a C-curve, thin samples of the alloy are solution heat treated and quenched very rapidly in a salt bath to a given temperature, held at that temperature for a period of time, and rapidly quenched again, this time to room temperature. The sample is then age-hardened and its hardness measured. This procedure is repeated for a large number of samples at different holding temperatures and holding times. Figure 14(b) shows three different C-curves, each corresponding to a different hardness ratio, HR: as shown in Fig. 14(b), the C-curve is named as such because it is a C-shaped locus of points on temperature-time coordinates corresponding to equal hardness values. The general features of the TTT diagram are dearly manifested in the C-curve: high and low temperatures require large times to attain a given precipitation, ξ_c, that would result in the desired hardness, while intermediate temperatures demand much smaller times for the same precipitation and same hardness [13].

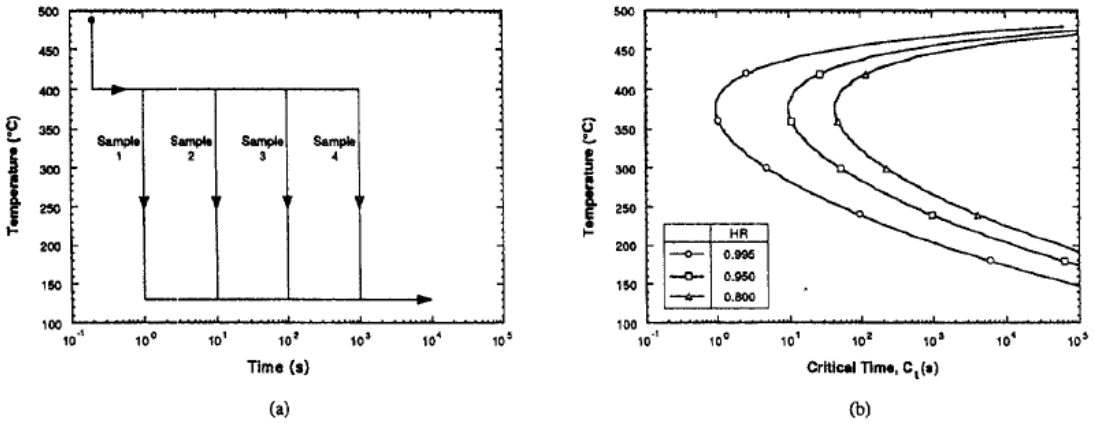

Figure 14. (a) Delayed quenching technique used to determine the C-curve and (b) C-curves for aluminium 2024-T6.

In general, while C-curves for different aluminum alloys are similar in shape, their relative positions on temperature-time coordinates depend on the values of k_2-k_5 which are determined using the iterative non-linear fitting procedure. The values of the constants for different aluminium alloys are displayed in Table 8.

Table 8. Values of constants k2-k5 for different aluminium alloys.

Alloy	Constants			
	k_2 (s)	k_3 (J mol^{-1})	k_4 (K)	k_5 (J mol^{-1})
A356-T6 [9]	3.0×10^{-11}	64	764	130000
A357-T6 [9]	1.1×10^{-11}	154	750	131000
2017A-T4 [18]	6.8×10^{-21}	5794	900	206784
2024-T6 [13]	2.38×10^{-12}	1310	840	147000
6061-T6 [18]	5.1×10^{-8}	978	822	94182
7050-T76 [19]	2.2×10^{-19}	5190	850	180000
7075-T6 [19]	4.1×10^{-13}	1050	780	140000
7175-T73 [18]	7.6×10^{-10}	412	750	112200
Al-2,7Cu-1,6Li-T8 [20]	1.8×10^{-8}	1520	870	102000

REFERENCES

[1] C.M. Estey, S.L. Cockcroft, D.M. Maijer, C. Hermesmannb, Materials Science and Engineering A 383 (2004) 245–251

[2] J. L. Cavazos, R. Colás, Materials Science and Engineering A363 (2003) 171–178

[3] L. Pedersen, L. Arnberg, Metallurgical and Materials Transaction A, Volume 32A (March 2001), pp.525-532

[4] Th. Herding, O. Kessler, F. Hoffmann, P. Mayr, Material Science Forum Vols.396-402 (2002) pp. 869-874

[5] J.L. Cavazos, R. Colas, Material Characterization 47 (2001), pp. 175-179

[6] M.F. Komarova, N.N. Buynov, L.I. Kaganovich, Phys. Met. Metallogr. 36 (1973), p.72.

[7] S. Shivkumar, S. Ricci, C. Keller, D. Apelian, J. Heat Treat. 8 (1990), p.63.

[8] W. Evancho, J.T.Stanley, Metallurgical transaction, 1974, 5, 43-47.

[9] P.A. Rometsch, G.B. Schaffer, Int. J. Cast Metals Res.,2000, pp.431-439J.

[10] P.A. Rometsch, M.J. Starink, Material Science & Engineering, 2003, pp. 255-265

[11] M. Shuhui, A Methodology to Predict the Effects of Quench Rates on Mechanical of Casting Aluminum Alloys, Ph.D. Thesis

[12] D. H. Bratland, 0. Grong, H. Shercliff, 0. R. Myhr and S. TjØtta, Acta Mater. Vol. 45, No. I, pp. l-22, 1997

[13] J. D. Bernardin, I. Mudawart, Int. J. Heat Mass Transfer. Vol. 38, No. 5, pp. 869873, 1995

[14] ASM International, Heat treatment of aluminum alloys, ASM Metals Handbook, Vol.4, pp. 841-861.

[15] P.A. Rometsch, G.B. Schaffer, Materials Science and Engineering A325, 2002, pp. 424-434.

[16] H.R. Shercliff, M.F. Ashby, Acta Metall. Mater. 38 (1990) 1789.

[17] F. Bonollo, S. Odorizzi, Numerical Simulation of Foundry Processes. SGE, Padova (2001).

[18] G.P. Dolan, J.S. Robinson, J. of Materials Processing Technology 153–154 (2004) 346–351

[19] W.L. Fink, L.A. Willey, Trans. AIME 175 (1948) 414–427

[20] J.T. Staley, R.D. Doherty, A.P. Jaworski, Physical Metallurgy and materials science 1993, vol. 24, 11, pp. 2417-2427

ARTICLE 5

VALIDATION OF NUMERICAL SIMULATION CODE IN THE DEVELOPMENT OF AN AUTOMOTIVE COMPONENT

Fabio Grosselle*, Giulio Timelli*, Franco Bonollo*, Nicola Gramegna**

* Department of Management and Engineering – DTG
University of Padova
I-36100 Vicenza
ITALY

** Enginsoft Spa
I-35129 Padova,
ITALY

To be Submitted in: Journal of Materials Processing Technology .

ABSTRACT
An integrated approach to design considers all life cycle aspects of a component since the design stage. From the manufacturing process to the demolition, all variables are taken into account in order to develop a component with increasing quality and well-known potentiality reducing, at the same time, costs and time to market.
These requirements are nowadays a must for automotive companies as a consequence of a growing competitiveness and a more and more complex market.
In order to achieve this objective, the numerical simulation process plays a key role because it allows to predict the evolution of a component during both manufacturing process and working life in the early stages of its development.
Especially for a casting component, the possibility to forecast defects, microstructure and mechanical properties reduces costs and efforts improving quality and soundness.
In this paper, a validation of the results provided by the commercial MAGMASOFT® v4.6 software is proposed. The study was carried out in the development of A356 aluminium alloy mono-cylinder engine block, cast by means of Low Pressure Die Casting. Therefore, the comparison between experimental data and simulation results was performed in terms of solidification time, porosity and die temperature along with microstructure features and mechanical properties in as-cast state and after heat treatment. The comparison showed the good accuracy and reliability of simulation code in the forecasting the overall properties of casting and how the simulation can be very useful in design stage.

KEYWORDS
Casting simulation, aluminium, process simulation, microstructural properties, mechanical properties, low pressure die casting.

INTRODUCTION

Aluminium continues to expand in automotive applications being driven by weight reduction and its associated benefits [1]. At the same time, the development a components with increasing quality and well-known potentiality at low costs and short time to market is nowadays a must for automotive companies as a consequence of an enhanced competitiveness and a more and more complex market.

This purpose is achievable by means of process simulation that, taking basis in the modelling of process or physical phenomena, allows to determine the viability of a process or to optimize the process parameters reducing the variability of the system[2].

In today's industrial production plants, state-of-the-art software systems are used to analyze different loading conditions in order to determine the strength and durability of a product. Similarly, production companies are using simulation for manufacturing processes, such as, for example, casting and forging. Advances in computational mechanics, such as the FEA Finite-Element Method, have also made their way into modern production facilities a long time ago. Again, clear advantages of simulation are shortened product development cycles, improved assessments of product quality, and importantly, savings in experimental time and equipment [3-5].

Considering its industrial infrastructure, the area of manufacturing process simulation shouldn't be regarded as a separate domain of computation. A multi-scale simultaneous engineering approach can improve quality and performance of components that come from a unique combination of design, processing, microstructural evolution features, and not from a simple casting operation [6].

The numerical simulation of foundry processes is mainly based on the solving of the equations [7]:

- in fluid dynamics, such as Navier–Stokes equation, for the filling of the cavity by means of a molten metal;
- in heat transfer, such as Fourier equation, for solidification and cooling of the alloy.
- in physical metallurgy for solid state transformation, related with thermodynamics and kinetics.

The filling and solidification are the basic aspects of the casting process simulation to predict the defects and the microstructure evolution in view of the final inhomogeneous mechanical properties.

In addition, the full integrated method needs to include the residual stress and strain distribution in the casting at room temperature. Due to different degrees of constraint by the mould and casting shape (e.g. various thickness and cooling rate), the non uniform contraction of the casting during the solidification as well as in quenching operation, can generate distortion, hot tears or cold crack initiation reducing strengthening and ductility of casting.

The simulation code allows the prediction of the microstructure evolution of the alloy and defect formation during the whole production process. In this way, final mechanical properties in as-cast temper and after heat treatment can be also predicted and, thus, they can be used as an input to structural simulation programs such as ANSYS or ABAQUS, and thereby be able to make good progress in design [8].

In this study, the validation of results provided by a commercial simulation software is proposed considering A356 aluminium alloy mono-cylinder engine block, cast by means of Low Pressure Die Casting. The comparison between simulation and experimental data in terms of solidification time, porosity and die temperature along with microstructure features and mechanical properties is discussed.

CASTING

The component studied was a mono-cylinder engine block. It was cast by means conventional low pressure die casting (LPDC) process using primary A356 aluminium alloy (7.2 Si, 0.09 Cu, 0.1 Fe, 0.1 Mn, 0.41 Mg, Zn 0.08, balance Al, contents in wt-%). Strontium was added to modify the Al–Si eutectic. Casting and the die are shown in Figure 1(a) and (b), respectively.

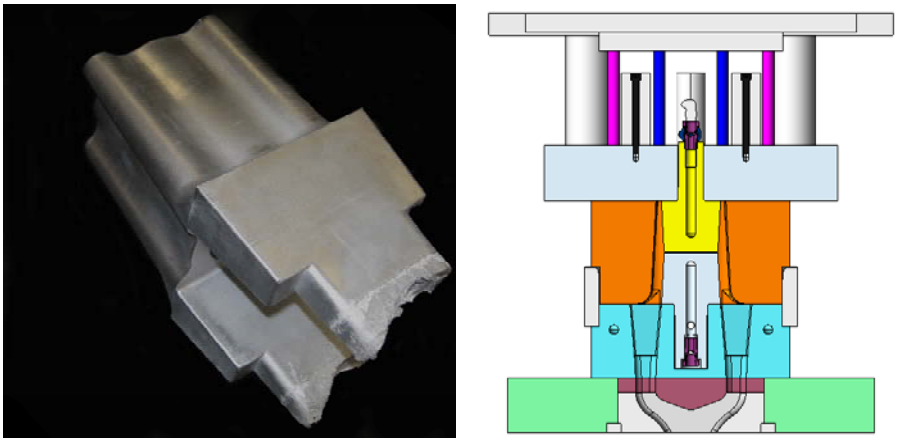

(a) (b)

Figure 1. (a) The mono-cylinder engine block and (b) mould die used for the production of castings.

The material was first melted in an electric-resistance furnace setup at 720±5°C. The pressure and time ramp of filling were set up in order to minimize the turbulence of molten metal inside the die cavity. In addition the flow of water in ten cooling circuits was set up in order to optimize the gradient of solidification and avoid the formation of shrinkage porosity. All casting was controlled by means X-Ray to verify the good integrity of them.

A semi-permanent layer of DYCOTE® F34 coating was spray applied on the die walls at the temperature of about 200°C according to standard practice.

Before pouring the melt, the temperature of the die was increased to about 250±10°C. In order to evaluate the local temperature and assure a good reproducibility of the tests, thermal evolution of die was followed by the use of three thermocouples inserted in different zones.

With the aim of analyze the variation of mechanical properties and test the consistency of numerical simulation, two casting were subjected to different T6 heat treatment. Both the components were solubilised in an electric-resistance heated-air-circulating box-type muffle furnace at 540±1°C for 8 h.

After solutioning, one casting was air quenched and then artificially aged at 170±1°C for 3h. In turn, the other casting was subjected to water quenching at room temperature and artificial ageing at 170±1°C for 9h.

Consequently, samples were cut from different zones of casting, Figure 2, considering different solidification rate to quantify the microstructure features such as SDAS and iron rich intermetallics. Thereafter, they were mechanically prepared to a 3-μm finish with diamond paste and, finally, polished with a commercial fine silica slurry for metallographic investigations.

A light microscope and image processing software were then used. The measures were carried out considering of at least 8 photographs of each specimen to obtain a statistical average of the distribution. Average Secondary Dendrite Arm Spacing (SDAS) values were obtained using the linear intercept method, which involves

measuring the distances (spacing) between secondary dendrite arms along a line normal to the dendrite arms.

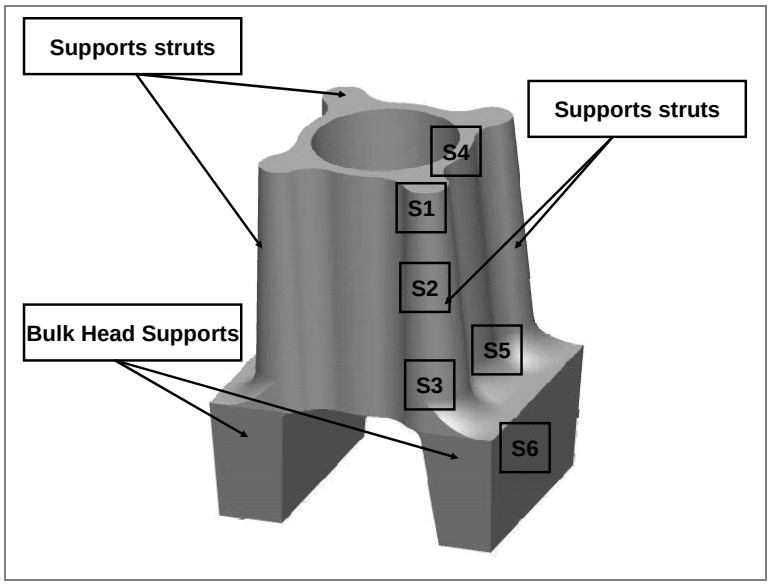

Figure 2. CAD geometry of the casting showing the sectioning scheme for metallurgical investigation and zones where tensile specimens were machined out.

Cylindrical tensile specimens were machined from the bulk-head supports and supports struts of casting according to ASTM-B577. Radiographic inspection has been performed on tensile specimens before mechanical testing, in order to assure an acceptable level of soundness.

The tensile tests were done on a computer controlled tensile testing machine. The crosshead speed used was 2 mm/min ($\dot{\varepsilon} \sim 10^{-3}$ s^{-1}). The strain was measured using a 25-mm extensometer. Experimental data were collected and processed to provide the average value of yield stress (YS, actually 0.2% proof stress), ultimate tensile strength (UTS) and elongation to fracture (s_f).

CASTING SIMULATION

The MAGMASOFT® v4.6 (2007) commercial software, with its module for low pressure die casting, was used for numerically simulating the filling and solidification behaviour of analysed component. The non-ferrous module was then used to predict microstructural features and mechanical properties.

Basic governing equations of the software are continuity equation, Navier–Stoke's equation, energy equation and volume of fluid (VoF) method for the free surface movement during the die filling. The numerical code employs the finite volume approach to convert differential equations into algebraic ones and solve them on a rectangular grid. The CAD model of the casting was drawn and imported in the simulation software where a controlled volume mesh of 132000 metal cells for the die cavity was automatically generated by the software. The initial conditions for numerical simulation were defined to reproduce the casting parameters. The pouring temperature was set at 720°C, while, for the die, the temperature for the first cycle was assumed to be at a uniform temperature of 250°C. In the subsequent cycles, the initial temperature in the die is taken to be the predicted temperature distribution at the end of the previous cycle. A number of 10–15 cycles were taken after the start up to reach a quasi-steady-state temperature in the die. The other physical constants and properties of the die and the alloys, and their evolution with temperature, were

chosen among those present in the software database, as well as the heat transfer coefficients (HTC), taking into account affecting parameters, like the type and thickness of coating, and the pouring temperature. Special attention was paid to the heat transfer coefficient for simulation of quenching. The coefficient defines the flux of heat from the component to the medium and than the quenching cooling rate and it depends on time and combination of casting shape and direction of immersion. An optimisation inverse method can be adopted to determine the heat transfer coefficient during quenching starting from the temperature-time curves measured in the real process. The same approach was originally applied to define the heat transfer coefficient between metal and die mould with or without coating.
To define the whole set of boundary conditions in the model, the process parameters (e.g. regarding the filling and cooling cycle) and the cycle time, acquired from the casting process, were imported in the software, increasing the reliability of numerical simulation. Virtual thermocouples were inserted in the different zones of the die in order to control the temperature profiles and to compare these values with the real ones. Solidification time was assessed via numerical simulation code in order to predict the final microstructure of the casting. The mechanical properties of the aluminium cast alloy were predicted by using the newly developed add-on module to the simulation software.

RESULTS AND DISCUSSION

In next sections, the results provided by numerical simulation code in terms of filling and solidification processes as well as of microstructural and mechanical properties are reported and discussed. In addition, the use of Yield Stress distribution as input for F.E.M. software and the comparison between classic approach and process/structure integrated approach in the analysis of stress and fatigue strength are proposed.

1. FILLING AND SOLIDIFICATION PROCESS

The possibility to visualize the evolution of filling in the time allows to analyze the degree of turbulence of the molten metal in the cavity; thus, the susceptibility to incorporate gas, to form oxide inclusions or to produce “splash” or “shotting” phenomena can be investigated. In addition, the temperature distribution indentifies regions in which too much fast solidification may take place leading to an un-correct filling of die. In Figure 3, the distribution of temperature for the mono-cylinder at 60% and 95% of filling process can be displayed.

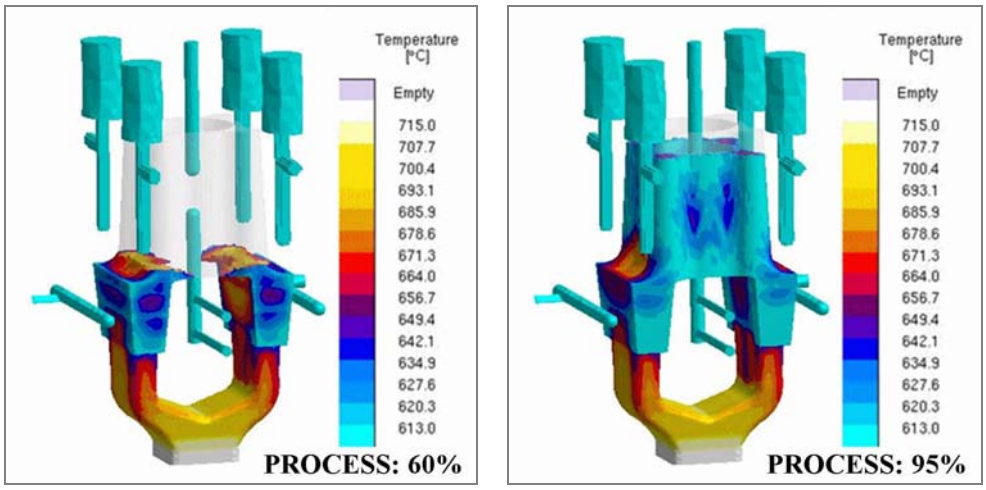

(a) (b)

Figure 3. Distribution of temperature during filling at (a) 60% and (b) 95% of the process.

The results shows that the flow of molten metal is quite laminar and the filling rate is in the typical ranges of a correct process; as consequence, no significant turbulence phenomena are likely to happen and, consequently, any dangerous gas entrapments is avoided. These results were confirmed by X-Ray investigation and metallurgical analysis that didn't reveal the presence of porosities with spherical morphology, typical for that kind of defect.

In addition, by the observation of temperature distribution, it can be noted that the temperature of liquid metal varies during the entire process from ~700°C to 613°C. Since the temperature of metal is always above the liquidus temperature, a gradual and complete filling of the die can be supposed.

When filling ends, solidification can start. In Figure 4, the distribution of temperature during solidification at 60% and 90% of the process is presented.

The analysis allows to visualize the gradient of solidification and to indentify the last zone of casting to solidify, as well. As consequence, the formation of "hot spot" and macro-shrinkage porosity can be detected. Furthermore, the effect of the cooling system on solidification rate can be investigated and the adjustments can be operated if necessary.

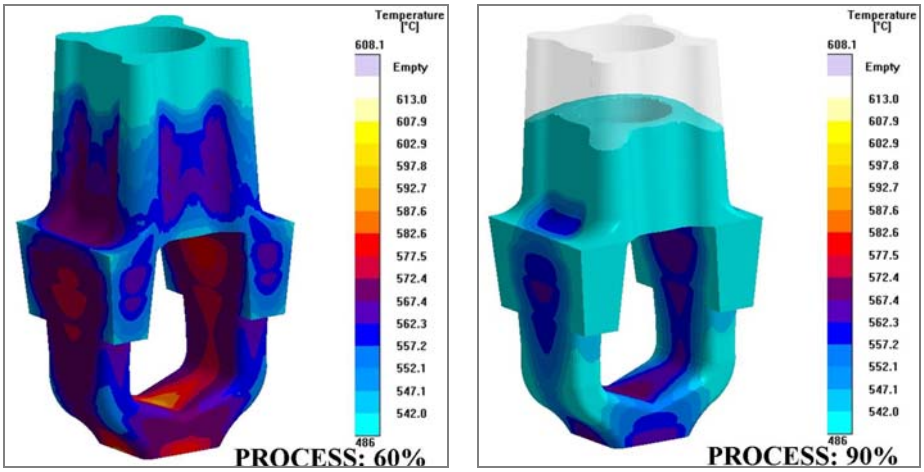

(a) (b)

Figure 4. Distribution of temperature during solidification at (a) 60% and (b) 90% of the solidification process.

As it can be observed that in general, the solidification gradually proceeds from the upper toward the bottom zone of engine block. Thus, in according with the LPDC principles, the last part to solidify is localized in the gating system. However, a localized zone with an higher temperature (~560°C) can be observed in top part of buck-head supports. Consequently the formation of internal shrinkage porosity can be promoted. This aspect was confirmed by the results shown in Figure 5. It refers to the *Porosity Criterion* analysis. This criterion allows to visualize the zones of the casting where the formation of shrinkage cavities are possible as consequence of un-correct filling of die due to the overcoming of the critical solid fraction. The value of this fraction depends on the combined effect of material and process. In general, for LPDC and Al alloy is around 30%. The result of simulation shows the presence of porosities in correspondence of the zone previously mentioned and it is also confirmed by the subsequent experimental investigation, Figure 5.

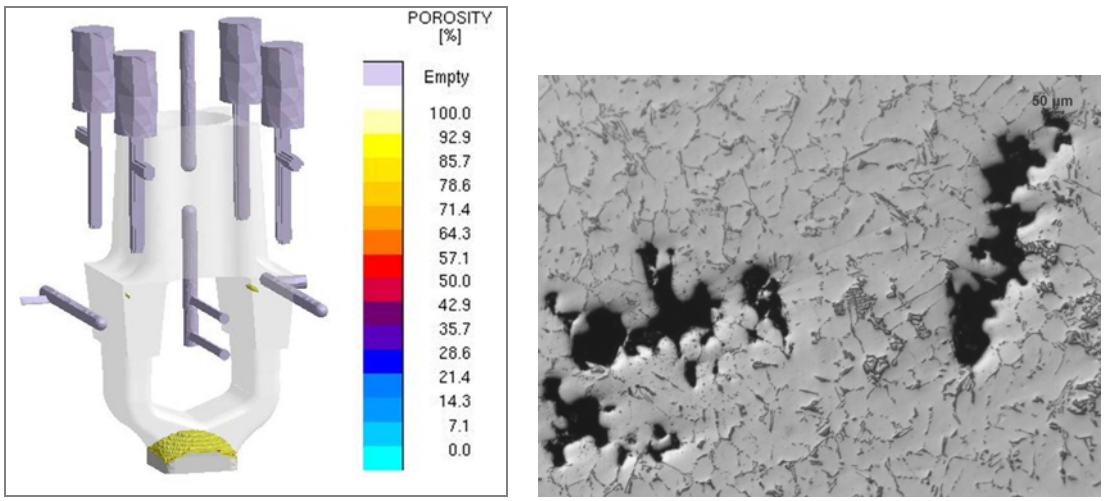

(a) (b)

Figure 5. Presence of porosity in bulk-head supports. (a) Results provided by numerical simulation and (b) results of experimental investigation.

In Figure 6 the distribution of solidification time can be observed.

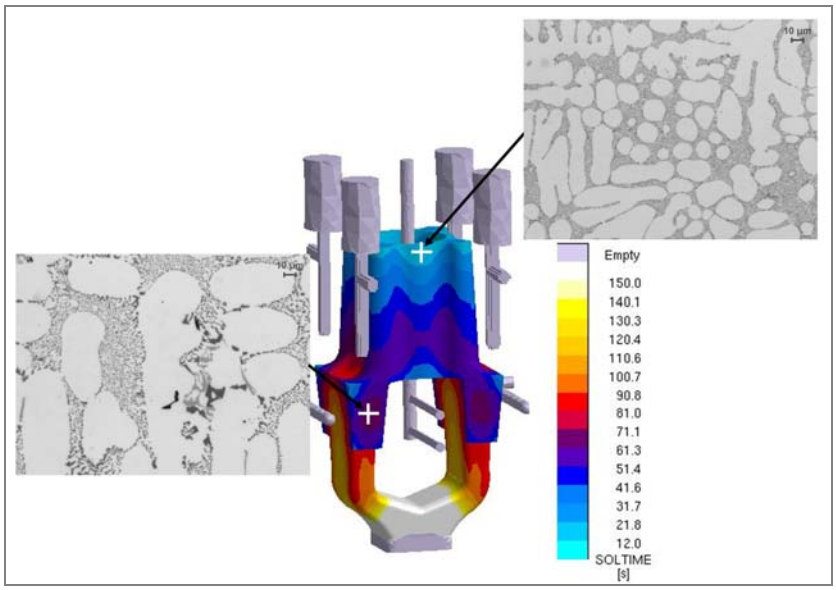

Figure 7. Solidification time required by the different zone of casting and microstructures in dependence of different thickness of the sections.

The total solidification time is about 150 sec. This is the time required for the solidification of massive sections of bulk-head supports while the thinner sections, in the top part of casting, require about 16 sec. Differences in solidification time reflect on the microstructure. As it can be noted, the coarseness of the microstructure varied inversely with the casting thickness, *i.e.* the solidification rate. Furthermore, in the more massive regions the formation of defects, such us micro-porosity or shrinkage porosity, is promoted.
In addition to filling and solidification process, the visualisation of the temperature distribution of the dies during can be useful in the determination of the amplitude of thermal cycle of the different regions and, consequently, in the description of the amount of the cooling actions. Furthermore, it allows to determine the more thermally stressed zones and, thus, susceptible of thermal fatigue.
In Figure 7, the temperature distribution of the die at 50% and at the end of solidification process is displayed.

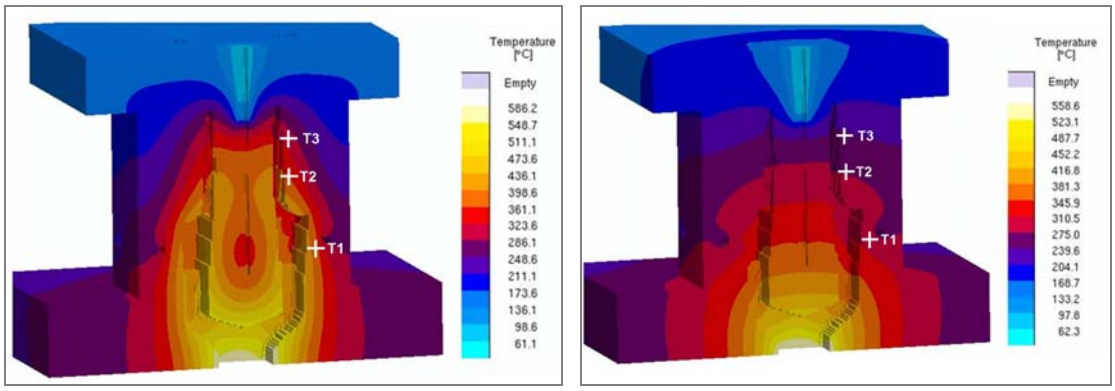

(a) (b)

Figure 7. Temperature distribution of the die (a) at the end of filling process and (b) at the end of solidification process.

When filling process is completed, the maximum average temperature is reached. In this condition, the temperature provided by simulation code is in the range between ~510°C and ~250°C. In detail, the highest temperature is measured in correspondence of in-gates and it decreases toward the top part of die. Due to the action of cooling circuits and the heat exchange between molten metal and die, as solidification proceeds, temperature decreases and, at the end of the process, the average temperature ranges between ~490°C and ~200°C. The comparison between virtual and real temperature values could be made by considering thermocouple T1 to T3. The results are reported in Table 1.

Table 1. Comparison between simulation results and experimental data for die temperature.

Thermocouples	Simulation results		Experimental data	
	End of filling	End of solidification	End of filling	End of solidification
T1	340°C	292°C	320°C	280°C
T2	342°C	274°C	316°C	276°C
T3	304°C	257°C	291°C	261°C

From the Table it can be noted that simulation tends to overestimate the temperature of the die both at the end of filling and at the end of solidification with an average error of ~ 5%. These differences can be associated to the heat transfer coefficient that

tends to underestimates the heat flow at high temperature along with the thermal inertia of thermocouples that cause delay in recording.

2. MICROSTRTUCTURAL OBSERVATION

The microstructure of casting consists mainly in dendrites of α-Al phase and well modified eutectic Al-Si. Iron-bearing intermetallics in form of Chinese script and Mg_2Si secondary phase can be also observed. Differences in solidification rate between upper and bottom part of casting reflect upon SDAS values as well as dimension of eutectic Silicon and Fe-rich particles. In general, a fine microstructure can be observed in the top part as consequence of thin section of the casting wall combined to the action of the cooling system. Vice-versa, in the bottom part, the high thickness of section leads to higher values of SDAS and coarser Si and Fe particles. In Table 1 the values of SDAS and Fe particles are collected.

Table 1. Values of SDAS and surface fraction and area of Fe-rich precipitates for the different samples.

Sample	SDAS (μm)	Fe-rich precipitates Surface fraction	Fe-rich precipitates Area (μm^2)
S1	21.9	1.21%	10.7
S2	27.2	1.15%	19.2
S3	32.0	1.11%	25.1
S4	15.9	0.87%	5.0
S5	37.5	0.67%	18.1
S6	33.5	0.97%	25.7

The distribution of SDAS provided by numerical code is shown in Figure 8. SDAS is described as a function of local solidification time by means of Equation 1, where t_s is the local solidification time, C and n are constants which are related to the material:

$$SDAS = C*ts^n \quad (1)$$

typical values of C and n for A356 alloy are 11.55 and 0.31.

In according with the distribution of local solidification time shown in Figure 5, it can be stated that SDAS varies from ~23 to ~40 μm in dependence of solidification rate.

In Figure 8 the comparison between experimental and simulation data is also provided. The best matching is obtained for the highest values of SDAS for which the average error is 4.6%; in turn, the experimental value is overestimated of 18.5% in the thinnest sections. However, it can be stated that the simulation enables the prediction of the local SDAS with good precision and reliability.

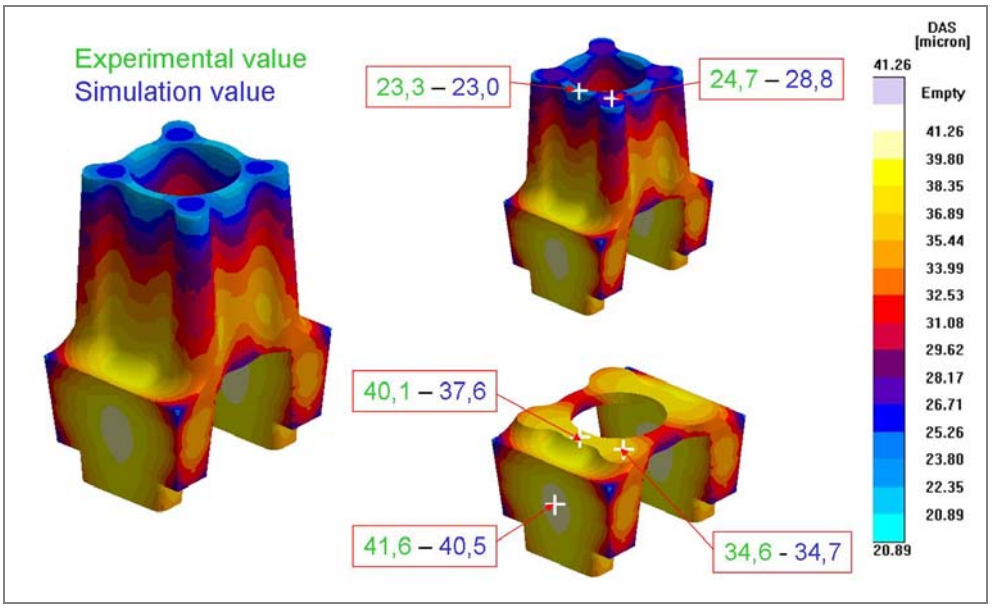

Figure 8. SDAS distribution provided by simulation code and comparison with experimental data.

It is well known that the mechanical properties of an aluminium alloy depend also on Fe-rich precipitate [9-10]. Iron-bearing phase can assume different morphology and shape in dependence of cooling rate and alloy composition. At lower iron level up to 0.8% and without addition of "neutralizer" element, the iron precipitates in form of β-Al_5FeSi needles precipitates [11]. These needles are very hard and brittle and have relatively low bond strength to the matrix. In addition, the acicular morphology promotes the fracture mechanism increasing the tension field around particles [12-13]. Manganese is often added in order to convert their morphology reducing the embrittlement and to alter the shape from sharp needles to a more compact type α-$Al_{15}(Fe,Mn)_3Si_2$ [11]. However, iron-reach needles are always present as long as iron and manganese are present. Another way to suppress the formation of these monoclinic Al_5FeSi-needles is by employing a high solidification rate to retain Fe in solid solution and/or to provide finely distributed hexagonal α-Al_8Fe_2Si with a skeleton-like morphology [11, 14-17]. The effect of cooling rate on size of Fe-rich precipitate can be appreciated in Figure 9 where the area of these particles is plotted in function of SDAS. A longer solidification time promotes growing mechanism and, thus, coarser particles can be observed. In particular, the average area varies linearly from ~5 to ~36 μm^2 as SDAS increases from ~16 to ~42μm. The dependence can be described by the following Equation:

$$\text{Area Fe-Bearing phase} = 1.19 \times \text{SDAS} - 14.6 \quad (2)$$

with a coefficient of determination R^2 of 0.98.
Since the presence of Fe-bearing phase affects negatively mechanical properties reducing the strengthening and the ductility of the alloy, the possibility to predict the local distribution of these phases can be useful in the localization of potential critical zones in the casting. Therefore, the Equation was implemented in the post-processor of simulation software to obtain the mapping of Fe-intermetallic phase for the whole casting. The result is shown in Figure 10.

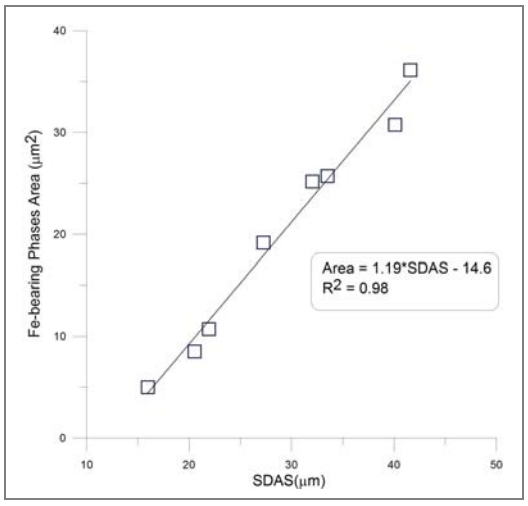

Figure 9. Variation in Fe-rich precipitate size as function of SDAS.

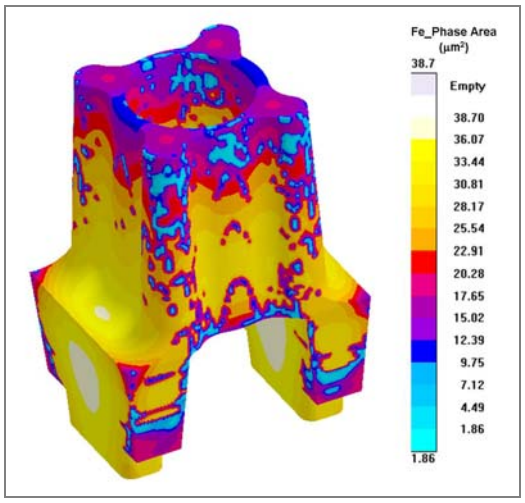

Figure 10. Mapping of Fe-bearing phase for whole casting.

However, due to its importance, simulation software was already able to predict the presence of Fe in terms of surface fraction as shown in Figure 11. The comparison between experimental and predicted values can be also observed.

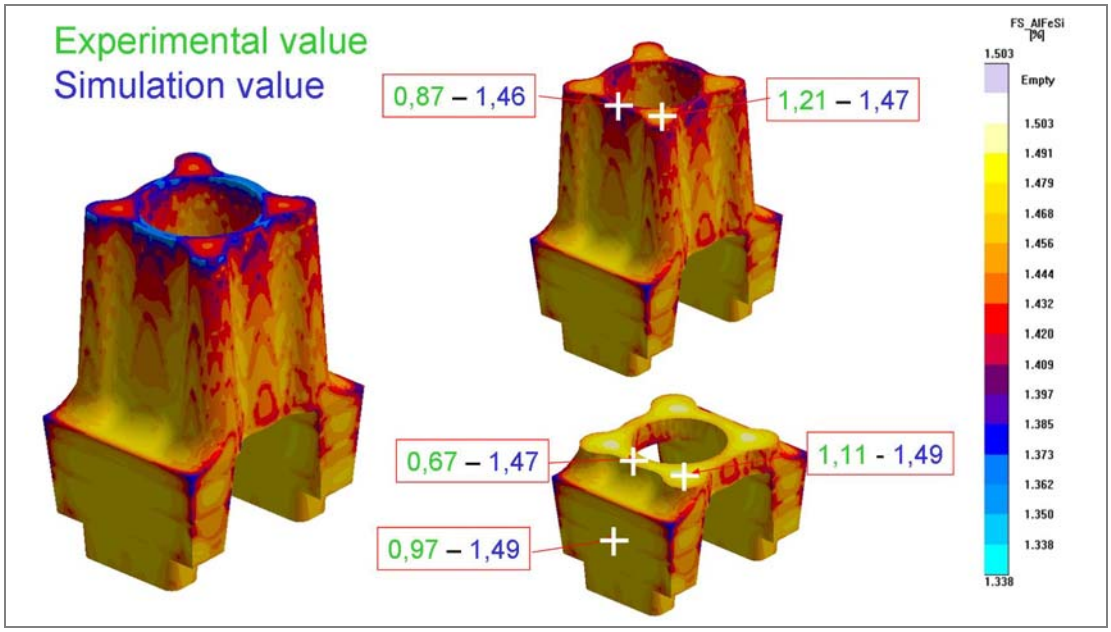

Figure 11. Distribution of fraction surface of Fe-bearing phase provided by simulation code and comparison with experimental data.

It can be seen that, in general there is no evident correlation between solidification rate and surface fraction of Fe-reach precipitate. While the experimental values vary in the interval between 0.87% and 1.21%, the numerical simulation provides an almost constant value of 1.46%. Thus, the simulation code tends to over-estimate the value of surface fraction with an average error of ~34%.
Even if some improvements seem to be necessary in order to refine the result of simulation, a good suggestion of possible critical area is provided.

3. MECHANICAL PROPERTIES

In Table 2 the experimental values of mechanical properties in as-cast temper and after heat treatment were collected.

Table 2. Average YS, UTS and s_f values for support struts and bulk-head support in as-cast and heat treated casting. (Standard deviation in parentheses).

	As-Cast temper			Heat treated temper*			Heat treated temper**		
	YS (MPa)	UTS (MPa)	s_f (%)	YS (MPa)	UTS (MPa)	s_f (%)	YS (MPa)	UTS (MPa)	s_f (%)
Support strut	111(1)	200(3)	7,5(1.5)	260(4)	314(11)	8,1(0.3)	113(5)	196(3)	13,0(1.7)
Bulk-head support	100(1)	134(16)	1,2(0.5)	230(2)	233(6)	5,7(0.4)	106(4)	195(3)	12,85(0.1)

* *solutioning: 540°C for 8 h; water quenching; ageing at 170°C for 9h.*
***solutioning: 540°C for 8 h; air quenching; ageing at 170°C for 3h.*

In general, lower mechanical properties are obtained in correspondence of bulk-head support due to a coarser microstructure as well as an increased amount of defects. The effect of defects can be also noted in the high value of standard deviation associated to UTS and s_f as well as in low value of ductility. From the table it can also be noted that the highest values of YS and UTS are obtained for water quenched. The higher cooling rate during water quenching promotes a better saturation of solid solution improving the mechanical properties after ageing. In detail, the average YS and UTS are 56% and 39% higher than those obtained in as-cast temper and 56% and 28% higher than those for air quenched casting.
However, if air quenching is considered, it can be seen that the main improvement is in ductility. This is due to a reduction of micro-stresses between α-Al matrix and un-coherent Mg_2Si precipitates as consequence of low cooling rate during air quenching.
The results provided by simulation code for mechanical properties in as-cast temper are shown in Figure 11(a)-(c). The effect of defects, *i.*e. porosities and Fe-intermetallic phase, has been assumed as degrading the mechanical performance, especially the ultimate tensile strength and elongation to fracture.

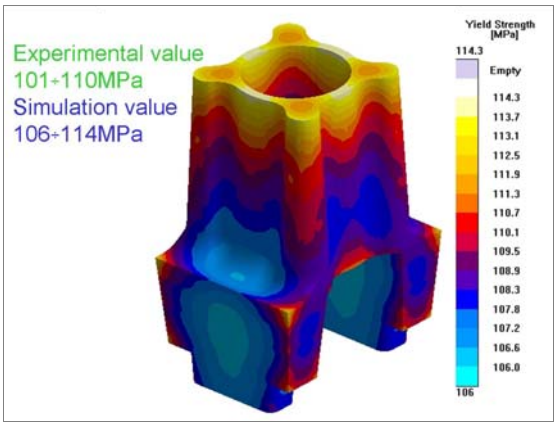

(a)

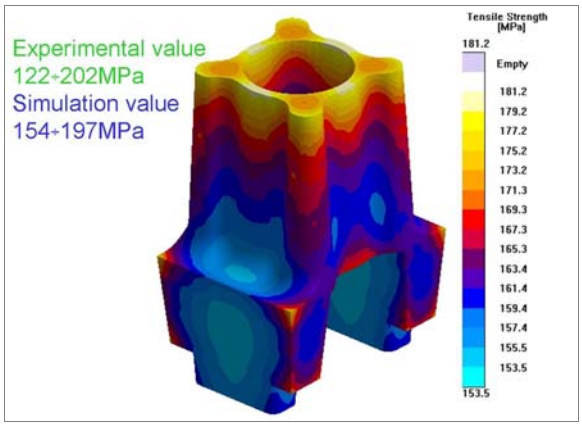

(b)

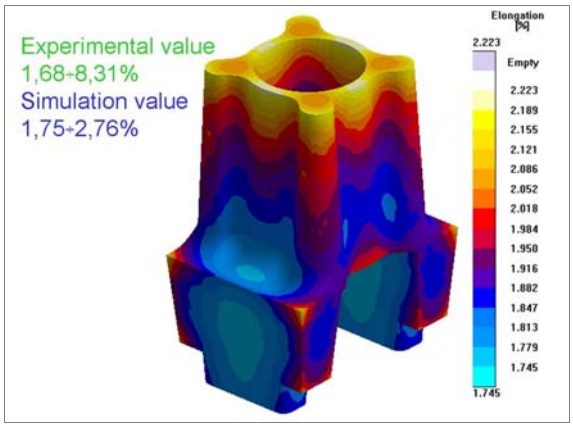

(c)

Figure 12. Distribution of (a) Yield Stress, (b) Ultimate Tensile Strength and (c) elongation to fracture provided by simulation code and comparison with experimental data.

A good agreement between numerical simulation and experimental data for YS and UTS can be pointed out. While the YS values can be assumed constant varying in the range between 106-118 MPa, UTS values vary from 154MPa in bulk-head support to 194 MPa in the top zone, reflecting the dependence of tensile properties on SDAS and microstructure coarseness [18]. On the other hand, the prediction of elongation needs of some improvements even if the distribution of values seems to be almost reasonable. Simulation values are in the range of 1.75-2.76% while measured data vary from 1.68% to 8.31%. This difference can be attributed to the presence of defects that increase the spread in values. Even if in simulation a quality factor is taken into account to consider the effect of defect in reducing the ductility of casting, it is difficult to reproducing exactly the high variability of values. Consequently, it is worth to note that values of elongation to fracture are underestimated by numerical code that allows, in this way, equally a good design of component.

Along with the properties in as-cast temper, in the development of Aluminum casting it is important to know also the properties after heat treatment. Nowadays, the only property that can be predicted with accuracy is Yield Strength. A model describing the influence of different quenching cooling rate as well as the influence of the ageing parameters on kinetic precipitation of secondary phases was recently implemented in simulation code. In Figure 13 the results of distribution of Yield Stress after heat treatment are shown.

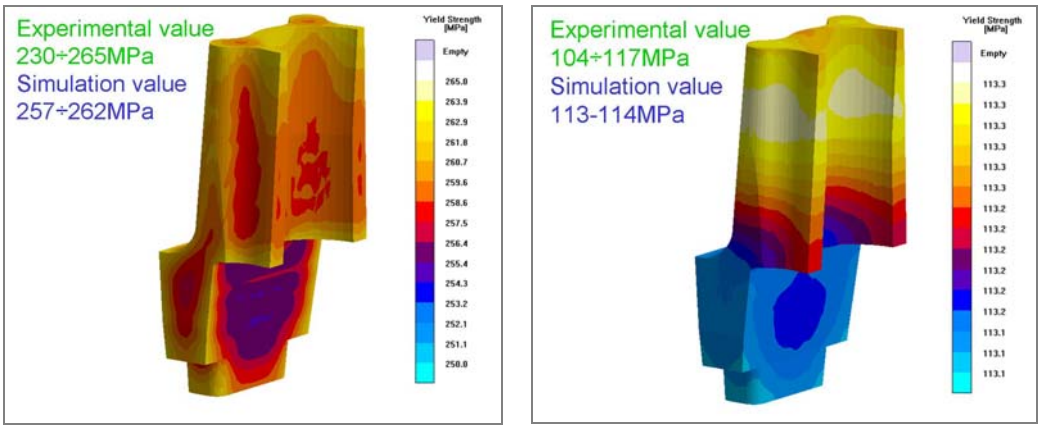

Figure 13. Distribution of Yield Stress, (a) YS after aging for the water heat treatment (b) YS after aging for the air heat treatment.

As it can be seen, the numerical simulation provides value of YS in the range between 116-118MPa and 257-262 for air and water quenched castings, respectively. These values vary in the same interval of experimental data ranging in the interval 104-117MPa and 230-265MPa with an average value of error is 3.6% for air quenched castings and 5.7% for water quenched. Thus, the simulation seems to be reliable, reproducing the experimental data with a good accuracy also for casting suitable of heat treatment.
The possibility to mapping the Yield Strength and, consequently, residual stresses as result of combined effect of alloy, component geometry, casting and heat treatment processes allows to obtain a more complete and realistic material model for structural F.E.M. analysis, as shown in Figure 14.

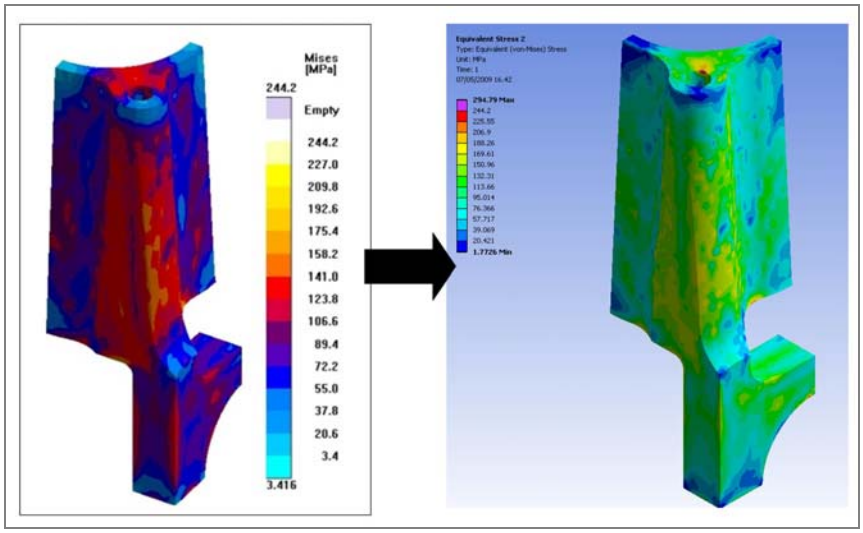

Figure 14: Residual stress (Von Mises result) after aging transferred to ANSYS

4. STRUCTURAL SIMULATION

A material model close to real properties of a component allows to obtain an improved stress and fatigue distributions provided by structural software in design stage. Consequently, in this work the comparison between the results obtained used a traditional elasto-plastic static model and those obtained using process/structure integrated approach is proposed.
Contour of Von Mises Equivalent stress is reported in Figure 15. For the both approaches, high value of Von Mises stress can be noted in the screw thread and in the great radius of curvature of the conjunction zone between liner and bearing where the failure is expected. The traditional approach provides values of ~67MPa and ~127MPa for the two zones respectively. In turn, the process /structure integrated approach shows higher stress values (~250MPa for screw thread and ~146MPa for curvature radius). In addition, it can be noted that this latter approach allows to obtain a more detailed local distribution of stresses describing, in this way, with more accuracy the stress intensity in correspondence of more critical zones of the component.

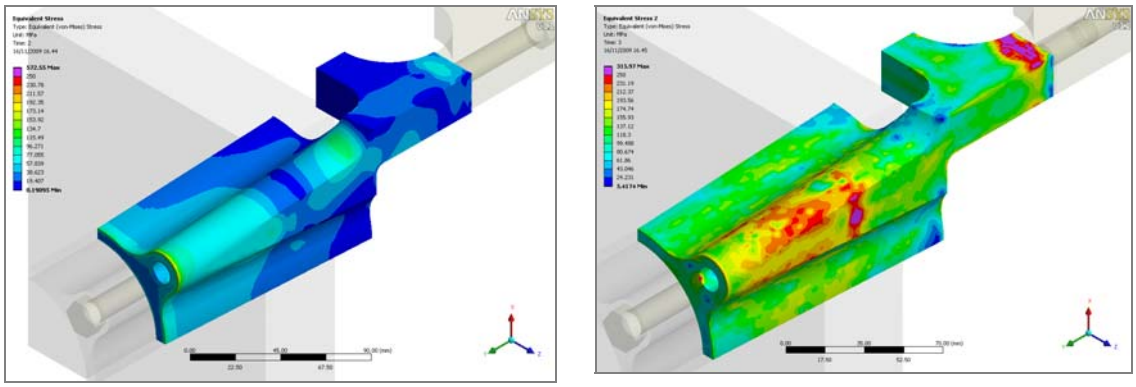

(a) (b)

Figure 15 – (a) Von Mises equivalent stress – Classic approach (b) Von Mises equivalent stress – process/structure integrated approach

The same considerations can be made if fatigue behaviuor is taken into account. Of course, the fatigue analysis includes three areas: materials, analysis, and results evaluation. In particular, the preliminary fatigue material properties are the guide for the simulation comparison and the fatigue results depends on the performed stress solution with constant amplitude. Fatigue material tests are usually conducted in a uniaxial loading under a fixed or zero mean stress state for cost reason; a multi-axial correction can be applied to convert the from a multiaxial stress state to a uniaxial one and a "signed" Von-Mises stress may be chosen where the Von-Mises stress takes the sign of the largest absolute principal stress. Using this approach, in Figures 16 and 17 the comparison between the two methods is shown for alternating stress constant-amplitude fatigue test until failure. The analysis was performed according to Goodman Smith diagram and considering the triaxality effect in a solid body. In addition, the Wöhler S-N diagram describes the possible number of life cycles of the component.

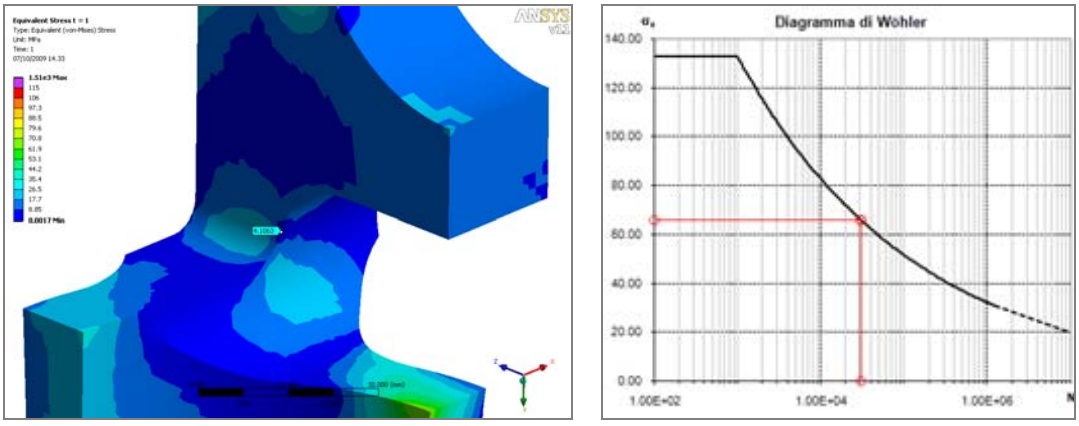

Figure 16. Result of fatigue analysis according to UNI8634 – Classic approach

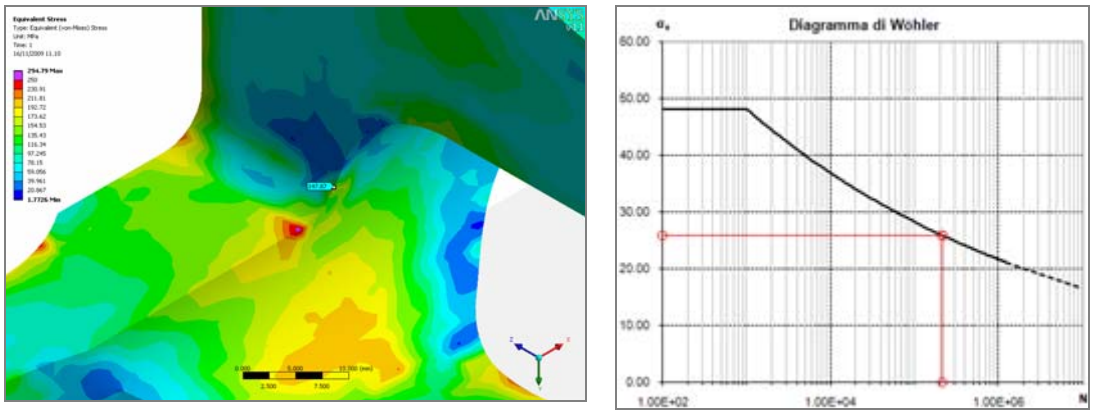

Figure 17. Result of fatigue analysis according to UNI8634 – process/structure integrated approach

From the Figures it can be noted that the fatigue verification carried out in according to UNI ENV 1999-2:2002 (or UNI8634) reference rules for aluminum structures show the verified stress point where 100 MPa maximum stress and 40 MPa as minimum values are defining the stress amplitude. Furthermore, the number of estimated cycles changes from 30000 to 220000 in the internal radius point in agreement with the real tests and considering the same Wöhler sloping factor for both approaches. On the other hand the results obtained by adopting the integrated methodology vary between 143 MPa (min) and 100 MPa (max) with a increment of cycles to the end of life for the 50% of fatigue failure probability.

CONCLUSION

In this work, the results provided by a commercial simulation software were used and experimentally validated to develop a low pressure die casting mono-cylinder engine block. Following remarks can be done:

- Numerical simulation results reproduce the experimental data with a good accuracy. Consequently, it can be stated that numerical simulation is a useful tool for the reduction of time and costs in the design stage.
- A multi-scale evolution of the numerical simulation systems is required for a complete determination of the material mechanical properties. This approach includes, beyond the traditional macro-scale approach, a suitable micro-modelling for micro-defect prediction and the elaboration of the microstructure characteristics.
- The casting and heat treatment simulation output the material microstructure and mechanical properties to evaluate the real performance of the material.
- In any different point of the component the effect of the residual stress can be positive or negative in term of fatigue life, but in any case the new full process-product design increase the component reliability and the company competitiveness.

Acknowledgement

We would like to thank Roberto Molina of Teksid Aluminium for the technical support. Some models and procedure applied to this project are output of NADIA project in FP6_Priority3_NMP (www.nadiaproject.org).

REFERENCES

[1] Haizhi, Ye, 2003. An Overview of the Development of Al-Si-Alloy Based Material for Engine Applications, J. Mater. Eng. Perform. 12, 288-296

[2] S. Kalpakjian, S. R. Schmid, 2002. Manufacturing Processes for Engineering Materials. Prentice Hall.

[3] Gramegna, N., Merlo, R., Pirola, 2005. L. The CAE design chain concept applied to automotive engine blocks. In: Proceedings of 9th Intenational ATA Conference, Florence, Italy.

[4] Gramegna, N., Magistretti, C., 2004. Virtual prototyping approach for the design of the diecast furniture components". In: Proceedings of High Tech Diecasting, Montichiari (Brescia), Italy.

[5] Gramegna, N., 2007. Using CAE tools to apply advanced materials and processes in automotive research. In: Proceedings of EnginSoft CAE Users' Meeting 2007, Bergamo, Italy.

[6] Gramegna, N., 2007. NADIA: New Automotive components Designed for and manufactured by Intelligent processing of light Alloys., In: Proceedings of EUROMAT 2007, Nuremberg, Germany.

[7] Bonollo, F., Odorizzi, S, 2001. Numerical Simulation of Foundry processes. SGE, Italy.

[8] Seifeddine, S., Sjögren, T., Svensson, I. L., 2007. Use of simulation to predict microstructure and mechanical properties in an-cast aluminium cylinder head-comparison with experiments. Mater. Sci. Technol. 25, 12-22.

[9] Niu, X.P, Hu, B.H., Hao, S.W., 1998. Effect of iron on the microstructure and mechanical properties of Al die-casting alloys. J. Mater. Sci. Letters 17, 1727-1729.

[10] Dinnis, C.M., Taylor, J.A., Dahle, A.K., 2005. As-cast morphology of iron-intermetallics in Al–Si foundry alloys. Scr. Mater. 53, 955–958.

[11] Seffeidine, S., Johansson, S., Svensson, I.L., 2008. The influence of cooling rate and manganese content on the β-Al5FeSi phase formation and mechanical properties of Al–Si-based alloys, Mater. Sci. Eng, A490 25, 385-390.

[12] Wang, Q.G., Cáceres, C.H., 1998. Fracture mode in Al-Si-Mg casting alloys. Mater. Sci. Eng, A241 1, 72-82

[13] Wang, Q.G., Cáceres, C.H., Griffiths, J.R., 2003. Damage by eutectic particle cracking in aluminum casting alloys A356/357. Metall. Mater. Trans. A 34, 2901-2912.

[14] Wang, L., Apelian, D., Makhlouf, M., 1999. Iron-Bearing Compounds in Al-Si Die-Casting Alloys: Their morphology and conditions under which they form. AFS Trans.146, 231–238.

[15] Shabestari, S.G., Gruzleski, J.E, 1994. The effect of solidification condition and chemistry on the formation and morphology of complex intermetallic compounds in aluminium-silicon alloys, Cast Met. 6, 217–224.

[16] Ma, Z., Samuel, A.M., Samuel, F.H., 2004. Effect of iron and cooling rate on tensile properties of B319.2 alloys in non-modified and Sr-modified conditions. AFS Trans, 131–140.

[17] Gowri, S., Samuel, F.H., 1994. Effect of alloying elements on the solidification characteristics and microstructure of Al-Si-Cu-Mg-Fe 380 alloy. Metall. Trans. A 25A, 437–448.

[18] Grosselle, F., Timelli, G., Bonollo, F., Tiziani, A., Della Corte,E., 2009. Correlation between microstructure and mechanical properties of Al-Si cast alloy. Metall. Ital. 6, 25-32.